National Technical University of Athens

School of Electrical and Computer Engineering

NATIONAL TECHNICAL UNIVERSITY OF ATHENS

SCHOOL OF ELECTRICAL AND COMPUTER ENGINEERING

DIVISION OF ELECTROMAGNETICS, ELECTROOPTICS AND ELECTRONIC MATERIALS

PH.D. THESIS

APPLICATION OF QUANTUM COMPUTING TECHNIQUES AND QUANTUM INFORMATION THEORY IN PLASMA PHYSICS

Koukoutsis Efstratios

SUPERVISOR: Professor Elias Glytsis, School of Electrical and Computer Engineering, National Technical University of Athens

Athens, February 2025

Submitted in part fulfillment of the requirements for the degree of Doctor of Philosophy in Electrical and Computer Engineering of National Technical University of Athens.

National Technical University of Athens

School of Electrical and Computer Engineering

NATIONAL TECHNICAL UNIVERSITY OF ATHENS

SCHOOL OF ELECTRICAL AND COMPUTER ENGINEERING

DIVISION OF ELECTROMAGNETICS, ELECTROOPTICS AND ELECTRONIC MATERIALS

PH.D. THESIS

APPLICATION OF QUANTUM COMPUTING TECHNIQUES AND QUANTUM INFORMATION THEORY IN PLASMA PHYSICS

Koukoutsis Efstratios

SUPERVISION COMMITTEE

Professor Elias Glytsis

Associate Professor Ioannis Kominis

Associate Professor Konstantinos Politopoulos

Approved by the examination committee on February 11, 2025.

Professor NTUA *Elias Glytsis*, Signature:

Associate Professor NTUA *Ioannis Kominis*, Signature:

Associate Professor NTUA *Kostantinos Politopoulos*, Signature:

Assistant Professor NTUA *Christos Tsironis*, Signature:

Professor Emeritus NTUA *Kyriakos Hizanidis*, Signature:

Professor NTUA *Georgios Gikioris*, Signature:

Professor NTUA *Leonidas Tsetseris*, Signature:

Athens, February 2025

National Technical University of Athens

School of Electrical and
Computer Engineering

DISCLAIMER ON ACADEMIC ETHICS AND INTELLECTUAL PROPERTY RIGHTS
Being fully aware of the implications of copyright laws, I expressly state that this diploma thesis, as well as the electronic files and source codes developed or modified in the course of this thesis, are solely the product of my personal work and do not infringe any rights of intellectual property, personality and personal data of third parties, do not contain work / contributions of third parties for which the permission of the authors / beneficiaries is required and are not a product of partial or complete plagiarism, while the sources used are limited to the bibliographic references only and meet the rules of scientific citing. The points where I have used ideas, text, files and / or sources of other authors are clearly mentioned in the text with the appropriate citation and the relevant complete reference is included in the bibliographic references section. I fully, individually and personally undertake all legal and administrative consequences that may arise in the event that it is proven, in the course of time, that this thesis or part of it does not belong to me because it is a product of plagiarism.

Signrature:

Efstratios Koukoutsis, Ph.D NTUA, February 2025.

Abstract in Greek

Η κβαντική υπολογιστική (QC) και η επιστήμη της κβαντικής πληροφορίας (QIS) αποτελούν ταχέως αναπτυσσόμενους τομείς στη σύγχρονη επιστήμη και τεχνολογία, παρέχοντας τη δυνατότητα επίλυσης ορισμένων υπολογιστικών προβλημάτων με εκθετικά μεγαλύτερη ταχύτητα από τις κλασικές μεθόδους. Ως εκ τούτου, παρατηρείται έντονο ενδιαφέρον από διάφορους επιστημονικούς και τεχνολογικούς κλάδους για την ταυτοποίηση προβλημάτων και τον σχεδιασμό κβαντικών αλγορίθμων που επιδεικνύουν ''κβαντικό πλεονέκτημα'' σε σχέση με τις αντίστοιχες κλασικές μεθόδους. Συγκεκριμένα, η παρούσα εργασία εστιάζει στην διάδοση και τη σκέδαση ηλεκτρομαγνητικών κυμάτων σε μαγνητισμένο πλάσμα και πολύπλοκα ηλεκτρομαγνητικά υλικά, μελετώντας και ενσωματώνοντας τις εξισώσεις του Μάξγουελ (Maxwell) στο πλαίσιο της κβαντικής υπολογιστικής.

Η διατριβή οργανώνεται ως εξής: Το Κεφάλαιο 1 περιγράφει την τρέχουσα κατάσταση της έρευνας σχετικά με την κβαντική υπολογιστική στη φυσική πλάσματος. Παρουσιάζονται επίσης οι στόχοι και το όραμα της διατριβής. Στο Κεφάλαιο 2 περιγράφονται βασικές έννοιες της κβαντικής μηχανικής, της κβαντικής υπολογιστικής και των ανοικτών κβαντικών συστημάτων, οι οποίες αποτελούν τη θεωρητική βάση για τις επόμενες ενότητες. Το Κεφάλαιο 3 αναλύει τη θεωρητική διατύπωση και τις αλγοριθμικές τεχνικές που απαιτούνται για την κβαντική αναπαράσταση των εξισώσεων Maxwell. Στο Κεφάλαιο 4 παρουσιάζεται μια συστηματική προσέγγιση για την κβαντική προσομοίωση της διάδοσης και της σκέδασης ηλεκτρομαγνητικών κυμάτων σε πολύπλοκα μέσα και μαγνητισμένο πλάσμα. Τέλος, το Κεφάλαιο 5 αξιολογεί την πιθανή επίδραση αυτής της έρευνας τόσο στις εφαρμογές της κβαντικής υπολογιστικής στη φυσική πλάσματος όσο και στις συνεισφορές της φυσικής πλάσματος στην προώθηση των κβαντικών τεχνολογιών. Συζητούνται επίσης προτάσεις για μελλοντική έρευνα και ανοιχτά ζητήματα.

Λέξεις Κλειδιά

Κβαντική υπολογιστική, Φυσική πλάσματος, Εξισώσεις Maxwell, Διάδοση και σκέδαση ηλεκτρομαγνητικών κυμάτων.

Abstract

The prospect that, for a range of problems, quantum computers could be exponentially faster than conventional computers has led to an enhanced interest in quantum computer sciences. Naturally, this raises the question of identifying suitable physical problems that can leverage these quantum resources for alternative numerical approaches. In this direction, the present thesis aims to explore integrating Maxwell equations within the quantum computation and information framework, focusing on electromagnetic wave propagation and scattering in magnetized plasmas and complex media. However, the goal is not to chase after a so called "quantum advantage" as it cannot be actually verified and tested in the Noisy Intermediate-Scale Quantum (NISQ) era. Instead, the objective is to identify the possibilities, limitations, and quantum resources required for a future quantum implementation of a realistic contemporary physical problem closely related to magnetic confinement fusion.

This thesis is structured as follows: Chapter 1 provides a brief overview of the motivation and current research status of quantum computing for plasma physics, along with the general objectives and vision of the manuscript. Chapter 2 introduces fundamental perquisites from quantum mechanics and quantum computing and algorithms to open quantum systems. Chapter 3 encompasses all the theoretical elements and insights, as well as the quantum algorithmic techniques required to eventually arrive in Chapter 4. There, a systematic approach to quantum representation and simulation simulation of Maxwell equations in complex media and magnetized plasmas is presented. Finally, Chapter 5 assesses the impact of the proposed research on both "quantum for plasmas" and "plasmas for quantum" perspectives and provides suggestions and open problems for future research and improvements.

Keywords

Quantum computing, Plasma physics, Maxwell equations, Electromagnetic wave propagation and scattering.

Extended Abstract in Greek

Τα τελευταία χρόνια, η ανάπτυξη κβαντικών υπολογιστικών συστημάτων και τεχνολογιών, έχει ανοίξει νέες προοπτικές για την εφαρμογή της κβαντικής υπολογιστικής σε ένα ευρύ φάσμα επιστημονικών και τεχνολογικών προβλημάτων. Ειδικότερα, το πεδίο των κβαντικών αλγορίθμων συνεχώς επεκτείνεται, περιλαμβάνοντας τεχνικές όπως οι κβαντικοί μετασχηματισμοί Fourier, οι αλγόριθμοι αναζήτησης τύπου Grover, και οι μέθοδοι κβαντικής μηχανικής μάθησης, που στοχεύουν στη βελτιστοποίηση και στην επιτάχυνση σύνθετων υπολογισμών.

Η αναζήτηση εναλλακτικών μεθόδων υλοποίησης υπολογισμών δεν περιορίζεται αποκλειστικά στο πεδίο της κβαντικής υπολογιστικής. Αντίθετα, αποτελεί αντικείμενο ευρύτερης έρευνας τα τελευταία χρόνια π.χ. νευρομορφικά δίκτυα (neuromorphic networks), καθώς οι υπολογιστικές απαιτήσεις αυξάνονται συνεχώς, ενώ είναι δεδομένο ότι οι σύγχρονες υπολογιστικές μηχανές κάποια στιγμή θα αγγίξουν τα όριά τους.

Συνεπώς, στο πλαίσιο της εξερεύνησης των υπολογιστικών δυνατοτήτων αλλά και της προοπτικής εφαρμογής των κβαντικών υπλογιστικών μεθόδων σε κλασσικά φυσικά προβλήματα, η παρούσα διατριβή μελετάει την σύγκλιση των κβαντικών τεχνολογιών με τον τομέα της φυσικής πλάσματος και σύντηξης όπου οι υπολογιστικές προκλήσεις είναι κρίσιμες για τη μελέτη των πολύπλοκων φυσικών διεργασιών που λαμβάνουν χώρα στο πλάσμα. Συγκεκριμένα, η παρούσα εργασία εστιάζει στην διάδοση και τη σκέδαση ηλεκτρομαγνητικών κυμάτων σε μαγνητισμένο πλάσμα και πολύπλοκα ηλεκτρομαγνητικά υλικά, μελετώντας και ενσωματώνοντας τις εξισώσεις του Μάξγουελ (Maxwell) στο πλαίσιο της κβαντικής υπολογιστικής.

Τα ηλεκτρομαγνητικά κύματα, που περιγράφονται από τις εξισώσεις Maxwell, διαδραματίζουν κεντρικό ρόλο σε σύγχρονες τεχνολογικές εφαρμογές από τις τηλεπικοινωνίες μέχρι τη θέρμανση πλάσματος σε πειράματα σύντηξης. Στον τομέα της μαγνητικής σύντηξης, τα ηλεκτρομαγνητικά κύματα είναι απαραίτητα για τον μετριασμό των αστάθειων, την οδήγηση ρεύματος, τη θέρμανση και τον έλεγχο της θερμοκρασίας του πλάσματος. Παρότι η θεωρητική κατανόηση της δυναμικής των ηλεκτρομαγντητικών κυμάτων σε μαγνητισμένο πλάσμα και άλλα πολύπλοκα υλικά έχει εδραιωθεί, η ανάπτυξη υπολογιστικών μοντέλων που μπορούν να περιγράψουν με ακρίβεια αυτά τα φαινόμενα υπο ρεαλιστικές πειραματικές συνθήκες παραμένουν ένα κρίσιμο πεδίο έρευνας. Η παρούσα διατριβή εξετάζει την κβαντική αναδιατύπωση των εξισώσεων Maxwell, με στόχο:

1. Την θεωρητική μελέτη και αξιολόγηση των περιορισμών και δυνατοτήτων της κβαντικής υπλογιστικής θεώρησης στις κλασσικές εξισώσεις Maxwell.

2. Την πρόταση και μελέτη κβαντικών αλγορίθμων και των κβαντικών πόρων που

απαιτούνται για την προσομοίωση των εξισώσεων Maxwell στην εποχή των Κβαντικών Υπολογιστών με Θόρυβο (NISQ) και πέρα από αυτή.

Acknowledgments

I would like to express my gratitude to my family for a lifetime of encouragement and care. I am equally indebted to Georgia for her love and support over the past few years and to my friends, who stood by me during challenging times.

The completion of this thesis would not have been possible without the invaluable guidance and mentorship of Professor Emeritus Kyriakos Hizanidis. His wisdom and encouragement have allowed me to grow as a scientist, fostering my intellectual curiosity through countless discussions and shared ideas.

I extend my deepest appreciation to Principal Researcher Abhay K. Ram and Professor George Vahala for their generous advice and support, which were instrumental in guiding me through every stage of this work. I am also grateful to my supervisor, Professor Elias Glytsis, for his cooperative and calm demeanor, which were a source of reassurance throughout this journey.

Special thanks are due to Associate Professor Yannis Kominis, who introduced me to the Laboratory of Plasma, Electron Beam, and Nonlinear Optics, and to Associate Professor Konstantinos Politopoulos, whose assistance with various administrative processes was greatly appreciated.

I would also like to acknowledge the contributions of my collaborators, Senior Researcher Panagiotis Papagiannis and Assistant Professor Christos Tsironis, for their support in numerous scientific endeavors. Finally, I extend my thanks to all my colleagues at NTUA for their insightful discussions, and encouragement.

This work has been carried out within the framework of the EUROfusion Consortium, funded by the European Union via the Euratom Research and Training Programme (Grant Agreement No 101052200 — EUROfusion). Views and opinions expressed are however those of the author(s) only and do not necessarily reflect those of the European Union or the European Commission. Neither the European Union nor the European Commission can be held responsible for them. The author also acknowledges funding and support from the *Basic Research Program, NTUA, PEVE.*

Contents

List of Figures

Chapter 1

Introduction

1.1 Motivation and scope

Since the introduction of quantum mechanics in 1925, that profoundly enhanced our understanding of nature's physical laws and established it as the second pillar of modern physics (alongside the theory of general relativity), today we are in the midst of the second quantum revolution [1, 2]. Quantum Computing (QC) and Quantum Information Science (QIS) have emerged at the forefront of the contemporary technological advancements due to the novel and exotic capabilities of quantum systems in terms of computation and information processing [3–5]. Subsequently, the research endeavor around the theoretical and experimental verification of quantum protocols' supremacy over their classical counterparts, is growing exponentially leading to pioneering applications in various fields in industry and science. Illustrative examples can be found in the respective areas of medicine [6], optimization and machine learning [7], dynamical systems [8], fluid dynamics [9] and many others.

These rapid advancements in quantum technologies have ignited the interest of plasma and fusion science community to integrate the novel and powerful quantum computational techniques into the notoriously complex and demanding in computational resources, field of plasma physics. Particularly, in 2018, the United States Department of Energy has made public a technical report titled "Quantum for Fusion, Fusion for Quantum" [10] that was highlighting several opportunities for leveraging quantum computing and quantum technologies for scientific discoveries and technology advances in fusion and plasma physics. As a result, unique research directions relevant to applications of QC and QIS to plasma physics have emerged [11–13] in the subsequent years. The impact of those works as well as the interdisciplinary nature of plasma physics have facilitated a paradigm shift towards quantum computing for addressing many different plasma physics problems.

The main contributions of the present thesis, motivated by these pioneering research directions, is the quantum reformulation of Maxwell equations and the subsequent quan-

tum simulation of electrodynamics in complex media such as magnetized plasmas. In summary:

1. Reformulating Maxwell equations for dispersion-less media as a quantum Schrodinger equation with explicit unitary dynamics. Following this, a Qubit Lattice Algorithm (QLA) reflecting a Quantum Walk (QW) process is employed for quantum simulation of electromagnetic propagation and scattering, with numerical results from the corresponding classical implementation.

2. Analyzing the complexity of a potential quantum implementation of the algorithm.

3. Developing a QW based quantum algorithm for simulating electromagnetic wave propagation in cold magnetized plasmas, along with the complexity analysis of the algorithm.

4. Introducing dissipation and using quantum simulation techniques inspired by open quantum systems to evaluate the algortihms' required quantum resources to accurately capture the transient dissipative dynamics.

But, why Maxwell equations?
Electromagnetic waves are ubiquitous in nature and play a crucial role in various applications ranging from communications to heating of thermonuclear fusion plasma. In all these applications, to predict the behaviour and obtain physical insight on the electromagnetic wave dynamics one can solely rely on the computational simulation of Maxwell equations. Specifically, in magnetic confinement fusion experiments electromagnetic waves play a vital part to mitigation of instabilities, current-drive and heating as well as plasma temperature control. While the theoretical and analytical foundations for electromagnetic wave propagation in magnetized plasmas have long been establish [14, 15] and remain an active field of research, the focus has shifted to construction of computational models that can accurately capture the physics of wave propagation in realistic fusion experiments [16].

Consequently, the scope of the proposed research is two-fold. Initially, it aims to prepare the plasma physics community to leverage quantum computers for fundamental aspects of fusion plasma physics. Whereupon, it seeks to establish quantum computing as a prominent simulation and validation tool in the field of computational electromagnetism with the potential to breakthrough the computational studies of electromagnetic wave dynamics in plasma fusion and beyond in the near future.

Chapter 2

A Primer to Quantum Computing and Quantum Information Science

2.1 A prelude to quantum mechanics

This section serves as a brief exposition to quantum mechanics and the related notation, for the unfamiliar reader to prepare for the material in the following chapters. For a thorough and comprehensive introduction to the mathematical and physical aspects of quantum mechanics, there is a plethora of excellent textbooks [17–21] for the interested reader to consult.

2.1.1 States and Hilbert space

A quantum state, denoted with $|\psi\rangle$ (ket), is an element of a Hilbert space $\mathscr{H}$. A Hilbert space $\mathscr{H}$, is a linear vector space $\mathscr{V}$ over the field of complex numbers $\mathscr{F} = \mathbb{C}$, equipped with the standard triplet of linear operations $(+, \cdot, \langle|\rangle)$,

$$+ : \mathscr{V} \times \mathscr{V} \to \mathscr{V} \quad \text{(addition)}, \tag{2.1}$$

$$\cdot : \mathbb{C} \times \mathscr{V} \to \mathscr{V} \quad \text{(scalar multiplication)}, \tag{2.2}$$

$$\langle|\rangle : \mathscr{V} \times \mathscr{V} \to \mathbb{C} \quad \text{(inner product)}. \tag{2.3}$$

The dual space $\mathscr{H}^*$ of the Hilbert space $\mathscr{H}$, contains functional elements denoted with $\langle\psi|$ (bra). Due to Hilbert space reflexivity, $\mathscr{H} = \mathscr{H}^{**}$, the dual pairing $(\langle\phi|, |\psi\rangle)$ is respectively equivalent to the inner product $(|\phi\rangle, |\psi\rangle)$. Thus, the inner product $(|\phi\rangle, |\psi\rangle)$ between the states $|\psi\rangle, |\phi\rangle \in \mathscr{H}$ can be compactly represented as $\langle\phi|\psi\rangle$. This formalism is called the bra-ket notation of quantum mechanics and was firstly introduced by Dirac [17]. The relation between the state $|\psi\rangle \in \mathscr{H}$ and its dual $\langle\psi| \in \mathscr{H}^*$ is

$$(|\psi\rangle)^\dagger = \langle\psi|, \tag{2.4}$$

where the superscript † indicates the complex conjugate transposition operation.

Using the inner product structure of $\mathscr{H}$, it is possible to define the norm $\|\psi\|$ of the state $|\psi\rangle$ as

$$\|\psi\| = \sqrt{\langle\psi|\psi\rangle} \geq 0, \quad \|\psi\| = 0 \text{ iff } |\psi\rangle = 0. \tag{2.5}$$

Two states $|\phi\rangle, |\psi\rangle \in \mathscr{H}$ satisfying $\langle\phi|\psi\rangle = 0$, are orthogonal and can be written as $|\phi\rangle \perp |\psi\rangle$. If also, the norm of the states is $\|\psi\| = \|\phi\| = 1$, then the states are called orthonormal. Given a specific orthonormal basis $\{|e_j\rangle\}$ of the Hilbert space $\mathscr{H}$ (assuming that the Hilbert space is finite dimensional, $dim(\mathscr{H}) < \infty$) the arbitrary state $|\psi\rangle \in \mathscr{H}$ is expressed as

$$|\psi\rangle = \sum_j^{dim(\mathscr{H})} c_j |e_j\rangle, \quad c_j = \langle e_j|\psi\rangle \in \mathbb{C}. \tag{2.6}$$

An admissible quantum state in the form of Eq.(2.6) obeys the normalization condition $\sum_j |c_j|^2 = 1$. As such, the complex numbers c_j constitute the probability amplitudes to find the particle in the state $|e_j\rangle$.

2.1.2 Operators and observables

A map $\hat{T} : \mathscr{H} \to \mathscr{H}$ is a linear operator in Hilbert space if,

$$\hat{T}(a|\psi\rangle + b|\phi\rangle) = a\hat{T}|\psi\rangle + b\hat{T}|\phi\rangle, \quad |\psi\rangle, |\phi\rangle \in \mathscr{H}, \quad a, b \in \mathbb{C}. \tag{2.7}$$

Expressing the operator $\hat{T}$ into a specific orthonormal basis of Hilbert space results into the outer product expression

$$\hat{T} = \sum_{ij} T_{ij} |e_i\rangle\langle e_j|, \quad T_{ij} = \langle e_i|\hat{T}|e_j\rangle, \tag{2.8}$$

where T_{ij} is the matrix representation of the operator. From Eq.(2.8), it can be directly deduced that the unity operator $\hat{I}|\psi\rangle = |\psi\rangle$ is

$$\hat{I} = \sum_j |e_j\rangle\langle e_j|. \tag{2.9}$$

In analogous way with Eq.(2.4), the dual mapping $\hat{T}^\dagger : \mathscr{H}^* \to \mathscr{H}^*$, is defined as

$$\langle\psi|\hat{T}^\dagger = (\hat{T}|\psi\rangle)^\dagger \tag{2.10}$$

where $\hat{T}^\dagger$ is the complex conjugate transpose operator, $T^\dagger_{ij} = T^*_{ji}$.

Quantum mechanics is a physical theory, so it has to describe reality by accurately providing physical quantities of interest such as position, momentum, energy etc. These meaningful physical quantities are defined as observables and are associated with a Her-

mitian operator. An operator $\hat{T}$ is Hermitian iff,

$$\langle\phi|(\hat{T}|\psi\rangle) = (\langle\phi|\hat{T})|\psi\rangle \equiv \langle\phi|\hat{T}|\psi\rangle, \quad \hat{T} = \hat{T}^{\dagger}, \quad |\phi\rangle, |\psi\rangle \in \mathscr{H}. \tag{2.11}$$

Hermitian operators admit spectral decomposition with real eigenvalues and the respective eigenvectors form a orhtonormal basis in Hilbert space $\mathscr{H}$, [22]. Utilizing this aspect, given a Hermitian operator, for example the energy operator $\hat{E}$, it is possible to expresses the arbitrary state $|\psi\rangle \in \mathscr{H}$ through the eigenvectors-basis $\{|E_j\rangle\}$ of $\hat{E}$,

$$|\psi\rangle = \sum_j d_j |E_j\rangle, \quad d_j \in \mathbb{C}. \tag{2.12}$$

Therefore, the quantity $\langle\psi|\hat{E}|\psi\rangle$

$$\langle\psi|\hat{E}|\psi\rangle = \sum_j |d_j|^2 \lambda_j \in \mathbb{R}, \tag{2.13}$$

represents the mean value $\langle\hat{E}\rangle$ of the energy operator $\hat{E}$, with λ_j being its respective eigenvalues. Equation (2.13) reflects that the observable physical quantities are the real eigenvalues of the corresponding Hermitian operator. For instance, the probability to measure the energy $E = \lambda_k$ of the system in state (2.12), is $p_k = |d_k|^2$.

A different kind of operator that plays a crucial role in quantum mechanics is the unitary operator. An operator $\hat{U}$ is unitary iff,

$$\hat{U}\hat{U}^{\dagger} = \hat{U}^{\dagger}\hat{U} = \hat{I}, \quad \hat{U}^{-1} = \hat{U}^{\dagger}. \tag{2.14}$$

Unitary operators are isometries, i.e they preserve the inner product structure. This can been easily verified by constructing the state $|\phi\rangle = \hat{U}|\psi\rangle$, then

$$\langle\phi|\phi\rangle = \langle\psi|U^{\dagger}\hat{U}|\psi\rangle = \langle\psi|\psi\rangle. \tag{2.15}$$

In terms of physical context, Eq.(2.15) implies that unitary operators are probability preserving.

2.1.3 Postulates of quantum mechanics

- Postulate 1: The evolution of a closed quantum system is dictated by the Schrodinger equation

$$i\frac{\partial|\psi\rangle}{\partial t} = \hat{H}|\psi\rangle, \quad \hat{H} = \hat{H}^{\dagger}. \tag{2.16}$$

  According to Stone's theorem [23], there is a one-to-one correspondence between Hermitian operators acting on Hilbert space $\mathscr{H}$ and one-parameter families $\hat{U}_{t\in\mathbb{R}}$

of unitary operators. Therefore, the Hermitian operator $\hat{H}$ generates unitary time evolution, $\hat{U} = \exp\{-it\hat{H}\}$.

The unitary dynamics of Schrodinger equation (2.16) convey the probability conservation that has to be present in a closed system,

$$|\psi(t)\rangle = \hat{U}\,|\psi_0\rangle\,, \quad \frac{\partial\,\langle\psi(t)|\psi(t)\rangle}{\partial t} = 0 \Leftrightarrow \langle\psi(t)|\psi(t)\rangle = \langle\psi_0|\psi_0\rangle\,, \tag{2.17}$$

with $|\psi_0\rangle$ the initial state at $t = 0$.

- Postulate 2: A quantum measurement is described by a collection of measurement operators $\{\hat{M}_m\}$ acting on a state $|\psi\rangle \in \mathscr{H}$ of the system being measured. After the measurement the probability $p(m)$ to obtain the outcome m is

$$p(m) = \langle\psi|\hat{M}_m^\dagger\hat{M}_m|\psi\rangle\,, \tag{2.18}$$

and the post-measurement state $|\psi\rangle'$ now reads

$$|\psi\rangle' = \frac{\hat{M}_m\,|\psi\rangle}{\sqrt{p(m)}}. \tag{2.19}$$

The aforementioned definition of measurements is the most general one, encompassing projective as well as Positive Operator-Valued Measure (POVM) measurements. Projective measurements $\hat{P}_m$ are described by Hermitian operators–observables as delineated in Sec.2.1.2,

$$\hat{P}_m = |e_m\rangle\,\langle e_m|\,, \quad \hat{P}_m = \hat{P}_m^\dagger, \quad \hat{P}_m^2 = \hat{P}_m, \tag{2.20}$$

with $|e_m\rangle$ an eigenvector of a Hermitian–observable–operator. The possible outcomes from such a measurement corresponds to the eigenvalues λ_m of the observable operator. On the other hand, POVM measurements denoted with $\hat{E}_m = \hat{M}_m^\dagger\hat{M}_m$ are usually used in cases where the post-measurement state is not of particular interest but the measurement statistics and the related disclosed information matters the most. A characteristic example is the use of POVM measurements to distinguish between two quantum states with a certain success probability [24].

- Postulate 3: The state space of a composite quantum system is the tensor product of the Hilbert spaces of the component quantum systems.

We define the tensor product operation $\otimes$ between two Hilbert spaces $\mathscr{H}_1$ and $\mathscr{H}_2$ as

$$\otimes : \mathscr{H}_1 \times \mathscr{H}_2 \to \mathscr{H}\,, \tag{2.21}$$

with $dim(\mathscr{H}) = dim(\mathscr{H}_1) \times dim(\mathscr{H}_2)$. Hence, a general bipartite quantum state $|\psi\rangle$ can be represented in a prescribed basis $\{|e_k\rangle = |e_i\rangle \otimes |e_j\rangle\}$

$$|\psi\rangle = \sum_{k}^{dim(\mathscr{H})} a_k |e_k\rangle, \quad a_k \in \mathbb{C}, \tag{2.22}$$

where $|e_i\rangle \otimes |e_j\rangle$ now translates into the Kronecker product [22] between the basis vectors $\{|e_i\rangle\}$ and $\{|e_j\rangle\}$ of the Hilbert spaces $\mathscr{H}_1$ and $\mathscr{H}_2$ respectively. Most of the times, for brevity purposes, the tensor product notation will be suppressed, so $|e_i\rangle \otimes |e_j\rangle \equiv |e_i\rangle |e_j\rangle \equiv |e_i e_j\rangle$. A direct consequence of definition (2.22) is that the tensor product state space $\mathscr{H}$ contains non-separable states,

$$\exists |\psi\rangle \in \mathscr{H} \Rightarrow |\psi\rangle \neq |\psi_1\rangle \otimes |\psi_2\rangle, \quad |\psi_1\rangle \in \mathscr{H}_1, \ |\psi_2\rangle \in \mathscr{H}_2. \tag{2.23}$$

In the following sections it will be showcased that these non-separable states, characterized as entangled, play a pivotal role on the computational prowess of quantum computers as well as in the quantum information theory.

2.1.4 Density operator formalism

In the previous sections the pure state formalism of quantum mechanics was illustrated; The quantum system was described by the state $|\psi\rangle \in \mathscr{H}$ with absolute certainty. However, a quantum system can be in one of a number of pure states $|\psi_i\rangle$ with probability p_i. Thus, to deal now with an ensemble of pure states $\{p_i, |\psi_i\rangle\}$ the density operator or density matrix formalism is employed. The density operator of a quantum system is defined though,

$$\rho = \sum_i p_i |\psi_i\rangle \langle\psi_i|, \quad \sum_i p_i = 1. \tag{2.24}$$

A density operator ρ is associated with an ensemble iff,

- $Tr(\rho) = 1$, and
- ρ is a positive definite operator.

The Tr notation stands for the trace operation. The density matrix for pure states is $Tr(\rho^2) = 1$, whereas for mixed states, i.e. states that are characterized by lack of maximal knowledge about them, $Tr(\rho^2) < 1$.

The quantum postulates for the pure states can be equivalently expressed in terms of the density matrix formalism as follows:

$$i\frac{\partial \rho(t)}{\partial t} = [\hat{H}, \rho], \quad \rho(t) = \hat{U}\rho_0\hat{U}^\dagger \quad \text{(Postulate 1)}, \tag{2.25}$$

where $[,]$ is the commutator operator, $[\hat{A},\hat{B}] = \hat{A}\hat{B} - \hat{B}\hat{A}$, and ρ_0 is the initial density matrix at $t = 0$.

$$p(m) = Tr(\hat{M}_m^\dagger \hat{M}_m \rho), \quad \rho' = \frac{\hat{M}_m \rho \hat{M}_m^\dagger}{p(m)} \quad \text{(Postulate 2).} \tag{2.26}$$

A bipartite separable state ρ_{AB} of a quantum system composed of subsystems–A and B with density matrices ρ_A and ρ_B respectively, reads

$$\rho_{AB} = \rho_A \otimes \rho_B \quad \text{(Postulate 3).} \tag{2.27}$$

Perhaps the most powerful application of the density operator formalism is on the characterization of the composite quantum systems. For a bipartite system as in Eq.(2.27), we define the partial trace operation with respect to subsystem–B to be

$$Tr_B(\rho_{AB}) = \rho_A Tr(\rho_B) = \rho_A. \tag{2.28}$$

The partial trace formula (2.28) enables us to efficiently compute the purity of the density matrix of the subsystem of interest and identify entanglement.

Before proceeding to the next section, the reader is advised to refer to Ref.[19] for a detailed and quantum informational-wise exposition of the aforementioned concepts.

2.2 Fundamental concepts in quantum computing

Embarking on our exploration of quantum computing and quantum information, a valuable reference is the seminal textbook by Nielsen and Chuang [25]. The reader is encouraged to consult it for additional clarification on the presented material.

2.2.1 Qubits and quantum gates

The fundamental carrier of quantum information, the quantum bit–qubit, is a coherent quantum state that resides in a two dimensional Hilbert space $\mathscr{H}_2$,

$$|\psi\rangle = a|0\rangle + b|1\rangle, \quad a,b \in \mathbb{C}, \quad |a|^2 + |b|^2 = 1, \tag{2.29}$$

where the basis vectors $\{|0\rangle, |1\rangle\}$ constitute the so called computational basis. Immediately, from the mere definition of qubit (2.29) it is evident that the superposition structure of a qubit as a pure state contains richer information compared to the the classical bit which can be represented as a quantum mixed state ρ_{bit},

$$\rho_{bit} = |a|^2 |0\rangle\langle 0| + |b|^2 |1\rangle\langle 1|. \tag{2.30}$$

An illustrative representation of the qubit is the Bloch sphere representation, Fig.2.1, which exploits the isomorphism between the complex two-dimensional Hilbert space $\mathscr{H}_2$ and the S^3 surface of a unit three-dimensional sphere,

$$|\psi\rangle = \cos\frac{\theta}{2}|0\rangle + e^{i\phi}\sin\frac{\theta}{2}|1\rangle \quad \text{(Bloch sphere representation)}, \tag{2.31}$$

where the angles θ and ϕ are the azimuthal and polar angles respectively.

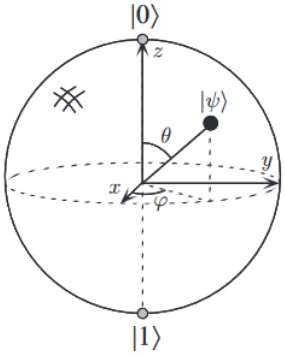

Figure 2.1: Bloch sphere representation of a qubit [25].

According to Postulate 1 the evolution of a closed system is unitary for the total probability to be conserved (see Eq.(2.17)). Therefore, only unitary operations–quantum gates– are admissible in the quantum computing framework. The most important single qubit gates are summarized as follows:

Pauli gates

$$\hat{X} = \begin{bmatrix} 0 & 1 \\ 1 & 0 \end{bmatrix}, \quad \hat{Y} = \begin{bmatrix} 0 & -i \\ i & 0 \end{bmatrix}, \quad \hat{Z} = \begin{bmatrix} 1 & 0 \\ 0 & -11 \end{bmatrix}, \tag{2.32}$$

Hadamard and Phase gates

$$\text{Hadamard gate:} \quad \hat{H} = \frac{1}{\sqrt{2}}\begin{bmatrix} 1 & 1 \\ 1 & -1 \end{bmatrix}, \quad \text{Phase gate:} \quad \hat{S} = \begin{bmatrix} 1 & 0 \\ 0 & i \end{bmatrix}, \tag{2.33}$$

Rotation gates

$$\hat{R}_x(\theta) = \begin{bmatrix} \cos\frac{\theta}{2} & -i\sin\frac{\theta}{2} \\ -i\sin\frac{\theta}{2} & \cos\frac{\theta}{2} \end{bmatrix}, \quad \hat{R}_y(\theta) = \begin{bmatrix} \cos\frac{\theta}{2} & -\sin\frac{\theta}{2} \\ \sin\frac{\theta}{2} & \cos\frac{\theta}{2} \end{bmatrix}, \quad \hat{R}_z(\theta) = \begin{bmatrix} e^{-i\theta/2} & 0 \\ 0 & e^{i\theta/2} \end{bmatrix}. \tag{2.34}$$

Allowing now n qubits to interact, the composite pure state according to the tensor product rule (2.21) in the third quantum mechanical postulate reads,

$$|\psi\rangle = \sum_{\substack{i=0 \\ j_i=\{0,1\}}}^{n-1} c_i\,|j_{n-1}j_{n-2}\ldots j_1 j_0\rangle\,, \quad |\psi\rangle \in \mathscr{H} = \mathscr{H}_2^{\otimes n}, \tag{2.35}$$

where the basis elements $|j_{n-1}j_{n-2}....j_1j_0\rangle$ consists of 2^n permutations of the binary elements $\{0,1\}$. The binary representation (2.35) can be easily re-expressed in the standard computational basis $\{|k\rangle\}, k = 0,1,...,2^n-1$ of the composite Hilbert space $\mathscr{H}_2^{\otimes n}$,

$$|\psi\rangle = \sum_{k=0}^{2^n-1} c_k |k\rangle, \quad k = j_{n-1}2^{n-1} + j_{n-2}2^{n-2} + ... + j_1 2^1 + j_0 2^0, \quad c_k \in \mathbb{C}. \tag{2.36}$$

Two things are to be taken from the state (2.36) and the resulting dimension of Hilbert space $\mathscr{H}$:

1. The dimension of the composite Hilbert space $\mathscr{H} = \mathscr{H}_2^{\otimes n}$ is exponentially large, $dim(\mathscr{H}) = 2^n$, in respect to the number of qubits. In contrast, the state space dimension of m classical bits scales as m. This implies that a quantum computer has an exponentially larger memory capacity compared to the classical machines.

2. The second element that stands out is that a state can carry an exponentially large amount of information (in the amplitudes c_k) due to the superposition structure, Eq.(2.36). This characteristic feature lies in the heart of quantum parallelism in which different information elements about the same object can be encoded in the the same quantum state and processed in parallel ways.

For $n = 2$ qubits, the four-dimensional space allows to introduce the simplest unitary controlled operation, the controlled-NOT (CNOT), that depending on the value the bit of the first–control–qubit, a Pauli $\hat{X}$ transformation is applied to the second–target–qubit. Then, the matrix representation of CNOT operation in the computational basis is,

$$\text{CNOT} = \begin{bmatrix} 1 & 0 & 0 & 0 \\ 0 & 1 & 0 & 0 \\ 0 & 0 & 0 & 1 \\ 0 & 0 & 1 & 0 \end{bmatrix}. \tag{2.37}$$

For example the action of CNOT gate into the 2-qubit state $\frac{1}{2}(|00\rangle + |11\rangle)$ results to $\frac{1}{2}(|0\rangle + |1\rangle)|0\rangle$. Notice how an initial non-separable, entangled, state has become separable through the CNOT action. In the same sense, it is possible to define a general controlled operation $C(\hat{U})$ of a general singe qubit unitary gate $\hat{U}$. More general, the action of a controlled operation $C^{m,k}(\hat{U})$ which applies the unitary $\hat{U}$ operator into the k–target qubit state $|\psi\rangle$, controlled by m qubits, is

$$C^{m,k}(\hat{U})|x_m...x_1x_0\rangle|\psi\rangle = |x_m...x_1x_0\rangle \hat{U}^{x_m\cdot....\cdot x_1\cdot x_0}|\psi\rangle, \quad \text{or} \quad C^{m,k}(\hat{U}). = \begin{bmatrix} \hat{I}_{(2^m\times 2^m)} & 0 \\ 0 & \hat{U} \end{bmatrix} \tag{2.38}$$

A useful example of a $m = 2, k = 1$ controlled gate is the Toffoli gate $C^{2,1}(\hat{X})$.

2.2.2 Quantum circuit model and gate decomposition

Applying different gates to multiple qubits can be extremely tedious in terms of the algebraic representation. Fortunately, there is an elegant way to depict the operations that apply to the different qubits thought quantum circuits.

A quantum circuit is composed by parallel horizontal lines representing the quantum wires. Each wire contains a qubit. Starting from the left-side, the input state is provided and the applied single qubit gates are depicted as boxes in the respective quantum wires. For controlled operations, control by the one–bit is depicted with solid black dot, whereas control by the zero–bit uses a hollow white dot. The outcome state is produced at the right side of the circuit. A measurement operation is depicted by a meter. Below, in Fig.2.2, the quantum circuit representation of important controlled gates is presented. The quantum

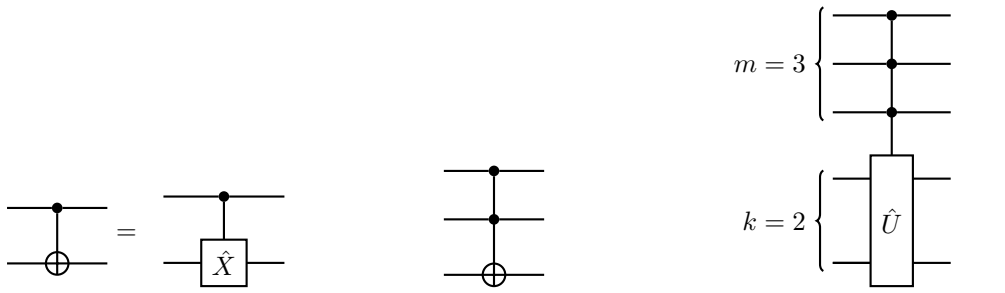

(a) CNOT gate. (b) Toffoli gate. (c) A multi-controlled gate.

Figure 2.2: Quantum circuit representation of different controlled operations.

circuit for preparing a two–qubit entangled Bell state is also presented in Fig.2.3.

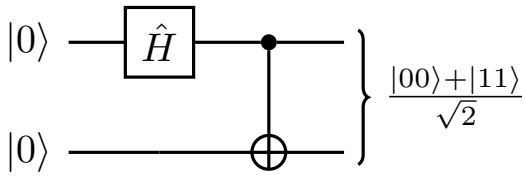

Figure 2.3: Quantum circuit representation of preparing a maximally entangled Bell state.

While the depiction of a sequence of unitary operations through quantum circuit is particularly useful, it has to be complemented with known decomposition of the applied operators into simple gates that consist a universal set, namely the Hadamard, CNOT, phase and $\pi/8$ gates, for fault tolerant quantum computation. Under this discrete universal set of gates any unitary operator can be approximated to arbitrary precision. Usually, it is sufficient to provide the decomposition of the unitary operator in a number of CNOTs and single-qubit gates as this set is also universal but not fault-tolerant. However, we must have in mind that approximating arbitrary unitary gates in terms of universal simple gates

is generally hard and it may requires an exponentially large number of universal gates. For example, the decomposition of a n qubit unitary operator into single-qubit and CNOT gates scales as $O(4^n n^2)$, with the big O being the standard asymptotic notation. However this situation is not viable as it directly affects the actual implementation efficiency of the quantum process to quantum hardware. Therefore, the search for optimized ("shallow"), in terms of the required numbers of gates, decomposition procedures [26–30] is considered extremely important as it is closely tied with the ability to implement and benchmark the proposed algorithms to present quantum hardware.

To illustrate the decomposition procedure we provide two important examples with the first being the decomposition of a single-qubit controlled operation $C^{1,1}(\hat{U})$ and the second one the decomposition of a two-level, two-qubit unitary operation. Based on the fact that any single-qubit operator $\hat{U}$ can be written in the form [25],

$$\hat{U} = e^{ia}\hat{A}\hat{X}\hat{B}\hat{X}\hat{C}, \quad \hat{A}\hat{B}\hat{C} = \hat{I}, \tag{2.39}$$

with a arbitrary phase, then the two-qubit controlled operator implementation in single qubit gates and CNOTs is presented in Fig.2.4. The phase gate $\hat{S}$ in the quantum circuit 2.4 is,

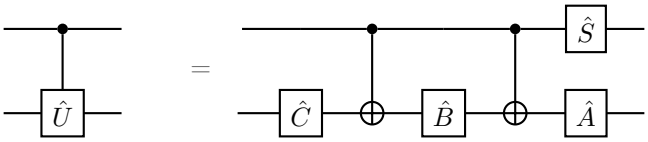

Figure 2.4: Decomposition of arbitrary two qubit controlled gate $C^{1,1}(\hat{U})$ to single-qubit and CNOT gates.

$$\hat{S} = \begin{bmatrix} 1 & 0 \\ 0 & e^{ia} \end{bmatrix}. \tag{2.40}$$

The next example pertains to decomposition of two-level unitary matrices into multi-controlled gates. A two-unitary matrix is a unitary matrix characterized by non-trivial action only in two or fewer components of the state vector. For instance, the following matrix is a two-level unitary $\hat{R}_y(\theta)$ rotation,

$$\hat{\mathscr{R}}_y(\theta) = \begin{bmatrix} 1 & 0 & 0 & 0 \\ 0 & \cos\frac{\theta}{2} & -\sin\frac{\theta}{2} & 0 \\ 0 & \sin\frac{\theta}{2} & \cos\frac{\theta}{2} & 0 \\ 0 & 0 & 0 & 1 \end{bmatrix}. \tag{2.41}$$

Applying the Gray code [25], the decomposition of the two-level matrix (2.41) into simpler controlled gates depicted in Fig.2.5. In addition, using the decomposition procedure of Fig.2.4, the two-level rotation matrix can be expressed solely in single-qubit gates and

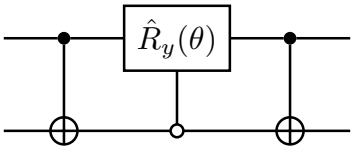

Figure 2.5: Decomposition of the two-level rotation matrix of Eq.(2.41) into simple controlled gates.

CNOTs. In general a two-level unitary matrix acting on n qubits, admits a breakdown to these elementary gates that scales as $O(n^2)$ [25].

The quantum circuit model naturally introduces three important parameters that have to be specified for a complete characterization of the operational specifics of a quantum algorithm. In particular, the term circuit depth conveys the number of qubits (number of quantum wires) that the algorithm requires for operation whereas the circuit depth reflects the number of elementary gates (or more properly, the maximum number of the gates acting on each quantum wire). Finally, an error ε of the proposed decomposition must always be accounted and its scaling in respect to both depth and width of the circuit.

2.3 Selected quantum algorithms

As a testimony of the computational prowess of quantum computers it is instructive to present some influential quantum algorithmic processes that exhibit quantum advantage compared to the classical counterparts and form the building blocks for various other algorithms.

2.3.1 The quantum Fourier transform

The quantum Fourier transform (QFT) is a quantum algorithm widely used as a subroutine in the quantum factoring protocol, phase estimation, quantum simulation as well as other interesting quantum algorithms. It efficiently transforms the quantum mechanical amplitudes of a N–dimensional input state to a different basis,

$$\sum_{j=0}^{N-1} x_j |j\rangle \rightarrow \sum_{k=0}^{N-1} y_k |k\rangle , \quad y_k = \frac{1}{\sqrt{N}} \sum_{j=0}^{N-1} x_j e^{2i\pi jk/N}. \tag{2.42}$$

To encode the transformation (2.42) into a quantum computer, first we assign the number N of the of the complex amplitudes to n qubits by setting $N = 2^n$. Then, the transformation

in Eq.(2.42) can be factorized [25] as

$$
\begin{aligned}
|j\rangle \rightarrow \frac{1}{2^{n/2}} \sum_{k=0}^{2^n-1} e^{2i\pi jk/2^n} &= \frac{1}{2^{n/2}} \bigotimes_{m=1}^{n} (|0\rangle + e^{2i\pi j 2^{-m}}|1\rangle) \\
&= \frac{1}{2^{n/2}} (|0\rangle + e^{2i\pi 0.j_n}|1\rangle)(|0\rangle + e^{2i\pi 0.j_{n-1}j_n}|1\rangle) \cdots (|0\rangle + e^{2i\pi 0.j_1 j_2 \ldots j_n}|1\rangle),
\end{aligned}
\tag{2.43}
$$

where in expression (2.43) the binary fraction form, $0.j_l j_{l+1} \ldots j_m = \frac{j_l}{2} + \frac{j_{l+1}}{4} + \ldots + \frac{j_m}{2^{m-l+1}}$ with $j_l = \{0,1\}$, has been employed. To quantum implement the decomposition of Eq.(2.43) into a circuit, we introduce the unitary phase gate $\hat{R}_k$,

$$
\hat{R}_k = \begin{bmatrix} 1 & 0 \\ 0 & e^{2i\pi/2^k} \end{bmatrix}. \tag{2.44}
$$

The respective quantum circuit implementation of the general n-qubit QFT is presented in [25]. In Fig.2.6, for the sake of clarity and completeness, the QFT for $n = 3$ qubits is presented along with the required SWAP gate.

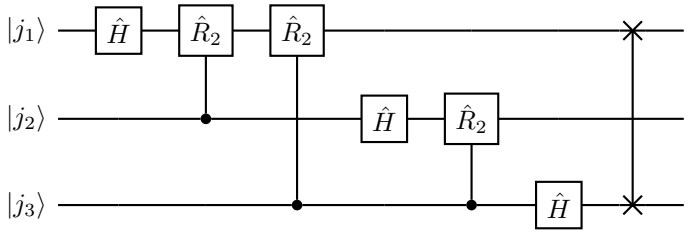

Figure 2.6: The quantum circuit implementation of QFT for $n = 3$ qubits.

For n qubits, the numbers of required elementary gates for implementing QFT scales as $\Theta(n^2)$, where the big Θ notation means that the number of gates is asymptotically bounded between $c_1 n^2$ and $c_2 n^2$ with $c_1, c_2 > 0$. However, the corresponding classical counterpart, the fast Fourier transfrom (FFT) requires $\Theta(n2^n)$ gates to calculate the 2^n amplitudes of the discrete Fourier transform. Therefore, an exponential quantum advantage in computational resources $\sim 2^n/n$ is achieved for the computation of the discrete Fourier transform compared to the classical FFT method.

The QFT algorithm is widely used as a sub-routine in other interesting quantum algorithms for phase estimation[25], factoring and computing the discrete logarithm [31], quantum signal processing (QSP) [32], solution of linear systems of equations [33] (HHL algorithm) and others.

2.3.2 Quantum simulation

Quantum simulation is the process of approximating the unitary quantum dynamics generated by the Hamiltonian operator in the Schrodinger equation (2.16), and has been the ba-

sis for simulation of dynamics for general classes of partial differential equations. Quantum simulation was first proposed by Feynman [34] recognising the intractability issue of classical digital computers to simulate the dynamics of typical quantum systems.

The first quantum simulation algorithm was explicitly presented by Lloyd [35] for simulation of a k-local Hamiltonian

$$\hat{H} = \sum_{i=1}^{l} \hat{H}_i, \tag{2.45}$$

which describes the interaction between n particles, where the Hamiltonian can be decomposed into l with each $\hat{H}_i$ acting only on k-particles. To efficiently compute the unitary evolution generated by Hamiltonian (2.45) we employ a first order Lie-Trotter-Suzuki product formula [36],

$$e^{-i\hat{H}t} = \left(\prod_{i=1}^{l} e^{-it/r\hat{H}_i}\right)^r + \varepsilon, \tag{2.46}$$

where the approximation error ε in Eq.(2.46) is

$$\varepsilon = \frac{t^2}{r}. \tag{2.47}$$

From Eq.(2.46), the problem boils down to find an efficient implementation for the each of the unitary gates $e^{-it/r\hat{H}_i}$ and apply it r times. But since $\hat{H}_i$ are k-local Hamiltonians their implementation is possible within $2^{2k} = O(1)$ elementary gates, as they act only within the k-qubit subspace of the total system, where $n >> k$. Notice that the former implementation cost is constant even with $n \to \infty$ due to the locality condition. Finally, the number of required operation for simulation of unitary dynamics within an prescribed error ε is $rl2^{2k}$. For local Hamiltonian the number of the individual $\hat{H}_i$'s scales as $O[poly(n)]$. Therefore, using the error expression (2.47), the overall complexity of the quantum simulation algorithm is

$$O[poly(n),\, t^2,\, 1/\varepsilon]. \tag{2.48}$$

Lloyd's quantum simulation algorithm is near optimal in time dependence but the error estimation is very crude assuming that the higher order terms are dominated by the lower ones. The latter issue was addressed in the work of Berry et al. [37] who provide an optimised complexity bound dependence on both $\left\|\hat{H}\right\|$ and t,

$$O_{Berry} \leq 2^{2(k+1)} n^2 \left\|\hat{H}\right\| t \exp\left\{2\sqrt{\ln 5 \ln\left(n\left\|\hat{H}\right\| t/\varepsilon\right)}\right\}. \tag{2.49}$$

In Eq.(2.49), $\left\|\hat{A}\right\|$ is the spectral norm of operator $\hat{A}$ i.e. its largest singular value. The complexity of Eq.(2.49) is close to linear for large $n\left\|\hat{H}\right\| t$ and applies to general sparse Hamiltonian operators.

In the following years various quantum simulation algorithms have been emerged for simulation of both quantum and classical systems the study of which is devoted in Chapter 3. Quantum simulation algorithms are important because they reflect the prospect of quantum computing to dominate the computational studies of complex quantum systems.

2.3.3 Quantum search

The third quantum algorithmic process presented here, regards the task of search through a search space of N elements. For example that could be to find the correct configuration (up or down) of n switches that successfully light up a lamp from the $N = 2^n$ different combinations. Classically this task requires $O(N)$ operations, albeit Grover's quantum search algorithm [25, 38] accomplishes the task using $O(\sqrt{N})$ operations.

To illustrate Grover's algorithm we begin be defining the Grover's oracle $\hat{O}$ that labels the solution of the problem– the n-bit correct configuration of switches– with one and the non-solution with zero through a function $f(x)$. Then, the operation of Grover's oracle to a arbitrary n-qubit encoded state $|x\rangle$ is

$$\hat{O}|x\rangle\left(\frac{|0\rangle-|1\rangle}{\sqrt{2}}\right)=(-1)^{f(x)}|x\rangle\left(\frac{|0\rangle-|1\rangle}{\sqrt{2}}\right). \tag{2.50}$$

Next the Grover diffusion operator $\hat{G}$ is defined as,

$$\hat{G}=(2|\psi\rangle\langle\psi|-\hat{I})\hat{O},\quad |\psi\rangle=\hat{H}^{\otimes n}|0\rangle^{\otimes n}=\frac{1}{\sqrt{N}}\sum_{x=0}^{N-1}|x\rangle. \tag{2.51}$$

Then, starting with the initial state $|0\rangle^{\otimes n}|1\rangle$ applying $r\approx\pi\sqrt{N}/4$ times the operator $\hat{G}$ we obtain,

$$\hat{G}^r(\hat{H}^{\otimes n}\otimes\hat{H})|0\rangle^{\otimes n}|1\rangle\approx|x_s\rangle\left(\frac{|0\rangle-|1\rangle}{\sqrt{2}}\right), \tag{2.52}$$

where $|x_s\rangle$ is the solution of the search with $f(x_s)=1$. Evidently, Grover's algorithm finds with probability $O(1)$ the proper x_s solution of the search problem with $O(\sqrt{N})$ calls–queries– of the oracle. The respective quantum circuit representation of Grover iteration (2.52) is presented in Fig.2.7.

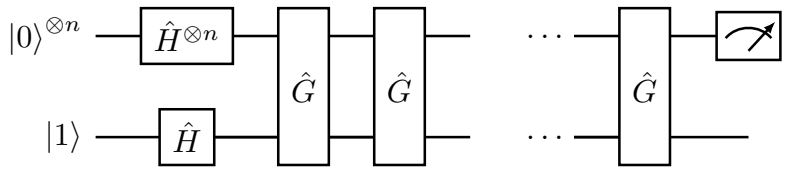

Figure 2.7: Quantum circuit for Grover's search algorithm. The Grover diffusion operator $\hat{G}$ is applied $O(\sqrt{N})$ times. Then, a measurement in the first register provides the x_s solution of the search problem with success probability $O(1)$.

A significant application of Grover's algorithm is in the amplitude estimation algorithm [39] which enables reading the amplitudes of a quantum state, an indispensable process in the information retrieval of classical amplitude encoded states.

2.4 Quantum noise

In the previous sections we have adhered to the unitary postulate for admissible operations in quantum theory. Here, we depart from this restriction by considering the quantum system to be open. Open quantum systems are subject to a rich spectrum of physical phenomena such as dissipation, deconherence and loss of information due to the interaction with a different system which is usually labeled as environment [40]. The existence of correlations-interaction between the open system and the environment breaks the unitary evolution, which translates into noise in the information transmission.

2.4.1 Quantum operations and Kraus representation

In Secs.2.1.3 and 2.1.4, the main operational transformations in quantum mechanics were described, namely the unitary operations and measurements. However, those two examples are only sub-cases of the evolution circumstances of a quantum state. Specifically, we define a general map $\hat{\mathscr{E}} : \mathscr{H}_1 \to \mathscr{H}_2$

$$\rho' = \hat{\mathscr{E}}(\rho), \tag{2.53}$$

that is called quantum operation that describes the change of the state ρ due to an occurring physical process. In general the super operator $\hat{\mathscr{E}}$ is non-unitary. For the quantum operation $\hat{\mathscr{E}}$ to map quantum states to other quantum states it has to be a completely positive and trace preserving (CPTP) even though it is possible to relax the complete positiveness to positive only operations (PTP).

To efficiently represent the map $\hat{\mathscr{E}}$, it is regarded that the subsequent dynamics arise from the interaction of the system of interest with an environment ρ_{env} as depicted in Fig.2.8. Thus, under the proposed scheme of Fig.2.8 the action of quantum operation $\hat{\mathscr{E}}$ reads,

$$\rho' = \hat{\mathscr{E}}(\rho) = Tr_{env}[\hat{U}(\rho \otimes \rho_{env})\hat{U}^{\dagger}]. \tag{2.54}$$

To explicitly calculate the expression (2.54) we assume that the environment state is initially on a specific eigenstate $\rho_{env} = |e_0\rangle\langle e_0|$, where $\{|e_m\rangle\}$ is a finite dimensional orthonormal basis of the environment state space. Thus, Eq.(2.54) obtains the form of an operator-sum representation,

$$\hat{\mathscr{E}}(\rho) = \sum_m \hat{K}_m \rho \hat{K}_m^{\dagger}, \quad \sum_m \hat{K}_m^{\dagger}\hat{K}_m = \hat{I}, \tag{2.55}$$

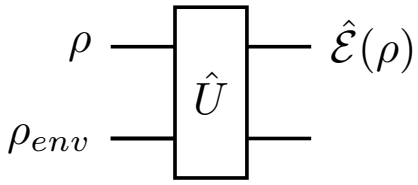

Figure 2.8: Schematic representation of an open quantum system interacting with an environment described by the density matrix ρ_{env}. The quantum operation $\hat{\mathscr{E}}$ describes the resulting non-unitary dynamics from this interaction and the dynamical change $\rho \rightarrow \hat{\mathscr{E}}(\rho)$. The combined system is closed and evolves under a unitary operator $\hat{U}$.

the so-called Kraus representation [25, 40]. The Kraus operators $\hat{K}_m$ cannot be unitary and are provided by

$$\hat{K}_m = \langle e_k|\hat{U}|e_0\rangle\,. \tag{2.56}$$

The Kraus representation Eq.(2.55) suggests that the principal system undergoes a probabilistic non-unitary transformation as result of the interaction with the environment, i.e introducing a Markovian type of noise in the system.

In quantum computing and information, many times instead of the quantum operation, the term quantum channel is used, with the scope that a quantum operation is a transmission channel of information about the change of the quantum state. A prototypical single qubit quantum channel that will be exploited later is the amplitude damping (AD) channel which reflects noise effects related to energy dissipation from the quantum system. The respective Kraus representation is,

$$\hat{\mathscr{E}}_{AD}(\rho) = \hat{K}_0\rho\hat{K}_0^\dagger + \hat{K}_1\rho\hat{K}_1^\dagger, \tag{2.57}$$

with

$$\hat{K}_0 = \begin{bmatrix} 1 & 0 \\ 0 & \sqrt{1-\gamma} \end{bmatrix}, \quad \hat{K}_1 = \begin{bmatrix} 0 & \sqrt{\gamma} \\ 0 & 0 \end{bmatrix}. \tag{2.58}$$

One physical system that the AD channel models, is the the spontaneous emission of a photon under the transition $|1\rangle \rightarrow |0\rangle$, with probability $\gamma = \sin^2\theta$. Hence, the environment plays the role of the photonic recipient in the vacuum state $|0\rangle$. The quantum circuit implementation for the AD process is represented in Fig.2.9.

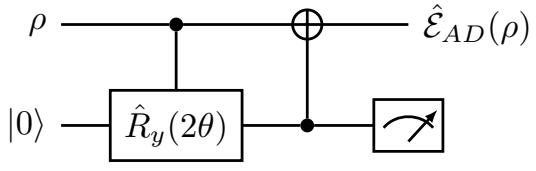

Figure 2.9: Quantum circuit implementation for the amplitude damping channel.

2.4.2 Master equation

In the previous section the Kraus representation has been illustrated. The main advantage of the formulation is the affine representation of the environment, as it is not required to have exact knowledge of the physics pertain to the environment. On the other hand, it lacks the time-evolution differential form that its unitary evolution counterpart, the Eq.(2.25), possesses.

Starting from the Kraus representation Eq.(2.55), expanding for a small time advancement $t \to t + \delta t$ and keeping only terms to first order in δt [40],

$$\hat{K}_0(\delta t) = \hat{I} - i\delta t(\hat{H}_0 - i\hat{H}_{diss}), \quad \hat{H}_{diss} = -\frac{1}{2}\sum_m \gamma_m \hat{L}_m^\dagger \hat{L}_m, \quad \hat{K}_{m>0}(\delta t) = \sqrt{\gamma_m \delta t}\hat{L}_m \tag{2.59}$$

we arrive at the celebrated Gorini-Kossakowski-Sudarshan-Lindblad (GKLS) master equation [41, 42]

$$\frac{\partial \rho}{\partial t} = -i[\hat{H}_0, \rho] + \sum_m \gamma_m \left(\hat{L}_m \rho \hat{L}_m^\dagger - \frac{1}{2}\{\hat{L}_m^\dagger \hat{L}_m, \rho\} \right), \tag{2.60}$$

where the $\hat{L}$ operators are called the Lidbland operators or jump operators and the second sum term is the dissipator. The operation $\{,\}$ in Eq.(2.60) denotes the anti-commutator. The GKLS master equation (2.60) can be compactly written as,

$$\frac{\partial \rho}{\partial t} = -i(\hat{H}_{eff}\rho - i\rho\hat{H}_{eff}^\dagger) + \sum_m \gamma_m \hat{L}_m \rho \hat{L}_m^\dagger, \quad \hat{H}_{eff} = \hat{H}_0 + i\hat{H}_{diss}. \tag{2.61}$$

Consequently, the effective non-Hermitian Hamiltonian $\hat{H}_{eff}$ in Eq.(2.61) generates the dissipative dynamics.

Chapter 3

Quantum Rerpesentation and Simulation

The main theme of this chapter is to establish the theoretical and computational quantum blocks that will be utilized in Chapter 4 for implementing Maxwell's equations in complex electromagnetic media within a quantum setting.

3.1 The role of representation

As briefly outlined in Sec.2.3.2, the task of quantum simulation involves the quantum implementation of the dynamical evolution operator generated by the linear partial differential equation,

$$i\frac{\partial\left|\boldsymbol{\psi}(\boldsymbol{r},t)\right\rangle}{\partial t}=\hat{D}(\boldsymbol{r},t)\left|\boldsymbol{\psi}(\boldsymbol{r},t)\right\rangle, \quad \left|\boldsymbol{\psi}\right\rangle\in\mathscr{H}, \tag{3.1}$$

where $\hat{D}$ is the generator of dynamics and $\mathscr{H}$ denotes the Hilbert space. Although equation (3.1) describes both classical and quantum evolution, in the classical case the operator $\hat{D}$ is not an observable. Thus, we refrain from using the Hamiltonian operator notation $\hat{H}$.

In Sec.2.2 it was established that for a quantum operation to be admissible it must be unitary. This requirement arises directly from the unitary evolution dictated by the Schrodinger equation in Eq.(2.16) with $\hat{D}=\hat{D}^{\dagger}$. However, when $\hat{D}\neq\hat{D}^{\dagger}$, the evolution is in general non-unitary except in cases where certain symmetries are present. This raises two natural questions:

- Are there theoretical approaches to address the challenges posed by non-unitary dynamics?
- On the same hand, how can a classical state be expressed in terms of quantum resources?

In this initial section, we will address fundamental questions surrounding the relation-

ship between classical and quantum frameworks before transitioning to a more computational perspective.

3.1.1 Dyson maps

Since quantum computers operate using unitary gates, it is highly beneficial to identify dynamical systems that exhibit unitary evolution, promoting them as prime candidates for immediate quantum simulation. In this context, we provide the following result:

For the linear dynamics of a system described by the partial differential equation

$$i\frac{\partial|\boldsymbol{\psi}\rangle}{\partial t}=\hat{D}|\boldsymbol{\psi}\rangle, \quad |\boldsymbol{\psi}\rangle\in\mathscr{H}, \quad \hat{D}^{\dagger}\neq\hat{D}, \tag{3.2}$$

if the system possesses a quadratic positive definite globally conserved quantity $\Theta=\langle\boldsymbol{\psi}|\hat{\Theta}|\boldsymbol{\psi}\rangle$ with,

$$\frac{\partial\Theta}{\partial t}=0\Leftrightarrow\hat{\Theta}\hat{D}^{\dagger}-\hat{\Theta}\hat{D}=0, \quad \hat{\Theta}^{\dagger}=\hat{\Theta}, \quad \hat{\Theta}>0, \tag{3.3}$$

then, an endomorphism $\hat{\eta}$ can be constructed, such that

$$\hat{\Theta}=\hat{\eta}^{\dagger}\hat{\eta}, \quad |\boldsymbol{\Psi}\rangle=\hat{\eta}|\boldsymbol{\psi}\rangle, \quad \hat{\eta}:\mathscr{H}\rightarrow\mathscr{H}, \tag{3.4}$$

transforming Eq.(3.2) into the following explicit Hermitian structure Schrodinger representation:

$$i\frac{\partial|\boldsymbol{\Psi}\rangle}{\partial t}=\hat{\eta}\hat{D}\hat{\eta}^{-1}|\boldsymbol{\Psi}\rangle=\hat{D}_{\eta}|\boldsymbol{\Psi}\rangle, \quad |\boldsymbol{\Psi}\rangle\in\mathscr{H}. \tag{3.5}$$

The operator $\hat{\eta}$ is called a Dyson map originally introduced in the study of complex quantum many-body Hamiltonians [43].

From a classical perspective this result should not be surprising as Θ satisfies the requirements for being a Lyapunov function, indicating the stability of the dynamics. However, from a quantum perspective, the discovery that non-Hermitian Hamiltonians can possess a real spectrum and generate unitary dynamics was groundbreaking. This revelation began with the seminal work of Bender and Boettcher [44], opening an entirely new field of non-Hermitian Quantum Mechanics [45–51]. In this framework, the operator $\hat{\Theta}$ is referred as the metric operator and is closely associated with the underlying symmetries of the quantum system. Specifically, rewriting Eq.(3.3),

$$\hat{D}^{\dagger}=\hat{\Theta}\hat{D}\hat{\Theta}^{-1}, \tag{3.6}$$

one obtains the pseudo-Hermicity condition for an invertible metric $\hat{\Theta}$ which implies that the initially non-Hermitian operator $\hat{D}$ in Hilbert space $\mathscr{H}$ is Hermitian in the weighted

Hilbert space $\mathscr{H}_\Theta$ under the inner product,

$$\langle \boldsymbol{\phi} | \boldsymbol{\psi} \rangle_\Theta = \langle \boldsymbol{\phi} | \hat{\Theta} | \boldsymbol{\psi} \rangle, \quad |\boldsymbol{\psi}\rangle, |\boldsymbol{\phi}\rangle \in \mathscr{H}_\Theta. \tag{3.7}$$

As a result, the $\mathscr{PT}$ symmetry can be understood as a specific choice of the metric $\hat{\Theta}$, corresponding to the existence of a conserved quantity. On a final note, while the existence of a Hermitian positive definite metric $\hat{\Theta}$ satisfying the pseudo-Hermicity relation (3.6) ensures the Hermicity of operator $\hat{D}$ in the weighted "physical" Hilbert space $\mathscr{H}_\Theta$, applications in quantum computing require the Dyson representation Eq.(3.5) such that that the operator $\hat{D}_\eta$ is Hermitian in the initial computational space $\mathscr{H}$. The interconnection of the Dyson map with the different spaces is presented in Fig.3.1.

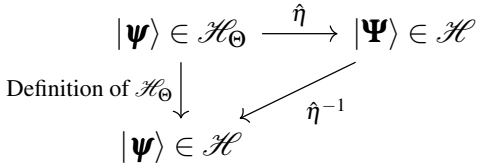

Figure 3.1: The dual role of the Dyson map. It endows the structure of the weighted space $\mathscr{H}_\Theta$ into the initial Hilbert space $\mathscr{H}$ through an isometry and serves as a different but not equivalent representation of elements $|\boldsymbol{\psi}\rangle$ and $|\boldsymbol{\Psi}\rangle$ belonging to $\mathscr{H}$.

The key takeaway from the preceding discussion is that if a physical system with linear dynamics possesses a positive-definite conserved quantity, this quantity can serve as a metric to construct an explicitly unitary evolution suitable for quantum computing applications.

To bridge these concepts—which may initially appear abstract and unrelated to the standard toolbox of a plasma physicist lets consider the Force Operator formalism of the linearized ideal MHD [52],

$$\frac{\partial^2 \boldsymbol{\xi}}{\partial t^2} = \hat{F}\boldsymbol{\xi}, \quad \hat{F} = \hat{F}^\dagger, \tag{3.8}$$

where $\boldsymbol{\xi}$ is the Lagrangian displacement vector from an equilibrium. Assuming $\boldsymbol{\xi}(\boldsymbol{r},t) = \boldsymbol{\xi}_r(\boldsymbol{r})e^{-i\omega t}$ Eq.(3.8) becomes an eigenvalue problem,

$$\hat{F}\boldsymbol{\xi}_r = -\omega^2 \boldsymbol{\xi}_r, \tag{3.9}$$

from which we deduce that when the force operator $\hat{F}$ is positive definite then $\omega^2 < 0$ resulting in MHD instabilities, whereas for the negative definite case, $\omega^2 > 0$ represents stable dynamics (MHD waves). The Hermicity of the force operator in ideal MHD enforces that the energy E_{MHD} is conserved,

$$E_{MHD}(t) = \frac{1}{2}\int_{\mathscr{V}} (\boldsymbol{v}^\dagger \boldsymbol{v} - \boldsymbol{\xi}^\dagger \hat{F}\boldsymbol{\xi}) d\boldsymbol{r} = \text{constant}, \quad \boldsymbol{v} = \frac{\partial \boldsymbol{\xi}}{\partial t}, \quad \mathscr{V} \subset \mathbb{R}^3. \tag{3.10}$$

We now reformulate Eq.(3.8) as a first order differential equation,

$$i\frac{\partial \boldsymbol{\psi}}{\partial t} = \hat{D}\boldsymbol{\psi}, \quad \boldsymbol{\psi} = \begin{bmatrix} \boldsymbol{\xi} \\ \boldsymbol{v} \end{bmatrix}, \quad \hat{D} = i\begin{bmatrix} 0 & 1 \\ \hat{F} & 0 \end{bmatrix}. \tag{3.11}$$

By defining the energy operator $\hat{E}_{MHD}$,

$$\hat{E}_{MHD} = \begin{bmatrix} -\hat{F} & 0 \\ 0 & 1 \end{bmatrix}, \tag{3.12}$$

it is evident from Eq.(3.10) that,

$$E_{MHD}(t) = \int_{\mathscr{V}} \boldsymbol{\psi}^{\dagger}\hat{E}\boldsymbol{\psi} d\,\boldsymbol{r} = constant \tag{3.13}$$

In addition, the energy operator is positive definite if and only if the force operator is negative definite, $\hat{F} < 0$ reflecting the stable wave case. Therefore, the energy operator fulfills the conditions in Eq.(3.3) and can used as a metric $\hat{\Theta} = \hat{E}_{MHD}$. An mediate Dyson map is,

$$\hat{\eta} = \begin{bmatrix} (-\hat{F})^{1/2} & 0 \\ 0 & 1 \end{bmatrix}, \quad \boldsymbol{\Psi} = \hat{\eta}\,\boldsymbol{\psi}, \tag{3.14}$$

under which, Eq.(3.11) becomes a first order MHD wave equation,

$$i\frac{\partial \boldsymbol{\Psi}}{\partial t} = \hat{D}_{\eta}\boldsymbol{\Psi}, \quad \hat{D}_{\eta} = \hat{D}_{\eta}^{\dagger}, \quad \hat{D}_{\eta} = \begin{bmatrix} 0 & i\hat{G} \\ -i\hat{G} & 0 \end{bmatrix}, \quad \text{with} \quad \hat{G} = (-\hat{F})^{1/2}. \tag{3.15}$$

Evidently, these considerations coincide with the MHD stability energy principle [52]. Moreover, through the Dyson map, we explicitly obtained the Hermitian MHD wave evolution equation (3.15), which admits unitary evolution and is therefore suitable for implementation on a quantum computer.

3.1.2 Quantum encoding

To represent a classical d-dimensional continuous state $\boldsymbol{\psi}(\boldsymbol{r},t)$ defined in $\mathscr{V} \subset \mathbb{R}^3$,

$$\boldsymbol{\psi}(\boldsymbol{r},t) = \sum_{i=1}^{d} \psi_i(\boldsymbol{r},t)e_i, \tag{3.16}$$

where e_i denotes the standard orthonormal basis in $\mathbb{R}^d$, as a n-qubit quantum superposition state, a finite spatial discretization is required. To achieve this quantization we perform an amplitude encoding of the classical state (3.16) by defining two registers of qubits as follows:

The first register denoted with $\{|q\rangle\}$, $q = 0,1,..,d-1$ stores the information on the

amplitudes and therefore requires $n_q = \log_2(d)$ qubits. The second register accommodates the information related to the discretization. Suppose we discretize the configuration space $\mathscr{V} = [x_0, x_0 + L_x] \times [y_0, y_0 + L_y] \times [z_0, z_0 + L_z]$ into a lattice consisted of $N = N_x N_y N_z$ nodes, where the separation length along each axis is $\delta_i = L_i/N_i$, for $i = x, y, z$. Then, the spatial register $\{|p\rangle\}$ is formed containing $n_p = \log_2(N) = \log_2(N_x) + \log_2(N_y) + \log_2(N_z) = n_{px} + n_{py} + n_{pz}$ qubits with

$$|p_i\rangle = |i_0 + p_i \delta_i\rangle, \quad p_i = 0, 1, ..., N_i - 1, \quad \text{for} \quad i = x, y, z. \tag{3.17}$$

As a result the classical state in Eq.(3.16) translates into the $n = n_q + n_p$–qubits quantum state,

$$\boldsymbol{\psi}(\boldsymbol{r}, t) \leftrightarrow |\boldsymbol{\psi}(t)\rangle = \sum_{q=0}^{d-1} \sum_{p=0}^{2^{n_p}-1} \psi_{qp}(t) |q\rangle |p\rangle. \tag{3.18}$$

In Eq.(3.18), the binary representation of Eq.(2.36) has been employed in the expression $|p_x\rangle \otimes |p_y\rangle \otimes |p_z\rangle = |p\rangle$ for compactness.

Notice that, as seen Eq.(3.18) the quantum memory of a quantum computer exponentially larger compared to a classical machine. For instance, storing the amplitudes of a $d = 10$ dimensional classical state in a $3D$ lattice with $N = 1000^3$ cites requires only $n \sim 34$ qubits.

3.2 Quantum simulation for unitary dynamics

Having established a proper linear Hermitian Schrodinger representation with unitary dynamics either naturally or induced via a Dyson map) for the problem at hand, a wide range of quantum simulation techniques can be applied. These include Trotterization and product formulas [37, 53, 54], Quantum Signal Processing (QSP) [32, 55, 56], Taylor series [57] and Linear Combinations of Unitaries (LCU) [58, 59] and quantum walks [60]. A comprehensive and comparative review of these simulation methods including their implementation scaling can be found in [61].

Among the aforementioned plethora of available simulation techniques the required ones for implementing Maxwell equations in plasmas and other dielectrics in the following chapter are a multi-dimensional quantum walk (QW) namely the Qubit Lattice Algorithm (QLA) and the LCU method.

3.2.1 Quantum walks (QW) and Qubit lattice algorithm (QLA)

Returning our attention to the quantum simulation of the linear dynamics in terms of the Schrodinger representation (3.1) with $\hat{D} = \hat{D}^\dagger$ and based on the quantum encoding in Eq.(3.18) we now outline the characteristics of the simulation algorithmic framework.

Discrete time QW are the quantum counterparts of classical random walks [62, 63]. Their prioritization as a quantum simulation technique [60] over the aforementioned quantum algorithms is motivated by the fact that that quantum walks on regular lattices can give rise to wave equations for relativistic particles in the continuum limit [64–67]. This property is particularly important for our studies, as we will see in the next chapter, where the quantum implementation of Maxwell equations requires a proper quantum representation in the form of a generalized multi-spinor Dirac-type equation. This extension involves incorporating multiple particles to increase the dimension of the coin-amplitude space $\mathscr{H}_C$, thereby extending quantum walk (QW) algorithms to multi-dimensional and multi-particle quantum secular automata [68, 69], quantum lattice Boltzmann [70] and, eventually, qubit lattice algorithms (QLA) [71].

In the standard notation of quantum walks, the dynamics of a particle are described by a walking exterior space $\mathscr{H}_S$ and an interior 2-dimensional Hilbert space $\mathscr{H}_C$ dubbed as the coin space. The walking process is applied between the vertex of the graph which in our case will be mapped as a lattice though the swift/streaming unitary operator $\hat{S}$ acting on the $|p\rangle \in \mathscr{H}_S$ register in respect of the coin register,

$$\hat{S} = |0\rangle\langle 0| \otimes |p+1\rangle\langle p| + |1\rangle\langle 1| \otimes |p-1\rangle\langle p|\,. \tag{3.19}$$

Selecting different coin operators $\hat{C}$ results to various non-trivial dynamics. Thus, the evolution of the state from time t to $t+\Delta t$ is

$$|\psi(t+\Delta t\rangle = \hat{S}(\hat{C}\otimes I)\,|\psi(t)\rangle\,. \tag{3.20}$$

Extending the evolution in Eq.(3.20) for a multi-particle d-dimensional space $\mathscr{H}_C$ for the evolution of states in Eq.(3.18) we define

1. a set of local unitary collision operators $\hat{C}_p$ acting in the amplitude $\{|q\rangle\}$ register for each lattice cite $|p\rangle$, and

2. a conditional unitary shift operator $\hat{S}$ acting in the $\{|p\rangle\}$ register.

The action of the shift operator in the computational basis reads,

$$\hat{S}^{+}\,|p\rangle = |p+1\rangle\,, \quad \hat{S}^{-}\,|p\rangle = |p-1\rangle\,, \quad \hat{S}^{-} = \hat{S}^{+\dagger}. \tag{3.21}$$

Then, the evolution of the state $|\psi(\boldsymbol{r},t)\rangle$ in time frame Δt

$$|\boldsymbol{\psi}(t+\Delta t)\rangle = \prod_p (C^q\hat{S}^{\pm})(C^p\hat{C}_p)\,|\boldsymbol{\psi}(\boldsymbol{r},t)\rangle = \hat{U}_{QLA}\,|\boldsymbol{\psi}(t)\rangle + O(\varepsilon^4), \quad \Delta t \sim \varepsilon^2, \quad \delta \sim \varepsilon, \tag{3.22}$$

which in the continuous limit $\delta \to 0$ recovers the evolution equation,

$$i\frac{\partial |\boldsymbol{\psi}(\boldsymbol{r},t)\rangle}{\partial t} = \hat{D}|\boldsymbol{\psi}(\boldsymbol{r},t)\rangle + O(\varepsilon^2). \tag{3.23}$$

In Eq.(3.22) the $C^{p,q}$ symbols in front of the collision and streaming operators denotes controlled operation in respect to the $\{|q\rangle\}$ and $\{|p\rangle\}$ registers.

The product evolution scheme in Eq.(3.22) offers three distinct advantages:

1. **Efficient quantum implementation of the streaming operation**

The streaming operator, defined in Eq.(3.21), is implemented explicitly using n_p-qubit operations, requiring an n_p-fold series of CNOT gates. These operations ultimately decompose into $0(n_p^2)$ single-qubit and CNOT gates [26]. Meanwhile, the local nature of

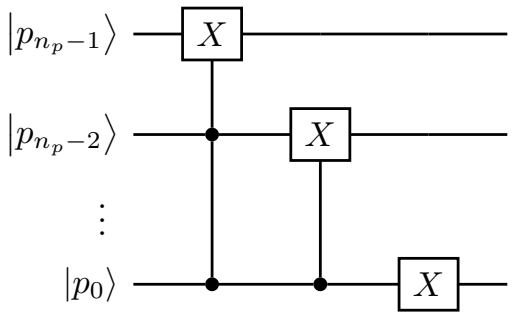

Figure 3.2: Quantum circuit implementation of the streaming $\hat{S}^+$operator within the n_p qubits with p_0 being the least significant bit.

the collision operators $\hat{C}$ permits a constant implementation scaling of $\mathrm{O}(n_q^2) = constant$, with the primary cost determined by the number of distinct, the number of the distinct C_p collision operators. Consequently, the general implementation cost of the product sequence in Eq.(3.22) scales as $O(2^{n_p} n_p^2)$. However, as will be demonstrated in Chapter 4 this scaling can be significantly reduced to an appealing $O[poly(n_p)]$ for quantum simulation of Maxwell equations in media with sufficiently localized inhomogeneities.

2. **Trotterization avoidance**

The QLA techniques circumvents the need for Trotterization [36] of the exponential evolution operator $\exp\{-it\hat{D}\}$ because relative phases generated by the collision operators accumulate to reproduce the desired dynamics.. The total error for a simulation time of $t_{total} = N_t \Delta t$ reads,

$$\varepsilon_{total} = \frac{t_{total}^2}{N_t}. \tag{3.24}$$

Notice how the error in Eq.(3.24) coincide with that of Lloyd's algorithm, Eq.(2.48), for the quantum simulation of local Hamiltonian dynamics.

3. **Explicit implementation scaling**

Finally, evolution sequence (3.22) is explicit, involving no oracle operations or undefined unitary gates with hidden implementation costs. This transparency makes the proposed QW-QLA algorithmic framework a strong candidate for practical testing on quantum hardware, as it reflects true scaling for potential quantum advantage compared to classical algorithms.

3.2.2 Application to Dirac equation

To provide a concrete example of the QLA prior to its implementation for Maxwell equations in plasmas, we apply it to the Dirac equation.

The Dirac equation [17, 20, 21] is one of the most celebrated equation in physics describing the quantum motion of a relativistic spin-$1/2$ particle,

$$\frac{\partial\,|\boldsymbol{\psi}\rangle}{\partial t}+c\hat{Z}\otimes\hat{X}\frac{\partial\,|\boldsymbol{\psi}\rangle}{\partial x}+c\hat{Z}\otimes\hat{Y}\frac{\partial\,|\boldsymbol{\psi}\rangle}{\partial y}+c\hat{Y}\otimes|1\rangle\frac{\partial\,|\boldsymbol{\psi}\rangle}{\partial z}+i\hat{X}\otimes\hat{I}\frac{mc^2}{h}\,|\boldsymbol{\psi}\rangle\,, \tag{3.25}$$

where $\hat{X},\hat{Y},\hat{Z}$ are the Pauli operators defined in Eq.(2.32) and the state $|\boldsymbol{\psi}\rangle$ is a four-spinor,

$$|\boldsymbol{\psi}\rangle=\begin{bmatrix}\psi_0\\ \psi_1\\ \psi_2\\ \psi_3\end{bmatrix},\quad n_q=2\text{ qubits}. \tag{3.26}$$

Following [72], setting $\varepsilon^2=mc^2\Delta t/h$ the evolution for the Dirac equation reads,

$$|\boldsymbol{\psi}(t+\Delta t\rangle=\hat{U}_X\hat{U}_Y\hat{U}_Z\hat{C}_x^{(1)}\,|\boldsymbol{\psi}(t)\rangle\,, \tag{3.27}$$

where the unitary operators $\hat{U}_i$ are QLA sequences of the form (3.22),

$$\hat{U}_X=\hat{S}^{-x}_{1,3}\hat{C}_y\hat{S}^{+x}_{1,3}\hat{C}_y^{\dagger}\hat{S}^{+x}_{0,1}\hat{C}_y\hat{S}^{-x}_{0,1}\hat{C}_y^{\dagger}, \tag{3.28}$$

$$\hat{U}_Y=\hat{S}^{-y}_{1,3}\hat{C}_x^{(2)\dagger}\hat{S}^{+y}_{1,3}\hat{C}_x^{(2)}\hat{S}^{+y}_{0,2}\hat{C}_x^{(2)\dagger}\hat{S}^{-y}_{0,2}\hat{C}_x^{(2)}, \tag{3.29}$$

$$\hat{U}_Z=\hat{S}^{+z}_{1,2}\hat{C}_x^{(1)}\hat{S}^{-z}_{1,2}\hat{C}_x^{(1)\dagger}\hat{S}^{+z}_{0,3}\hat{C}_x^{(1)}\hat{S}^{-z}_{0,3}\hat{C}_x^{(1)\dagger}. \tag{3.30}$$

In the QLA sequences Eqs.(3.28)-(3.30) the notation $\hat{S}_{i,j}$ implies conditional action of the swift operator $\hat{S}$ based on the i,j spinor amplitudes in Eq.(3.26). In addition, the participating coin/collision operators $\hat{C}$ are 2-qubit two-level rotation matrices of angle

$\theta \sim \delta \sim \varepsilon$ in the amplitude register,

$$\hat{C}_x^{(1)} = \hat{Z}\hat{R}_x(\theta)\hat{Z} \otimes \hat{I}, = \begin{bmatrix} \cos\theta/2 & 0 & i\sin\theta/2 & 0 \\ 0 & \cos\theta/2 & 0 & i\sin\theta/2 \\ i\sin\theta/2 & 0 & \cos\theta/2 & 0 \\ 0 & i\sin\theta/2 & 0 & \cos\theta/2 \end{bmatrix}, \tag{3.31}$$

$$\hat{C}_x^{(2)} = \hat{I} \otimes \hat{Z}\hat{R}_x(\theta)\hat{Z} = \begin{bmatrix} \cos\theta/2 & i\sin\theta/2 & 0 & 0 \\ i\sin\theta/2 & \cos\theta/2 & 0 & 0 \\ 0 & 0 & \cos\theta/2 & i\sin\theta/2 \\ 0 & 0 & i\sin\theta/2 & \cos\theta/2 \end{bmatrix}, \tag{3.32}$$

$$\hat{C}_y = \hat{I} \otimes \hat{X}\hat{R}_y(\theta)\hat{X} = \begin{bmatrix} \cos\theta/2 & -\sin\theta/2 & 0 & 0 \\ \sin\theta/2 & \cos\theta/2 & 0 & 0 \\ 0 & 0 & \cos\theta/2 & -\sin\theta/2 \\ 0 & 0 & \sin\theta/2 & \cos\theta/2 \end{bmatrix}. \tag{3.33}$$

In expressions (3.31)-(3.33) the rotation gates $\hat{R}_x$ and $\hat{R}_y$ have been defined in Eq.(2.34).

Since the algorithmic sequence (3.27) θ depends only on a finite number of collision operators which do not depend on the lattice cite that they act on, the total implementation of the QLA requires $O(n_p^2)$ elementary gates for the streaming operators and 3 gates for the decomposition of each collision operators as depicted in Fig.3.3 Therefore, implementing the evolution sequence (3.27) within error ε for time δt requires $O(n_p^2)$ simple gates which is equivalent to simulating the exponential evolution operator with the Quantum Fourier Transform (QFT).

3.3 Breaking unitarity

As demonstrated in Sec.3.1.1, every linear and positive-definite conservative system possesses a Hermitian Schrodinger representation that admits unitary evolution, making it suitable for quantum simulation. However, many systems of interest, particularly dissipative ones, break the underlying symmetries, resulting in non-unitary evolution. Addressing this issue requires moving beyond the QLA product sequence of unitary operators to incorporate non-unitary operators within the unitary framework. Naturally, this cannot be achieved deterministically; instead, we must the praice of a probabilistic implementation to remain consistent with closed-system quantum theory.

Below, the Linear Combination of Unitaries (LCU) method is delineated, along with other dilation techniques for transforming a non-unitary operator into a unitary one within an enlarged Hilbert space.

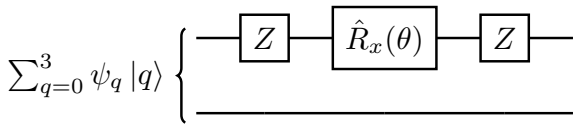

(a) Quantum circuit implementation of $\hat{C}_x^{(1)}$ operator in Eq.(3.31).

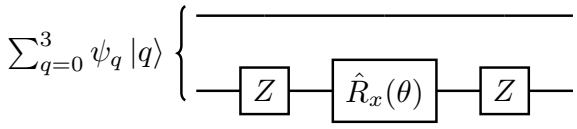

(b) Quantum circuit implementation of $\hat{C}_x^{(2)}$ operator in Eq.(3.32).

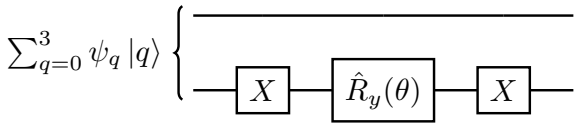

(c) Quantum circuit implementation of $\hat{C}_y$ operator in Eq.(3.33).

Figure 3.3: The quantum circuit implementation of the collision operators $\hat{C}$ in Eqs.(3.31)-(3.33).

3.3.1 The LCU method

Treating non-unitary quantum gates rely on duality quantum computing proposed initially in [73] and then further developed into the LCU method [58, 59, 74] for quantum simulation of unitary and non-unitary dynamics. In contrast with the algorithmic procedure of simulating the evolution through a sequence of unitary operators, the LCU method considers the implementation of weighted sums of unitary operators,

$$\hat{V} = \sum_i^N a_i \hat{U}_i, \quad \hat{U}_i \hat{U}_i^\dagger = \hat{I}, \quad a_i > 0. \tag{3.34}$$

To implement the sum (3.34) we define two unitary operators $\hat{U}_{prep}$ and $\hat{U}_{select}$ and an ancillary register composed of $m = \log_2 N$ qubits,

$$\hat{U}_{prep} \left|0^{\otimes m}\right\rangle = \frac{1}{\sqrt{a}} \sum_i \sqrt{a_i} |i\rangle, \quad a = \sum_i^N a_i, \tag{3.35}$$

$$\hat{U}_{select} = \sum_i |i\rangle \langle i| \otimes \hat{U}_i. \tag{3.36}$$

Then, the sequence of operators acting on the composite state produces,

$$\hat{U}_{prep}^{\dagger}\hat{U}_{select}\hat{U}_{prep}\left|0^{\otimes m}\right\rangle|\boldsymbol{\psi}\rangle=\frac{1}{a}\left|0^{\otimes m}\right\rangle\hat{V}|\boldsymbol{\psi}\rangle+|\perp\rangle\,, \tag{3.37}$$

where the $|\perp\rangle$ state is orthogonal to the $|0^{\otimes m}\rangle\hat{V}|\boldsymbol{\psi}\rangle$ state. Notice that the RHS of Eq.(3.37) is a superposition of the desired part and an othrogonal complement. Hence, a measurement in the ancillary register in respcet to the $|0\rangle=|0^{\otimes m}\rangle$ state implements the non-unitary operator $\hat{V}$ of Eq.(3.34) up to a normalization factor with probability,

$$p_{sucess}=\frac{\left\|\hat{V}|\psi\rangle\right\|^2}{a^2}. \tag{3.38}$$

The LCU implementation procedure of Eq.(3.37) is depicted in Fig.3.4.

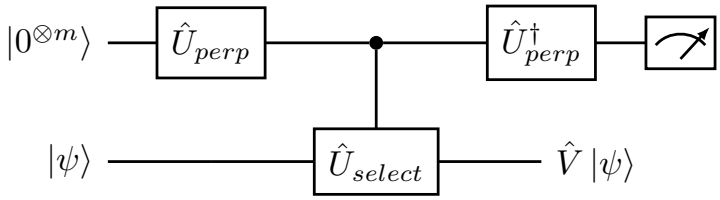

Figure 3.4: Schematic quantum circuit implementation of the LCU method Eq.(3.37) along with the measurement operation. The ancillary register has been traced out in the final outcome.

According to Eq.(3.38), the implementation success of the LCU method depends on the number of summands that the non-unitary operator $\hat{V}$ is decomposed of, $p_{sucess}\sim 1/N^2$. However, it can be proven that every non-unitary contraction operator $\left\|\hat{V}\right\|<1$, is the sum of three unitary operators, irrespectively of operator's dimension [75]. Hence, the LCU method can be implemented with only 2 extra ancillary qubits and with a reasonably feasible manner.

3.3.2 Dilation methods

An alternative approach to address non-unitary operators in quantum computing involves the use of dilation techniques. A unitary dilation of a non-unitary operator $\hat{V}$ in the Hilbert space $\mathscr{H}$ is defined as a unitary operator $\hat{V}_D$ in an enlarged Hilbert space $\mathscr{K}$ whose projection $\hat{P}_{\mathscr{H}}$ on the Hilbert space $\mathscr{H}\subset\mathscr{K}$ is the operator $\hat{V}$ [76],

$$\hat{P}_{\mathscr{H}}\hat{V}_D|_{\mathscr{H}}=\hat{V},\quad \hat{V}^{\dagger}\hat{V}=\hat{I}\text{ in }\mathscr{K}\,. \tag{3.39}$$

Dilation methods find extensive use in quantum computing for implementing non-Hermitian and open quantum systems dynamics [77–81].

3.3.2.1 Stinespring dilation

Returning to the Kraus representation in Eq.(2.55) for an open quantum system dynamics,

$$\hat{\mathscr{E}}(\rho) = \sum_{m=0}^{d^2-1} \hat{K}_m \rho \hat{K}_m^\dagger, \quad \sum_m \hat{K}_m^\dagger \hat{K}_m = \hat{I}, \tag{3.40}$$

it is possible to construct a unitary operator of the form,

$$\hat{U}_{S+E} = \begin{bmatrix} \hat{K}_0 & * & \dots \\ \hat{K}_1 & * & \dots \\ . & * & \dots \\ . & * & \dots \\ . & * & \dots \\ \hat{K}_{d^2-1} & * & \dots \end{bmatrix} \tag{3.41}$$

where the elements $*$ must be specified appropriately to ensure unitarity, and $d = 2^n$ represents the dimensionality of the operators involved

Therefore, the dimension of the unitary operator $\hat{U}_{S+E}$ is $d^2 2^n = 2^{3n}$ meaning that the dilated unitary evolution,

$$\rho'_{S+E} = \hat{U}_{S+E} \rho_{S+E} \hat{U}_{S+E}^\dagger \tag{3.42}$$

requires an ancillary environment (E) consisting of $2n$ qubits. Tracing out the environment component we retrieve the evolution Eq.(3.40) for the density matrix of the open system of interest $\rho_S = \rho$.

Although the size of the environment scales linearly with the number of qubits of the open system, Stinespring dilation provides a direct method for unitary implementation of open system dynamics in through the Kraus form. An application for the method for open lattice theories can be found in [82].

3.3.2.2 Sz.-Nagy dilation

In contrast to the Stinespring dilation, the Sz.-Nagy unitary dilation requires only a single extra ancillary qubit as an environment. From the trace-preserving property in Eq.(3.40) it follows that the Kraus operators are contractions, $\left\|\hat{K}_m\right\| \leq 1$. Consequently, the following operator is unitary,

$$\hat{U}_{\hat{K}_m} = \begin{bmatrix} \hat{K}_m & \hat{D}_{\hat{K}_m^\dagger} \\ \hat{D}_{\hat{K}_m} & \hat{K}_m^\dagger \end{bmatrix}, \quad \hat{D}_{\hat{K}_m} = \sqrt{I - \hat{K}_m^\dagger \hat{K}_m}. \tag{3.43}$$

In Eq.(3.43) the operator $\hat{D}_{\hat{K}_m}$ is the defect operator.

Therefore, instead of relying on the cost-ineffective implementation described in Eq.(3.41),

more advanced unitary algorithms can be constructed using only one ancillary qubit [83].

Chapter 4

A Quantum Computing Approach to Electromagnetic Wave Propagation in Complex Media and Cold Magnetized Plasmas

Classical Maxwell equations have recently emerged as a compelling set of differential equations for applying quantum algorithms [84–90], primarily due to their (**i**) inherent linearity within the linear response framework and (**ii**) broad applicability to various physical problems.

Albeit the significant contributions of the previous studies, most have focused on simplified models of wave propagation and scattering in either homogeneous or inhomogeneous scalar media. Such simplifications limit their practical relevance to realistic applications where the electromagnetic media response is anisotropic, inhomogeneous and potentially complex. In this direction, the goal of this chapter is to extend beyond these simplified models and incorporate the complex response of electromagnetic media within Maxwell equations.

Therefore, this chapter serves as the centerpiece of the research presented in this thesis, leveraging the theoretical and computational tools outlined in Chapter 3 to explore the prospect for quantum computing to revolutionize the computational studies on electromagnetic wave propagation in complex media and plasmas [91–97].

4.1 Classical Maxwell equations in complex electromagnetic media

The source free Maxwell equations [98, 99] for a medium, consist of two evolution equations namely the Faraday and Ampere equations,

$$\frac{\partial \boldsymbol{B}(\boldsymbol{r},t)}{\partial t} = -\boldsymbol{\nabla} \times \boldsymbol{E}(\boldsymbol{r},t), \quad \frac{\partial \boldsymbol{D}(\boldsymbol{r},t)}{\partial t} = \boldsymbol{\nabla} \times \boldsymbol{H}(\boldsymbol{r},t), \tag{4.1}$$

along with the divergence Gauss's laws,

$$\boldsymbol{\nabla} \cdot \boldsymbol{D}(\boldsymbol{r},t) = 0, \quad \boldsymbol{\nabla} \cdot \boldsymbol{B}(\boldsymbol{r},t) = 0. \tag{4.2}$$

Employing the six-vector formulation [100] for the electromagnetic fields $\boldsymbol{u} = (\boldsymbol{E},\boldsymbol{H})^T$ and their respective intensities $\boldsymbol{d} = (\boldsymbol{D},\boldsymbol{B})^T$, Maxwell equations (4.1), (4.2) are compactly written as

$$i\frac{\partial \boldsymbol{d}}{\partial t} = \hat{M}\boldsymbol{u}, \quad \boldsymbol{\nabla} \cdot \boldsymbol{d} = 0. \tag{4.3}$$

The Maxwell operator $\hat{M}$ in the Faraday-Ampere equation (4.3),

$$\hat{M} = i \begin{bmatrix} 0 & \boldsymbol{\nabla}\times \\ -\boldsymbol{\nabla}\times & 0 \end{bmatrix}, \tag{4.4}$$

is Hermitian in the Hilbert space $L^2(\mathscr{V} \subset \mathbb{R}^3, \mathbb{C})$ under the imposed Perfect Electric Conductor (PEC) Dirichlet boundary condition,

$$\boldsymbol{n}(\boldsymbol{r}) \times \boldsymbol{E} = 0 \quad \text{on the boundary} \quad \partial\mathscr{V}, \tag{4.5}$$

where $\boldsymbol{n}$ is the outward pointing normal at the boundary.

Maxwell equations in the form presented in Eq.(4.3) are under-determined. To self-consistently describe the evolution of the fields $\boldsymbol{u}$ it is necessary to consider the characteristics of the electromagnetic medium, which translate into the connection between the response vectors $\boldsymbol{d}$ and the applied electromagnetic field $\boldsymbol{u}$, known as the constitutive relations [101],

$$\boldsymbol{d}(\boldsymbol{r},t) = \hat{\mathscr{L}}\boldsymbol{u} = \hat{W}(\boldsymbol{r})\boldsymbol{u}(\boldsymbol{r},t) + \int_0^t \hat{G}(\boldsymbol{r},t-\tau)\boldsymbol{u}(\boldsymbol{r},\tau)d\tau. \tag{4.6}$$

The matrix $\hat{W}$ in Eq.(4.6) represents the instantaneous–optical–response of the medium, and it is a positive-definite, Hermitian and boundedly invertible operator. On the other hand, the susceptibility kernel $\hat{G}$ accounts for time-dispersion effects such as memory and dissipation. For simplicity we will assume only anisotropic media so the matrices $\hat{W}$

and $\hat{G}$ take the block-diagonal form,

$$\hat{W}(\boldsymbol{r}) = \begin{bmatrix} \hat{\varepsilon}(\boldsymbol{r}) & 0 \\ 0 & \hat{\mu}(\boldsymbol{r}) \end{bmatrix}, \quad \hat{G}(\boldsymbol{r},t) = \begin{bmatrix} \hat{K}^e(\boldsymbol{r},t) & 0 \\ 0 & \hat{K}^m(\boldsymbol{r},t) \end{bmatrix}, \tag{4.7}$$

where $\varepsilon(\boldsymbol{r})$ and $\mu(\boldsymbol{r})$ are the electric permittivity and magnetic permeability of the medium respectively and $\hat{K}^e(\boldsymbol{r},t)$ and $\hat{K}^m(\boldsymbol{r},t)$ are the electric and magnetic susceptibility kernels. The constitutive linear operator $\hat{\mathscr{L}}$ in Eq.(4.6) obeys the following physical postulates [101]:

1. *Determinism*, $\hat{\mathscr{L}}$ is a single valued operator and relates the cause fields $\boldsymbol{u}$ with the response fields $\boldsymbol{d}$.

2. *Linearity*, $\hat{\mathscr{L}}$ is a linear operator .

3. *Causality*, if $\boldsymbol{u} = 0$ for $t \leq \tau$, then $\hat{\mathscr{L}}\boldsymbol{u} = 0$ for $t \leq \tau$.

4. *Locality in space*, $\hat{\mathscr{L}}$ is a local operator with respect to the spatial variable $\boldsymbol{r} \in \mathscr{V} \subset \mathbb{R}^3$.

5. *Time translation invariance*, $\hat{\mathscr{L}}\boldsymbol{u}(\boldsymbol{r},t-\tau) = (\hat{\mathscr{L}}\boldsymbol{u})(\boldsymbol{r},t-\tau)$.

For more general constitutive relations relaxing the validity of the previous physical postulates along with their mathematical treatment, we direct the reader to [102].

Combining Eqs.(4.3) and (4.6) we obtain,

$$i\frac{\partial \boldsymbol{u}}{\partial t} = \hat{W}^{-1}\hat{M}\boldsymbol{u} - i\hat{G}_A * \boldsymbol{u}, \tag{4.8}$$

where the $\hat{X}*$ operation denotes the convolution operation with kernel $\hat{X}$,

$$\hat{G}_A = W^{-1}\frac{\partial \hat{G}}{\partial t}, \quad \hat{G}_A * \boldsymbol{u} = W^{-1}(\boldsymbol{r})\int_0^t \frac{\partial \hat{G}(\boldsymbol{r},t-\tau)}{\partial t}\boldsymbol{u}(\boldsymbol{r},\tau)d\,\tau \tag{4.9}$$

In derivation of Eq.(4.8) it is assumed that $\hat{G}(\boldsymbol{r},0) = 0$, else this extra term can be directly absorbed in the optical part. Finally, the divergence equations $\boldsymbol{\nabla}\cdot\boldsymbol{d} = 0$ are, in effect, initial conditions for the compact Maxwell equation (4.8), dictating that if the initial fields $\boldsymbol{u}(\boldsymbol{r},0) = \boldsymbol{u}_0$ satisfy the divergence equations $\boldsymbol{\nabla}\cdot(\hat{\mathscr{L}}\boldsymbol{u})(\boldsymbol{r},0) = 0$, then the derived fields $\boldsymbol{u}(\boldsymbol{r},t)$ will continue to satisfy these conditions for all $t > 0$.

Summarizing, we have accomplished to express the source free Maxwell equations Eqs.(4.1) and (4.2) as a initial value problem for the evolution of the electromagnetic fields $\boldsymbol{u} = (\boldsymbol{E},\boldsymbol{H})^T$ in a complex electromagnetic medium contained in a closed domain

$\mathscr{V} \subset \mathbb{R}^3$ with the following mathematical structure,

$$
\begin{aligned}
& i\frac{\partial \boldsymbol{u}}{\partial t} = \hat{D}\boldsymbol{u}, \quad \hat{D} = \hat{W}^{-1}\hat{M} - i\hat{G}_A*, \quad \boldsymbol{u} \in \mathscr{H} = L^2(\mathscr{V} \subset \mathbb{R}^3, \mathbb{C}). \\
& \boldsymbol{u}(\boldsymbol{r},0) = \boldsymbol{u}_0 \quad \text{such that} \quad \boldsymbol{\nabla} \cdot (\hat{\mathscr{L}}\boldsymbol{u})(\boldsymbol{r},0) = 0. \\
& \boldsymbol{n}(\boldsymbol{r}) \times \boldsymbol{E} = 0 \quad \text{on} \quad \partial\mathscr{V}.
\end{aligned}
\tag{4.10}
$$

The generator of dynamics $\hat{D}$ in Eq.(4.10) is linear with the $\hat{W}, \hat{M}$ operators being Hermitian in the Hilbert space $\mathscr{H}$. It is evident that Eq.(4.10) represents a Schrodinger-like formulation of the Maxwell equations, where the Hermicity of the operator $\hat{D}$ depends solely on the properties of the electromagnetic medium. Harnessing the theoretical and computational quantum tools presented in Chapter 3, our goal is to implement the electromagnetic Schrodinger equation in a quantum computer. In the next section, we proceed to do that starting with optical media, extending to the dispersion case, and finally incorporating dissipation.

4.2 Non-dispersive media

In many applications, dispersion can be safely neglected if the electromagnetic waves posses a very narrow frequency spectrum around a central value $\omega \approx \omega_0$ provided that,

$$
\frac{\mathrm{d}\hat{\tilde{G}}(\omega)}{\mathrm{d}\omega}\bigg|_{\omega_0} \approx 0. \tag{4.11}
$$

In Eq.(4.11) the operator $\hat{\tilde{G}}(\omega)$ is the Fourier-transformed variant of the operator $\hat{G}*$. The frequency window $\omega_0 \pm \delta\omega$ is referred as the transparency window. In such cases, the action of the operator $\hat{G}_A*$ in Eq.(4.8) can be neglected, and therefore the Maxwell equations take the simplified form,

$$
i\frac{\partial \boldsymbol{u}}{\partial t} = \hat{W}^{-1}\hat{M}\boldsymbol{u}. \tag{4.12}
$$

Before proceeding with any quantum implementation effort of the evolution of Maxwell equations in Eq.(4.12) an important observation regarding the generator of dynamics $\hat{D} = \hat{W}^{-1}\hat{M}$ has to be made. Even though $\hat{W}^{-1}$ is Hermitian, the product $\hat{D} = \hat{W}^{-1}\hat{M}$ is not generally Hermitian even for the trivial case of vacuum, ($\varepsilon = \varepsilon_0$, $\mu = \mu_0$) since $[\hat{W}^{-1}\ \hat{M}] \neq 0$. Therefore a suitable representation must be devised before constructing the quantum algorithm.

4.2.1 Homogeneous scalar media

In homogeneous media, the unitary evolution of Maxwell equations (4.12) can be retrieved using the Rieman-Silberstein-Weber (RSW) vector [103],

$$\boldsymbol{F}_{RSW} = \frac{1}{\sqrt{2}}\Big(\sqrt{\varepsilon}\boldsymbol{E} + i\frac{\boldsymbol{B}}{\sqrt{\mu}}\Big), \tag{4.13}$$

under which the Maxwell equations transforms into [104],

$$i\frac{\partial\,|\boldsymbol{\psi}\rangle}{\partial t} - v\hat{\boldsymbol{\gamma}}\cdot\hat{\boldsymbol{p}}\,|\boldsymbol{\psi}\rangle = 0, \quad |\boldsymbol{\psi}\rangle = \begin{bmatrix} -F_x + iF_y \\ F_z \\ F_z \\ F_x + iF_y \end{bmatrix} \in \mathbb{C}^4. \tag{4.14}$$

The quantum momentum operator $\hat{\boldsymbol{p}}$ has its usual representation $\hat{\boldsymbol{p}} = -i\nabla$ and $v = 1/\sqrt{\varepsilon\mu}$ is the speed of light within the medium. In addition, the matrix vector $\hat{\boldsymbol{\gamma}} = (\hat{\gamma}_x, \hat{\gamma}_y, \hat{\gamma}_z)$ contains the Dirac matrices

$$\hat{\gamma}_x = \begin{bmatrix} 0 & 0 & 1 & 0 \\ 0 & 0 & 0 & 1 \\ 1 & 0 & 0 & 0 \\ 0 & 1 & 0 & 0 \end{bmatrix}, \quad \hat{\gamma}_y = \begin{bmatrix} 0 & 0 & -i & 0 \\ 0 & 0 & 0 & -i \\ i & 0 & 0 & 0 \\ 0 & i & 0 & 0 \end{bmatrix}, \quad \hat{\gamma}_z = \begin{bmatrix} 1 & 0 & 0 & 0 \\ 0 & 1 & 0 & 0 \\ 0 & 0 & -1 & 0 \\ 0 & 0 & 0 & -1 \end{bmatrix}. \tag{4.15}$$

The apparent similarity of Eq.(4.14) with the quantum-mechanical Dirac equation in Eq.(3.25), (3.26) has led many authors to associate the RSW vector with the photon wave function [103, 105–107]. The four-dimensional status of the state $|\boldsymbol{\psi}\rangle$ in Eq.(4.14) arises from the inclusion of the Gauss laws $\boldsymbol{\nabla}\cdot\boldsymbol{u} = 0$ into the construction of optical-Dirac equation (4.14). This results in two linearly dependent entries F_z, as expected since the divergence laws define the initial conditions (see the relevant discussion at the end of Sec.4.1). From a computational standpoint, this unification of the evolution and Gauss's laws is advantageous because it ensures the divergence conditions are satisfied at each step. Theoretically, the roots of the optical-Dirac equation in Eq.(4.14) lie in the Clifford Geometric Algebra formulation of electromagnetism. For further details, the interested reader is referred to Sec.4.3.3 and [108, 109].

Similarly with Sec.3.2.2, the unitary evolution $\hat{U}$ of the optical Dirac equation (4.14) in the $x-y$ plane

$$\hat{U}(t) = \exp\{-itv\hat{\boldsymbol{\gamma}}\cdot\hat{\boldsymbol{p}}\}, \tag{4.16}$$

admits a QLA representation [91],

$$|\boldsymbol{\psi}(t+\Delta t)\rangle = \hat{V}_Y\hat{V}_X\,|\boldsymbol{\psi}(t+\Delta t)\rangle\,, \tag{4.17}$$

where the unitary operators $\hat{V}_X$, $\hat{V}_Y$ are given in terms of an interleaved sequence of coin-shift operators in an analogous way to Eq.(3.28), (3.29),

$$\hat{V}_X = \hat{S}^{01}_{+X}\hat{C}^{\dagger}_X\hat{S}^{01}_{-X}\hat{C}_X\hat{S}^{23}_{-X}\hat{C}^{\dagger}_X\hat{S}^{23}_{+X}\hat{C}_X\hat{S}^{01}_{-X}\hat{C}_X\hat{S}^{01}_{+X}\hat{C}^{\dagger}_X\hat{S}^{23}_{+X}\hat{C}_X\hat{S}^{23}_{-X}\hat{C}^{\dagger}_X, \tag{4.18}$$

$$\hat{V}_Y = \hat{S}^{23}_{+Y}\hat{C}^{\dagger}_Y\hat{S}^{23}_{-Y}\hat{C}_Y\hat{S}^{01}_{-Y}\hat{C}^{\dagger}_Y\hat{S}^{01}_{+Y}\hat{C}_Y\hat{S}^{23}_{-Y}\hat{C}_Y\hat{S}^{23}_{+Y}\hat{C}^{\dagger}_Y\hat{S}^{01}_{+Y}\hat{C}_Y\hat{S}^{01}_{-Y}\hat{C}^{\dagger}_Y. \tag{4.19}$$

Now there is only one collision/coin operator for each direction provided by the matrices,

$$\hat{C}_X = \begin{bmatrix} \cos\theta & 0 & \sin\theta & 0 \\ 0 & \cos\theta & 0 & \sin\theta \\ -\sin\theta & 0 & \cos\theta & 0 \\ 0 & -\sin\theta & 0 & \cos\theta \end{bmatrix}, \quad \hat{C}_Y = \begin{bmatrix} \cos\theta & 0 & i\sin\theta & 0 \\ 0 & \cos\theta & 0 & i\sin\theta \\ i\sin\theta & 0 & \cos\theta & 0 \\ 0 & i\sin\theta & 0 & \cos\theta \end{bmatrix}, \tag{4.20}$$

with rotation angle $\theta \sim \varepsilon/4$. On the other hand, the conditional action of the shift operator $\hat{S}^{q_i q_j}_{+X,Y}$ in respect to the q_i, q_j amplitudes has been provided in Eq.(3.21) along with the implementation quantum circuit of Fig.3.2. Decomposing the collision operators Eq.(4.20) into two-level rotations,

$$\hat{C}_X = \begin{bmatrix} \cos\theta & 0 & \sin\theta & 0 \\ 0 & 1 & 0 & 0 \\ -\sin\theta & 0 & \cos\theta & 0 \\ 0 & 0 & 0 & 1 \end{bmatrix} \begin{bmatrix} 1 & 0 & 0 & 0 \\ 0 & \cos\theta & 0 & \sin\theta \\ 0 & 0 & 1 & 0 \\ 0 & -\sin\theta & 0 & \cos\theta \end{bmatrix}, \tag{4.21}$$

$$\hat{C}_Y = \begin{bmatrix} \cos\theta & 0 & i\sin\theta & 0 \\ 0 & 1 & 0 & 0 \\ i\sin\theta & 0 & \cos\theta & 0 \\ 0 & 0 & 0 & 1 \end{bmatrix} \begin{bmatrix} 1 & 0 & 0 & 0 \\ 0 & \cos\theta & 0 & i\sin\theta \\ 0 & 0 & 1 & 0 \\ 0 & i\sin\theta & 0 & \cos\theta \end{bmatrix}, \tag{4.22}$$

we can construct their explicit quantum circuit implementation as depicted in Fig.4.1.

Since the action of the collision operators is only local in the $n_q = 2$-qubit register that means that their implementation is accomplished through $O(4)$ elementary gates. Therefore, implementing the full unitary evolution Eq.(4.17) requires $16(n_p^2 + n_q^2)$ single qubit and CNOT gates. The latter implies that our algorithm scales quadratically with the number of spatial qubits $O(n_p^2)$, rendering it implementable on present quantum hardware.

4.2.2 Extension to inhomogeneous and tensor media

4.2.2.1 Theoretical considerations

In contrast to establishing unitary evolution through the RSW vector for Maxwell equations in a homogeneous scalar medium, as illustrated in Sec.4.2.1, extending our considerations to inhomogeneous and tensor media requires returning to the starting point of

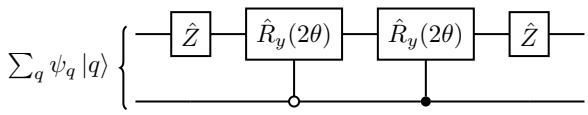

(a) Quantum circuit implementation of $\hat{C}_X$ operator in Eq.(4.21).

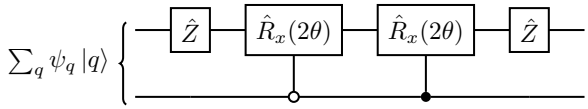

(b) Quantum circuit implementation of $\hat{C}_Y$ operator in Eq.(4.22).

Figure 4.1: The quantum circuit implementation of the collision operators $\hat{C}_X$ and $\hat{C}_Y$ in Eq.(4.20).

Eq.(4.12) to establish the appropriate conditions for unitary evolution.

Rewriting Maxwell equations in a general tensor and inhomogeneous medium, we have

$$i\frac{\partial \boldsymbol{u}}{\partial t} = \hat{W}^{-1}\hat{M}\boldsymbol{u}, \quad \hat{W} = \hat{W}(\boldsymbol{r}) = \begin{bmatrix} \hat{\varepsilon}(\boldsymbol{r}) & 0_{3\times 3} \\ 0_{3\times 3} & \hat{\mu}(\boldsymbol{r}) \end{bmatrix}, \tag{4.23}$$

where $\hat{\varepsilon}$ and $\hat{\mu}$ are the 3×3 permittivity and permeability matrices. Next we define the inner product,

$$\langle \boldsymbol{v}|\boldsymbol{u}\rangle = \int_{\mathscr{V}} \boldsymbol{v}^{\dagger}(\boldsymbol{r},t)\boldsymbol{u}(\boldsymbol{r},t)d\boldsymbol{r}, \quad \mathscr{V}\subset\mathbb{R}^3,\, t\in\mathscr{T}=[0,T], \tag{4.24}$$

where $\boldsymbol{u}(\boldsymbol{r},t)$ and $\boldsymbol{v}(\boldsymbol{r},t)$ are two solutions of Eq.(4.23) within the bounded domain defined by $\mathscr{V}$. We now explicitly show that the Maxwell operator $\hat{M}$ is Hermitian in the assigned Hilbert space $\mathscr{H} = L^2(\mathscr{V}\subset\mathbb{R}^3,\mathbb{C})$,

$$\begin{aligned} \left\langle \boldsymbol{v}\middle|\hat{M}\boldsymbol{u}\right\rangle &= i\int_{\Omega}\left(\boldsymbol{v}_1^*\cdot(\nabla\times\boldsymbol{u}_2) - \boldsymbol{v}_2^*\cdot(\nabla\times\boldsymbol{u}_1)\right)d^3\boldsymbol{r} \\ &= i\int_{\Omega}\left(\boldsymbol{u}_2\cdot(\nabla\times\boldsymbol{v}_1^*) - \boldsymbol{u}_1\cdot(\nabla\times\boldsymbol{v}_2^*)\right)d^3\boldsymbol{r} + i\int_{\partial\Omega}\left(\boldsymbol{v}_1^*\cdot(\hat{\boldsymbol{n}}\times\boldsymbol{u}_2) - \boldsymbol{v}_2^*\cdot(\hat{\boldsymbol{n}}\times\boldsymbol{u}_1)\right)dA \\ &= \left\langle \boldsymbol{v}\hat{M}\middle|\boldsymbol{u}\right\rangle. \end{aligned} \tag{4.25}$$

The transition from the second line of Eq.(4.25) to the desired result is due to the imposition of PEC boundary condition in Eq.(4.5). Thus, $\hat{M} = \hat{M}^{\dagger}$.

Following [110], the electromagnetic energy density is defined as,

$$U(\boldsymbol{r},t) = \int_0^t \boldsymbol{u}^{\dagger}\,\frac{\partial \boldsymbol{d}(\boldsymbol{r},\tau)}{\partial\tau}\,d\tau = \frac{1}{2}\boldsymbol{u}^{\dagger}\hat{W}\boldsymbol{u} + \int_0^t \boldsymbol{u}^{\dagger}(\boldsymbol{r},\tau)\,\hat{W}^A\,\frac{\partial \boldsymbol{u}(\boldsymbol{r},\tau)}{\partial\tau}\,d\tau, \tag{4.26}$$

where $\hat{W}^A = \left(\hat{W} - \hat{W}^{\dagger}\right)/2$ is the anti-Hermitian part of $\hat{W}$. Moreover, for a passive

medium [110] it applies that,

$$U(\boldsymbol{r},t) \geq 0, \quad \forall\, \boldsymbol{r} \in \mathscr{V}. \tag{4.27}$$

Then, from Eq.(4.26) it follows that $\hat{W}$ must be Hermitian and semi-positive definite,

$$\hat{W} = \hat{W}^{\dagger} \qquad \text{and} \qquad \hat{W} \geq 0. \tag{4.28}$$

Therefore, the total integrated stored electromagnetic energy E in a volume $\mathscr{V}$ is,

$$E(t) = \frac{1}{2} \int_{\mathscr{V}} \boldsymbol{u}^{\dagger}\, \hat{W}\, \boldsymbol{u}\, d^3\boldsymbol{r} \;\geq\; 0. \tag{4.29}$$

Integrating the Poynting theorem [101] over the $\mathscr{V}$ domain and making use of the divergence theorem, we obtain,

$$\frac{\partial E(t)}{\partial t} + \int_{\partial \mathscr{V}} \boldsymbol{S} \cdot \hat{\boldsymbol{n}}(\boldsymbol{r})\, dA = 0, \tag{4.30}$$

where dA is an elemental area on the surface $\partial\mathscr{V}$, $\hat{\boldsymbol{n}}$ is the outward pointing normal to $\partial\mathscr{V}$ and $\boldsymbol{S} = \boldsymbol{u}_1 \times \boldsymbol{u}_2$. From Eq.(4.30) and the PEC boundary condition (4.5) is follows that $E(t)$ is conserved,

$$E(t) = E(t=0) = \int_{\mathscr{V}} \boldsymbol{u}_0^{\dagger} \hat{W}(\boldsymbol{r})\, \boldsymbol{u}_0\, d^3\boldsymbol{r}. \tag{4.31}$$

As expected for a passive medium, there is no net dissipation or generation of electromagnetic energy within $\mathscr{V}$.

Inspecting Eqs.(4.28), (4.29) and (4.31) it is evident that the operator $\hat{W}$ fulfills the conditions of Eq.(3.3) for being a proper metric operator with $\hat{\Theta} = \hat{W}$. Indeed, in a manner analogous to Eq.(3.6),

$$\hat{D}^{\dagger} = \hat{M}\hat{W}^{-1} = \hat{W}\hat{W}^{-1}\hat{M}\hat{W}^{-1} = \hat{W}\hat{D}\hat{W}^{-1}. \tag{4.32}$$

Subsequently, the non-Hermitian operator $\hat{D}$ in Hilbert space $\mathscr{H}$ becomes Hermitian in the new weighted Hilbert space $\mathscr{H}_W$ under the inner product $\langle \boldsymbol{v}|\boldsymbol{u}\rangle_W = \langle \boldsymbol{v}|\hat{W}\boldsymbol{u}\rangle$,

$$\begin{aligned} \langle \boldsymbol{v}|\hat{D}\boldsymbol{u}\rangle_W &= \langle \boldsymbol{v}|\hat{M}\boldsymbol{u}\rangle = \langle \boldsymbol{v}\hat{M}\hat{W}^{-1}\hat{W}|\boldsymbol{u}\rangle \\ &= \langle \boldsymbol{v}\hat{M}\hat{W}^{-1}|\boldsymbol{u}\rangle_W = \langle \boldsymbol{v}\hat{D}|\boldsymbol{u}\rangle_W . \end{aligned} \tag{4.33}$$

Harnessing the Dyson map concept from Sec.3.1.1, there is an operator $\hat{\eta} : \mathscr{H} \to \mathscr{H}$ such that $\hat{\eta}^{\dagger}\hat{\eta} = \hat{W}$ with its explicit form provided by the following decompositions [22]:

- **Spectral decomposition**:

$$\hat{W}(\boldsymbol{r}) = \hat{U}^{\dagger}\hat{\Delta}(\boldsymbol{r})\hat{U} = \hat{U}^{\dagger}\sqrt{\hat{\Delta}(\boldsymbol{r})}\sqrt{\hat{\Delta}(\boldsymbol{r})}\hat{U} = \hat{\eta}^{\dagger}(\boldsymbol{r})\hat{\eta}(\boldsymbol{r}), \tag{4.34}$$

leading to the Dyson map,

$$\hat{\eta}(\boldsymbol{r}) = \sqrt{\hat{\Delta}(\boldsymbol{r})}\hat{U}. \tag{4.35}$$

- **Square root decomposition**:

$$\hat{W}(\boldsymbol{r}) = \hat{W}^{1/2}(\boldsymbol{r})\hat{W}^{1/2}(\boldsymbol{r}) = \hat{\eta}^{\dagger}(\boldsymbol{r})\hat{\eta}(\boldsymbol{r}), \tag{4.36}$$

with the corresponding Dyson map,

$$\hat{\eta}(\boldsymbol{r}) = \hat{W}^{1/2}(\boldsymbol{r}). \tag{4.37}$$

- **Cholesky decomposition**:

$$\hat{W}(\boldsymbol{r}) = \hat{T}^{\dagger}(\boldsymbol{r})\hat{T}(\boldsymbol{r}) = \hat{\eta}^{\dagger}(\boldsymbol{r})\hat{\eta}(\boldsymbol{r}), \tag{4.38}$$

giving the Dyson map,

$$\hat{\eta}(\boldsymbol{r}) = \hat{T}(\boldsymbol{r}). \tag{4.39}$$

For the spectral decomposition Eq.(4.34), $\hat{\Delta}(\boldsymbol{r}) = \lambda_i(\boldsymbol{r})\delta_{ij}$ (where no summation is implied over repeated indices) with $\lambda(\boldsymbol{r}) > 0$ and $\sqrt{\hat{\Delta}(\boldsymbol{r})} = \sqrt{\lambda_i(\boldsymbol{r})}\delta_{ij}$. For the Cholesky decomposition Eq.(4.38), the $\hat{T}$ matrix is an upper triangular matrix with positive diagonal elements. The specific choice of a Dyson map is determined by the decomposition scheme leading to a sparse $\hat{\eta}$.

Applying the Dyson map to Maxwell equations in Eq.(4.23) we obtain a Hermitian Schrodinger representation with an explicit unitary evolution,

$$i\frac{\partial \boldsymbol{\psi}}{\partial t} = \hat{\eta}(\boldsymbol{r})\hat{D}\hat{\eta}^{-1}(\boldsymbol{r})\boldsymbol{\psi} = \hat{D}_{\eta}\boldsymbol{\psi}, \quad \boldsymbol{\psi}(\boldsymbol{r},t) = e^{-it\hat{D}_{\eta}}\boldsymbol{\psi}_0(\boldsymbol{r}), \tag{4.40}$$

where $\boldsymbol{\psi} = \hat{\rho}\boldsymbol{u} \in \mathscr{H}$, and $\hat{D}_{\eta} = \hat{\eta}(\boldsymbol{r})\hat{D}\hat{\eta}^{-1}(\boldsymbol{r})$ is now Hermitian in $\mathscr{H}$.

As an illustration of the explicit form of Hermitian structured Maxwell equations in Eq.(4.40) we consider a non-magnetic, uniaxial dielectric medium,

$$\hat{\varepsilon}(\boldsymbol{r}) = \begin{bmatrix} \varepsilon_x(\boldsymbol{r}) & 0 & 0 \\ 0 & \varepsilon_x(\boldsymbol{r}) & 0 \\ 0 & 0 & \varepsilon_z(\boldsymbol{r}) \end{bmatrix}, \qquad \hat{\mu} = \mu_0 I_{3\times 3}. \tag{4.41}$$

A useful choice for a sparse Dyson map is,

$$\hat{\eta} = \hat{W}^{1/2} = \begin{bmatrix} \hat{\varepsilon}^{1/2} & 0_{3\times 3} \\ 0_{3\times 3} & \sqrt{\mu_0} I_{3\times 3}, \end{bmatrix}, \tag{4.42}$$

where,

$$\hat{\varepsilon}^{1/2}(\boldsymbol{r}) = \begin{bmatrix} \sqrt{\varepsilon_x(\boldsymbol{r})} & 0 & 0 \\ 0 & \sqrt{\varepsilon_x(\boldsymbol{r})} & 0 \\ 0 & 0 & \sqrt{\varepsilon_z(\boldsymbol{r}),} \end{bmatrix}. \tag{4.43}$$

Then, the Hermitian generator of dynamics $\hat{D}_\eta = \hat{\eta}\,\hat{D}\,\hat{\eta}^{-1}$ reads,

$$\hat{D}_\eta = \begin{bmatrix} 0_{3\times 3} & ic\hat{\boldsymbol{Z}}\cdot\hat{\boldsymbol{p}} \\ -ic\hat{\boldsymbol{p}}\cdot\hat{\boldsymbol{Z}}^\dagger & 0_{3\times 3} \end{bmatrix}, \tag{4.44}$$

where, in terms of the refractive index $n_i(\boldsymbol{r}) = \sqrt{\varepsilon_i(\boldsymbol{r})/\varepsilon_0}$, the components of $\hat{\boldsymbol{Z}} = (\hat{Z}_x, \hat{Z}_y, \hat{Z}_z)$ are

$$\hat{Z}_x = \begin{bmatrix} 0 & 0 & 0 \\ 0 & 0 & -\dfrac{i}{n_x(\boldsymbol{r})} \\ 0 & \dfrac{i}{n_z}(\boldsymbol{r}) & 0 \end{bmatrix}, \quad \hat{Z}_y = \begin{bmatrix} 0 & 0 & \dfrac{i}{n_x(\boldsymbol{r})} \\ 0 & 0 & 0 \\ -\dfrac{i}{n_z(\boldsymbol{r})} & 0 & 0 \end{bmatrix}, \quad \hat{Z}_z = \begin{bmatrix} 0 & -\dfrac{i}{n_x(\boldsymbol{r})} & 0 \\ \dfrac{i}{n_x(\boldsymbol{r})} & 0 & 0 \\ 0 & 0 & 0 \end{bmatrix}, \tag{4.45}$$

with $n_x = \sqrt{\varepsilon_x/\varepsilon_0}$ and $n_z = \sqrt{\varepsilon_z/\varepsilon_0}$ being the refraction indices in the x and z directions, respectively, and, as before $\hat{\boldsymbol{p}} = -i\nabla$.

Applying the unitary operator $\hat{L}$

$$\hat{L} = \frac{1}{\sqrt{2}} \begin{bmatrix} 1 & i \\ 1 & -i \end{bmatrix}, \tag{4.46}$$

in Eq.(4.40) results,

$$i\frac{\partial}{\partial t}\hat{L}\boldsymbol{\psi} = \left(\hat{L}\hat{D}_\eta\hat{L}^{-1}\right)\hat{L}\boldsymbol{\psi}. \tag{4.47}$$

Upon defining,

$$\boldsymbol{F}_r^{\pm} \;=\; \hat{L}\boldsymbol{\psi} \;=\; \hat{L}\hat{W}^{1/2}\boldsymbol{u} \;=\; \frac{1}{\sqrt{2}}\left(\hat{\varepsilon}^{1/2}(\boldsymbol{r})\,\boldsymbol{E} \pm \frac{i}{\sqrt{\mu_0}}\boldsymbol{B}\right), \tag{4.48}$$

the unitary evolution equation of Eq.(4.47) for a uniaxial anisotropic dielectric medium takes on the form,

$$i\frac{\partial}{\partial t}\begin{bmatrix} \boldsymbol{F}_r^+ \\ \boldsymbol{F}_r^- \end{bmatrix} = c\begin{bmatrix} (\boldsymbol{Z}\cdot\hat{\boldsymbol{p}})^H & -(\boldsymbol{Z}\cdot\hat{\boldsymbol{p}})^A \\ (\boldsymbol{Z}\cdot\hat{\boldsymbol{p}})^A & -(\boldsymbol{Z}\cdot\hat{\boldsymbol{p}})^H \end{bmatrix}\begin{bmatrix} \boldsymbol{F}_r^+ \\ \boldsymbol{F}_r^- \end{bmatrix}. \tag{4.49}$$

Here, the superscripts H and A represent the Hermitian and the anti-Hermitian parts of the operators in the parentheses. The definition in Eq.(4.48) generalizes the notion of the RSW vectors in Eq.(4.13) for an inhomogeneous and tensor dielectric medium.

4.2.2.2 Quantum algorithm

Having established the proper theoretical framework for the unitary evolution of Maxwell equation for non-dissipative inhomogeneous tensor media, we now proceed to construct the QLA algorithm and its corresponding quantum circuit implementation. For a general biaxial tensor dielectric, the state vector is given by:

$$\begin{bmatrix} n_x E_x \\ n_y E_y \\ n_z E_z \\ \mu_0^{1/2} H_x \\ \mu_0^{1/2} H_y \\ \mu_0^{1/2} H_z \end{bmatrix} = \begin{bmatrix} \psi_0 \\ \psi_1 \\ \psi_2 \\ \psi_3 \\ \psi_4 \\ \psi_5 \end{bmatrix} = \boldsymbol{\psi}, \quad q = 0, 1, ..., 5. \tag{4.50}$$

Assuming two-dimensional spatial dependence in the x-y plane, the decomposition of the Maxwell-Schrodinger equation (4.40) into Cartesian components yields,

$$\begin{aligned} &\frac{\partial \psi_0}{\partial t} = \frac{1}{n_x}\frac{\partial \psi_5}{\partial y}, \quad \frac{\partial \psi_1}{\partial t} = \frac{1}{n_y}\frac{\partial \psi_5}{\partial y}, \quad \frac{\partial \psi_2}{\partial t} = \frac{1}{n_z}\left[\frac{\partial \psi_4}{\partial y} - \frac{\partial \psi_3}{\partial x}\right], \\ &\frac{\partial \psi_3}{\partial t} = \frac{\partial (\psi_2/n_z)}{\partial y}, \quad \frac{\partial \psi_4}{\partial t} = \frac{\partial (\psi_2/n_z)}{\partial x}, \\ &\frac{\partial \psi_5}{\partial t} = -\frac{\partial (\psi_1/n_y)}{\partial x} + \frac{\partial (\psi_0/n_x)}{\partial n_y}. \end{aligned} \tag{4.51}$$

We discretize the two-dimensional space into a lattice with the spacing given by the ordering parameter $O(\delta)$. Then, we define the unitary collision operators in the x and y directions to be [95],

$$\hat{C}_X = \begin{bmatrix} 1 & 0 & 0 & 0 & 0 & 0 \\ 0 & \cos\theta_1 & 0 & 0 & 0 & -\sin\theta_1 \\ 0 & 0 & \cos\theta_2 & 0 & -\sin\theta_2 & 0 \\ 0 & 0 & 0 & 1 & 0 & 0 \\ 0 & 0 & \sin\theta_2 & 0 & \cos\theta_2 & 0 \\ 0 & \sin\theta_1 & 0 & 0 & 0 & \cos\theta_1 \end{bmatrix}, \tag{4.52}$$

$$\hat{C}_Y = \begin{bmatrix} \cos\theta_0 & 0 & 0 & 0 & 0 & \sin\theta_0 \\ 0 & 1 & 0 & 0 & 0 & 0 \\ 0 & 0 & \cos\theta_2 & \sin\theta_2 & 0 & 0 \\ 0 & 0 & -\sin\theta_2 & \cos\theta_2 & 0 & 0 \\ 0 & 0 & 0 & 0 & 1 & 0 \\ -\sin\theta_0 & 0 & 0 & 0 & 0 & \cos\theta_0 \end{bmatrix}. \tag{4.53}$$

In addition, to complete the walking process in the spatial $\{|p\rangle\}$ register, we define the

swift operator $\hat{S}_{q_i q_j}$ to denote a unitary streaming operator which shifts the amplitudes ψ_{q_i} and ψ_{q_j} one lattice unit along x and one lattice along y directions while leaving all the other amplitudes unaffected. Then, the QLA sequence along each direction to retrieve Eq.(4.51) without the refractive index derivatives is then given by:

$$\begin{aligned}\hat{U}_X &= \hat{S}_{25}^{+x}\hat{C}_X^{\dagger}\hat{S}_{25}^{-x}\hat{C}_X\hat{S}_{14}^{-x}\hat{C}_X^{\dagger}\hat{S}_{14}^{+x}\hat{C}_X\hat{S}_{25}^{-x}\hat{C}_X\hat{S}_{25}^{+x}\hat{C}_X^{\dagger}\hat{S}_{14}^{+x}\hat{C}_X\hat{S}_{14}^{-x}\hat{C}_X^{\dagger},\\ \hat{U}_Y &= \hat{S}_{25}^{+y}\hat{C}_Y^{\dagger}\hat{S}_{25}^{-y}\hat{C}_Y\hat{S}_{03}^{-y}\hat{C}_Y^{\dagger}\hat{S}_{03}^{+y}\hat{C}_Y\hat{S}_{25}^{-y}\hat{C}_Y\hat{S}_{25}^{+y}\hat{C}_Y^{\dagger}\hat{S}_{03}^{+y}\hat{C}_Y\hat{S}_{03}^{-y}\hat{C}_Y^{\dagger}.\end{aligned} \tag{4.54}$$

The terms in Eq.(4.51) that contain the derivatives of the refractive index are recovered through the following potential operators,

$$\hat{V}_X = \begin{bmatrix} 1 & 0 & 0 & 0 & 0 & 0 \\ 0 & 1 & 0 & 0 & 0 & 0 \\ 0 & 0 & 1 & 0 & 0 & 0 \\ 0 & 0 & -\sin\beta_2 & 0 & \cos\beta_2 & 0 \\ 0 & \sin\beta_0 & 0 & 0 & 0 & \cos\beta_0 \end{bmatrix} \tag{4.55}$$

and

$$\hat{V}_Y = \begin{bmatrix} 1 & 0 & 0 & 0 & 0 & 0 \\ 0 & 1 & 0 & 0 & 0 & 0 \\ 0 & 0 & 1 & 0 & 0 & 0 \\ 0 & 0 & \cos\beta_3 & \sin\beta_3 & 0 & 0 \\ -\sin\beta_1 & 0 & 0 & 0 & 0 & \cos\beta_1 \end{bmatrix}. \tag{4.56}$$

The angles θ_0, θ_1, θ_2, β_0, β_1, β_2, and β_3 that appearing in Eqs.(4.52), (4.53), (4.55), and (4.56) are chosen appropriately, such that the discretized system reproduces Eq.(4.51) to order δ^2 [95]. Thus, the evolution of the state vector $|\boldsymbol{\psi}\rangle$ from time t to $t+\Delta t$ is given by,

$$|\boldsymbol{\psi}(t+\Delta t)\rangle = \hat{V}_Y\hat{V}_X\hat{U}_Y\hat{U}_X\,|\boldsymbol{\psi}(t)\rangle\,. \tag{4.57}$$

Although we have proven that the continuous time evolution of the quantum representation of Maxwell equations, Eq.(4.51), is unitary, in the presented $O(\delta^2)$ discrete-time scheme, the external potential operators $\hat{V}_X, \hat{V}_Y$ are not unitary. This stems from the fragility of the unitary structure in perturbative schemes that do not employ Trotterization.

Using the quantum encoding in Eq.(3.18) and the two-level decomposition of $\hat{C}_X$ and $\hat{C}_Y$ matrices [93], their quantum circuit implementation is presented in Fig.4.2, whereas the streaming operators in each direction follow the implementation in Fig.3.2. The implementation scaling of the collision operators $\hat{C}_X$ and $\hat{C}_Y$ is constant due to the locality of the operators in the $\{|q\rangle\}$ register. However, because the angles $\theta_0, \theta_1, \theta_2$,

$$\theta_0 = \frac{\delta}{4n_x}, \quad \theta_1 = \frac{\delta}{4n_y}, \quad \theta_2 = \frac{\delta}{4n_z} \tag{4.58}$$

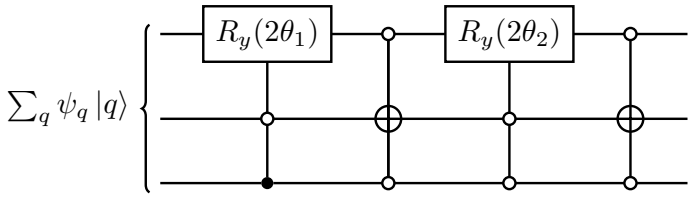

(a) Quantum circuit implementation of $\hat{C}_X$ operator in Eq.(4.52). The spatial dependence has been suppressed for simplicity.

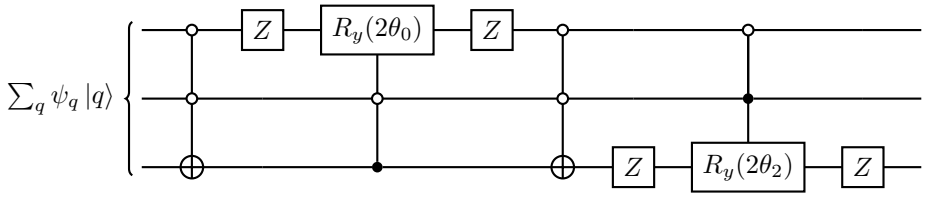

(b) Quantum circuit implementation of $\hat{C}_Y$ operator in Eq.(4.53). The spatial dependence has been suppressed for simplicity

Figure 4.2: The quantum circuit implementation of the collision operators $\hat{C}_X$ and $\hat{C}_Y$ in Eqs.(4.52) and (4.53).

are spatially dependent on the refractive index, the overall implementation cost for applying the collision operators in each lattice node is $O(2^{n_p})$. However, for physical applications, particularly relevant to electromagnetic wave scattering from inhomogeneities, these scattering structures are usually localized enabling us to reduce the encoding cost of the collision operators to $O[poly(n_p)]$. Taking into consideration the quadratic implementation scaling of streaming operator $\hat{S}$ in Fig.3.2 results into a polynomial implementation scaling $O[poly(n_p)]$ for the unitary sequence in Eq.(4.57).

Turning our attention to the implementation of the non-unitary operators $\hat{V}_X$ and $\hat{V}_Y$ in Eqs.(4.55) and (4.55), these are sparse matrices and can be decomposed into a sum of four unitary terms, respectively.

$$\hat{V}_{X,Y} = \frac{1}{2}\sum_{j=0}^{3} \hat{\hat{V}}_{jX,Y}, \tag{4.59}$$

with the unitary operators $\hat{\tilde{V}}_j$ to be defined as

$$\hat{\tilde{V}}_{0X} = \hat{\tilde{V}}_{0Y} = I_{6\times 6},$$

$$\hat{\tilde{V}}_{1X} = \begin{bmatrix} -1 & 0 & 0 & 0 & 0 & 0 \\ 0 & 1 & 0 & 0 & 0 & 0 \\ 0 & 0 & 1 & 0 & 0 & 0 \\ 0 & 0 & 0 & -1 & 0 & 0 \\ 0 & 0 & 0 & 0 & -1 & 0 \\ 0 & 0 & 0 & 0 & 0 & -1 \end{bmatrix}, \quad \hat{\tilde{V}}_{1Y} = \begin{bmatrix} 1 & 0 & 0 & 0 & 0 & 0 \\ 0 & -1 & 0 & 0 & 0 & 0 \\ 0 & 0 & 1 & 0 & 0 & 0 \\ 0 & 0 & 0 & -1 & 0 & 0 \\ 0 & 0 & 0 & 0 & -1 & 0 \\ 0 & 0 & 0 & 0 & 0 & -1 \end{bmatrix},$$

$$\hat{\tilde{V}}_{2X} = \begin{bmatrix} 1 & 0 & 0 & 0 & 0 & 0 \\ 0 & \cos\beta_0 & 0 & 0 & 0 & -\sin\beta_0 \\ 0 & 0 & \cos\beta_2 & 0 & \sin\beta_2 & 0 \\ 0 & 0 & 0 & 1 & 0 & 0 \\ 0 & 0 & -\sin\beta_2 & 0 & \cos\beta_2 & 0 \\ 0 & \sin\beta_0 & 0 & 0 & 0 & \cos\beta_0 \end{bmatrix}, \quad \hat{\tilde{V}}_{2Y} = \begin{bmatrix} \cos\beta_1 & 0 & 0 & 0 & 0 & \sin\beta_1 \\ 0 & 1 & 0 & 0 & 0 & 0 \\ 0 & 0 & -\sin\beta_3 & \cos\beta_3 & 0 & 0 \\ 0 & 0 & \cos\beta_3 & \sin\beta_3 & 0 & 0 \\ 0 & 0 & 0 & 0 & 1 & 0 \\ -\sin\beta_1 & 0 & 0 & 0 & 0 & \cos\beta_1 \end{bmatrix},$$

$$\hat{\tilde{V}}_{3X} = \begin{bmatrix} 1 & 0 & 0 & 0 & 0 & 0 \\ 0 & -\cos\beta_0 & 0 & 0 & 0 & \sin\beta_0 \\ 0 & 0 & -\cos\beta_2 & 0 & -\sin\beta_2 & 0 \\ 0 & 0 & 0 & 1 & 0 & 0 \\ 0 & 0 & -\sin\beta_2 & 0 & \cos\beta_2 & 0 \\ 0 & \sin\beta_0 & 0 & 0 & 0 & \cos\beta_0 \end{bmatrix}, \quad \hat{\tilde{V}}_{3Y} = \begin{bmatrix} -\cos\beta_1 & 0 & 0 & 0 & 0 & -\sin\beta_1 \\ 0 & 1 & 0 & 0 & 0 & 0 \\ 0 & 0 & \sin\beta_3 & -\cos\beta_3 & 0 & 0 \\ 0 & 0 & \cos\beta_3 & \sin\beta_3 & 0 & 0 \\ 0 & 0 & 0 & 0 & 1 & 0 \\ -\sin\beta_1 & 0 & 0 & 0 & 0 & \cos\beta_1 \end{bmatrix}. \tag{4.60}$$

As a result, the product structure of evolution in Eq. (4.57) now turns into a weighted sum of unitary operators,

$$\hat{U}_{ev} = \frac{1}{4}\sum_{j,k}^{3} \hat{\tilde{V}}_{jX}\hat{\tilde{V}}_{kY}\hat{U}_X\hat{U}_Y = \Big(\sum_{m=0}^{15}\hat{U}_m\Big)\hat{U}_X\hat{U}_Y. \tag{4.61}$$

that can naturally implemented through the LCU method. Specifically, following the LCU implementation process described in Sec.3.3.1, we consider an ancillary register of $n_m = \log_2 16 = 4$ qubits and define the following operators:

$$\begin{aligned} \hat{U}_{select} &= \sum_{m=0}^{15} |m\rangle\langle m| \otimes \hat{U}_m \\ \hat{U}_{prep} &: |0\rangle^{\otimes n_m} \rightarrow \frac{1}{4}\sum_{m=0}^{15} |m\rangle . \end{aligned} \tag{4.62}$$

Unitary operator $\hat{U}_{prep}$ represents state preparation in the ancillary register whereas implementation of operator $\hat{U}_{select}$ is similar to those presented in Fig.4.2 because $\hat{U}_m$ are composed of dual combinations of two-level matrices Eq.(4.60), containing rotations and $\hat{X}, \hat{Z}$ Pauli gates.

Applying the sequence $\hat{U}_{prep}\hat{U}_{select}\hat{U}_{prep}^{\dagger}$ we obtain the desired evolution, in accordance to Eq.(3.37) with success probability $p_{success} \sim 1/16$. This concludes the implementation process of evolution in Eq.(4.57) using $O[poly(n_p)]$ single qubit and CNOT gates.

On a final note, let us explore a potential quantum advantage of the QLA over the conventional Finite Difference Time Domain (FDTD) classical algorithm, which originated from the seminal work of Yee [111] for scalar media and was later extended to general dielectric tensor media in [112]. For a biaxial dielectric medium, the Yee FDTD algorithm updates the $\boldsymbol{u}$ electromagnetic fields in a staggered lattice. Thus, for a $x-y$ lattice consisting of N_xN_y nodes the number of operations for evolving the field in a time step Δt asymptotically scales as $O(N_xN_y)$. Conversely, for the QLA, we have shown that by leveraging the quantum walking process on a collocated lattice, the scaling for the same number of lattice nodes is $O[poly(log(N_xN_y))]$. For simplicity, assuming $N_x = N_y$, an indicating measure of potential quantum speedup S_1 is the ratio between the implementation cost of the FDTD algorithm and the quantum algorithm [113],

$$S_1 = \lim_{N\to\infty} \frac{\sum_k^M a_k \log^k N}{N^2} = \lim_{N\to\infty} \frac{a_M \log^M N}{N^2} \sim \lim_{N\to\infty} \frac{M!}{N^2}. \tag{4.63}$$

Here, M is the degree of the polynomial that characterizes the complexity in terms of resources of the quantum algorithm.

Equation (4.63) suggests that there is a possible exponential quantum speed-up of the QLA compared with the FDTD algorithm. In addition, even in the non-asymptotic regime, the QLA maintains an advantage over the FDTD method when the degree M, which reflects the locality of the scatterer, satisfies the condition $M! << N^2$. This condition ensures the computational implementation cost of the quantum algorithm remains significantly lower than that of the classical method for practical problem sizes.

4.2.2.3 Simulation results

To showcase what we expect to obtain from this quantum algorithmic process described thus far, as well as to benchmark the capabilities of the QLA we examine a 2D $x-y$ scattering of a wave-packet from scalar but non-dispersive localized inhomogeneities with refractive index $n = n(x,y)$, as displayed in Fig.4.3. The shape of the inhomogeneities, can be either a cylinder or a cone. The initial electromagnetic wave-packet $\boldsymbol{u}_0 = (E_{z0}(x), -B_{y0}(x))^T$ is a Gaussian envelope with internal oscillations, Fig.4.3b. The wave-packet propagates in the x-direction, from a vacuum $n = 1$ towards a localized dielectric inhomogeneous object with $n_{max}(x,y) = 2$. This polarization satisfies the initial divergence conditions. As the 1D vacuum wave-packet interacts with the 2D refractive index of the dielectric. the B_y field now becomes 2D, with $B_y(x,y,t)$. This self-consistently generates a $B_x(x,y,t)$ so that $\nabla \cdot \boldsymbol{B} = 0$ as well as a 2D $E_z(x,y,t)$. Throughout the QLA

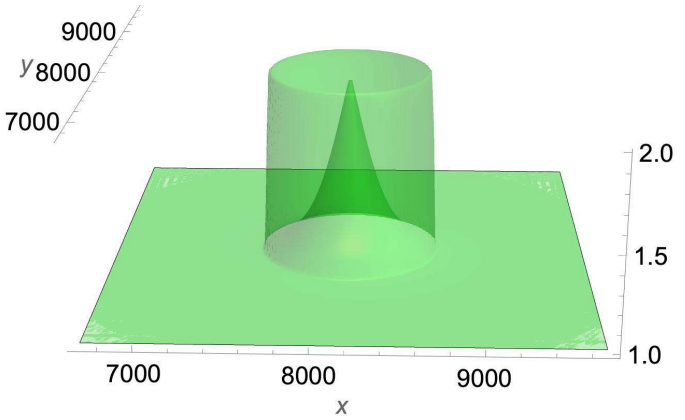

(a)

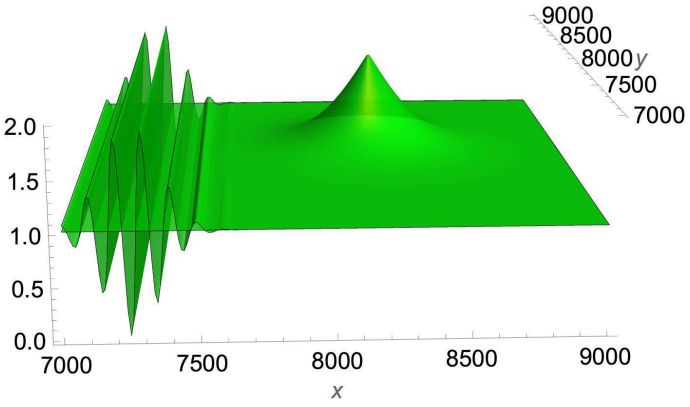

(b)

Figure 4.3: Two different inhomogeneity refractive index profiles $1 \leq n(x,y) \leq 2$ and the electric field $E_{z0}(x)$ of the incident wave-packet. The cylinder dielectric has strong spatial gradient near the vacuum-dielectric interface, while the conic dielectric has very weak spatial gradients. In Fig.4.3a these two profiles are shown superimposed. In Fig.4.3b the conic dielectric is shown together with the incident wave-packet (arbitrary normalization).

scattering simulation, $\nabla \cdot \boldsymbol{B}$ is monitored and is non-zero in very small isolated spatial regions with some time instants in which $max_{x,y}|\nabla \cdot \boldsymbol{B}/\boldsymbol{B_0}| \leq 0.006$. $\nabla \cdot \boldsymbol{D}$ is identically zero throughout the simulation. (For initial $E_{y0}(x)$-polarization, 2D QLA simulations retain $\nabla \cdot \boldsymbol{B} = 0$ identically zero for all time.)

In Fig.4.4, the wave-packet has interacted with the dielectric objects. The viewpoint is looking down from the z axis onto the $x-y$ plane. The apex of the cone is seen as a white dot, while the interior of the dielectric cylinder is in a somewhat darker color than the surrounding vacuum. In the case of a dielectric cone, Fig.4.4a, there is a mild slowing down of that part of the packet that is around the apex of the cone - since the phase velocity is reduced to $c/n(x,y)$. But, more importantly, one does not see any reflected part of the packet from the slowly varying boundary region between vacuum and dielectric. Basically the propagation is Wentzel–Kramers–Brillouin (WKB)-like. On the other hand,

there are immediate reflection fronts emitted back into the vacuum from the interaction of the wave-packet's oscillation peaks with the steep refractive index gradients in the boundary region of vacuum and cylinder dielectric, Fig.4.4b. There is also considerable retardation in the oscillation peaks within the dielectric cylinder as the refractive index away from the boundaries are $n = 2$. As mentioned earlier, the transmitted component of

(a) (b)

Figure 4.4: QLA scattering simulation of z-component of an electromagnetic pulse, E_{z0} off a dielectric inhomogeneity in the shape of a cone (Fig.4.3a), versus a cylindrical dielectric (Fig.4.3b). The perspective is looking down the z-axis onto the x-y plane. The full-wave simulation for the wave-cylinder encounter reveals strong initial reflection phenomena whereas the reflection is very weak in the cone case. This differentiation in the wave behavior is directly related to the steepness of the inhomogeneity gradient. The weak reflected wave from the cone corresponds to asymptotic WKB type of solution.

the initial wave-packet propagates into the respective dielectrics with phase velocity

$$v_{ph} = \frac{c}{n(x,y)} \tag{4.64}$$

because there is no dispersion in the media. However, the wave crests and the envelope along the y-direction possess different phase velocities during their propagation in the dielectric resulting in a lag between the interior and outer wave components. Ultimately, both dielectrics act as a focusing lens for the transmitted wave inside them. This latter behavior is clearly depicted in Fig.4.5.

As the bounded modes within the dielectric approach the vacuum boundary, the rapid change in the cylindrical dielectric object produces a secondary internal reflection that propagates back inside the cylinder. For the cone case, the slowly varying transition between the different regions contributes a negligible secondary reflection. Those secondary reflections, along with the secondary propagating wave-fronts in the vacuum region are presented in Fig.4.6.

The back and forth succession from Fig.4.6 to Fig.4.4 through higher order internal reflections in the cylindrical dielectric results in a radiating temporal pattern. It should be reminded that the presented algorithmic process is an initial value solver giving the

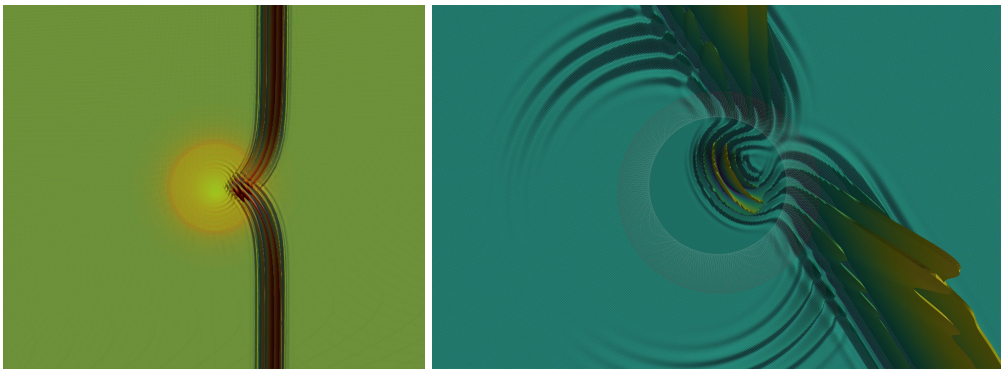

(a) (b)

Figure 4.5: The propagation of the transmitted wave within the conical and cylindrical dielectrics. The wave propagation is now distorted because the initial wave crests along the y axis diffract on the dielectric boundary. In both cases, Figs.4.5a, 4.5b, transmitted bounded modes are observed towards the exit point to vacuum.

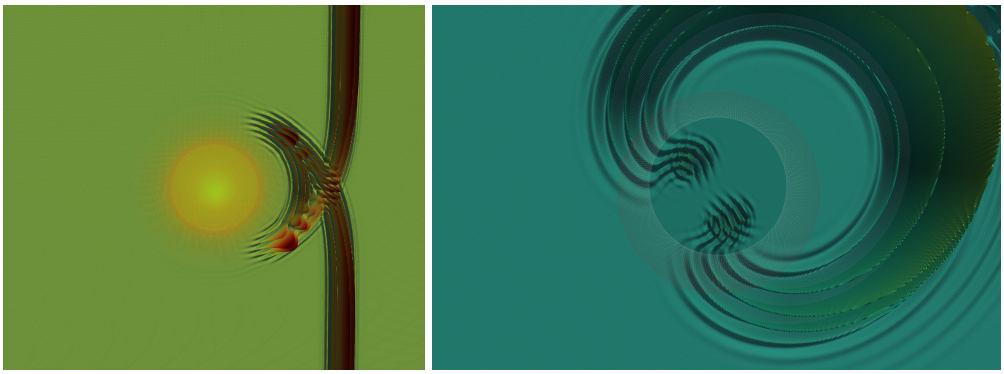

(a) (b)

Figure 4.6: The absence of internal reflections from the conical dielectric Fig.4.6a versus the internal reflections from the cylindrical dielectric Fig.4.6b. Similar to the behavior of the primary reflections in Fig.4.4 the inhomogeneity gradient of the dielectrics plays a pivotal role on the strength of the internal reflection.

temporal (and transient) evolution of the scattered field without the introduction of any internal boundary conditions to handle vacuum-dielectric effects. Most importantly, the simulations reveal that the QLA accurately grasps the interconnection of the transient behavior of waves with the inhomogeneity profile.

In all simulations, the total energy is conserved to the seventh significant digit. A numerical study of errors with respect to spatial resolution was performed in [71]. It indeed verified that the QLA performs better than 2nd order accuracy. This scaling was further verified in [114] for spinor Bose-Einstein Condensates. Finally, simulation results for scattering of Gaussian pulses from biaxial media can be found in [95].

4.3 Dispersive media and plasmas

In this section, we build upon the considerations for the non-dispersive media by presenting the theoretical framework for transforming the dispersive Maxwell equations Eq.(4.10) into a Hermitian structured Schrodinger representation for conservative dispersive media like scalar Lorentz media and gyrotropic media such as cold magnetized plasmas. Finally, we will examine the effect of dissipation in its simplest form, utilizing the LCU method and dilation techniques as outlined in Secs 3.3.1 and 3.3.2.

It is important to emphasize that the authors of Refs.[115–117] have demonstrated that Maxwell equations in passive, dissipative, and dispersive media can be formulated within a Hermitian Schrodinger framework. This is accomplished by extending the Hilbert space of the primary electromagnetic fields $\boldsymbol{E},\boldsymbol{H}$ with an appropriate set of auxiliary fields, derived using functional analysis techniques. However, the resulting Hermitian generator of dynamics operator $\hat{D}$ has a complex structure rendering it unsuitable for implementation of the underlying dynamics on a quantum computer. Therefore, a quantum representation of Maxwell equations that aligns with the principles of quantum information science (QIS) is required for their implementation in lossy and dispersive media.

For the cases of conservative Lorentz and gyrotropic media, following [117], we will formulate a quantum Schrodinger equation representation of classical Maxwell equations by introducing auxiliary electromagnetic fields related to the wave polarization and to the polarization density current.

4.3.1 Lorentz media

Lossless, scalar, and dispersive Lorentz media are characterized by scalar permittivity and permeability. Their general constitutive relations in the frequency domain are described as follows [117]:

$$\tilde{\varepsilon}(\boldsymbol{r},\omega)=\varepsilon_0\Big(1+\sum_{l=1}^{N_e}\frac{\Omega_{e,l}^2(\boldsymbol{r})}{\omega_{e,l}^2(\boldsymbol{r})-i\gamma_{e,l}(\boldsymbol{r})\omega-\omega^2}\Big), \tag{4.65}$$

$$\tilde{\mu}(\boldsymbol{r},\omega)=\mu_0\Big(1+\sum_{l=1}^{N_m}\frac{\Omega_{m,l}^2(\boldsymbol{r})}{\omega_{m,l}^2(\boldsymbol{r})-i\gamma_{m,l}(\boldsymbol{r})\omega-\omega^2}\Big). \tag{4.66}$$

Equations (4.65) and (4.66) describe the phenomenological Lorentz oscillator response model of bound charges in materials. Ω_e and Ω_m are the characteristic frequencies of the oscillator, whereas ω_e, ω_m are the resonant frequencies. The high frequency response of the medium is that of the vacuum with permittivity ε_0 and permeability μ_0. Finally, the $\gamma_{e,l}(\boldsymbol{r})$, $\gamma_{m,l}(\boldsymbol{r})\geq 0$ are the relaxation-dissipation rates. If $\gamma_e=0$ and $\gamma_m=0$, the medium is dispersive but lossless and for $\omega_e=0$ and $\omega_m=0$, we retrieve the Drude model for a simple metal. The connection between the susceptibility kernel $\hat{G}$ in Eq.(4.7) and the

constitutive relations Eqs.(4.65), (4.66) in the frequency domain is,

$$\hat{G}(\boldsymbol{r},t) = \frac{1}{2\pi}\int_{-\infty}^{\infty}\begin{bmatrix}\varepsilon(\boldsymbol{r},\omega)-\varepsilon_0 & 0\\ 0 & \mu(\boldsymbol{r},\omega)-\mu_0\end{bmatrix} e^{-i\omega t}\,d\omega. \tag{4.67}$$

Treating the lossless case we introduce the following auxiliary fields [117],

$$\mathbb{P}_l(\boldsymbol{r},t) = \frac{1}{2\pi}\int_0^t\int_{-\infty}^{\infty}\frac{e^{-i\omega(t-\tau)}}{\omega_{e,l}^2-\omega^2}\boldsymbol{E}(\boldsymbol{r},\tau)d\,\omega d\,\tau, \tag{4.68}$$

and

$$\mathbb{M}_l(\boldsymbol{r},t) = \frac{1}{2\pi}\int_0^t\int_{-\infty}^{\infty}\frac{e^{-i\omega(t-\tau)}}{\omega_{m,l}^2-\omega^2}\boldsymbol{H}(\boldsymbol{r},\tau)d\,\omega d\,\tau, \tag{4.69}$$

which are related to the electric $\boldsymbol{P}$ and magnetic $\boldsymbol{M}$ polarizability of the medium,

$$\boldsymbol{P}(\boldsymbol{r},t) = \varepsilon_0\sum_{l=1}^{N_e}\Omega_{e,l}^2\mathbb{P}_l, \quad \boldsymbol{M}(\boldsymbol{r},t) = \mu_0\sum_{l=1}^{N_m}\Omega_{m,l}^2\mathbb{M}_l. \tag{4.70}$$

Maxwell equations (4.8), together with the evolution equations for the auxiliary fields in Eqs.(4.68), (4.69) result in the following closed system of partial differential equations,

$$\begin{aligned} i\frac{\partial\boldsymbol{u}}{\partial t} &= \hat{W}_0^{-1}\hat{M}\boldsymbol{u} - i\sum_{l=1}^{N}\hat{\Omega}_l^2\mathscr{P}_{l,t},\\ i\frac{\partial\mathscr{P}_l}{\partial t} &= i\mathscr{P}_{l,t}, \qquad l=1,2...N,\\ i\frac{\partial\mathscr{P}_{l,t}}{\partial t} &= i\boldsymbol{u} - i\hat{\omega}_l^2\mathscr{P}_l, \qquad l=1,2...N, \end{aligned} \tag{4.71}$$

where $\boldsymbol{u} = (\boldsymbol{E},\boldsymbol{H})^T$, $\mathscr{P}_l = (\mathbb{P}_l,\mathbb{M}_l)^T$, $N = max\{N_e,N_m\}$ and the matrices $\hat{\Omega}_l^2$ and $\hat{\omega}_l^2$ are diagonal of the form,

$$\hat{\Omega}_l^2 = \begin{bmatrix}\Omega_{e,l}^2 & 0\\ 0 & \Omega_{m,l}^2\end{bmatrix}, \quad \hat{\omega}_l^2 = \begin{bmatrix}\omega_{e,l}^2 & 0\\ 0 & \omega_{m,l}^2\end{bmatrix}. \tag{4.72}$$

Upon applying the Dyson transform [93],

$$\hat{\eta} = diag(\hat{W}_0^{1/2},\hat{W}_0^{1/2}\hat{\Omega}_l\hat{\omega}_l,W_0^{1/2}\hat{\Omega}_l), \tag{4.73}$$

to Eq.(4.71), we obtain a Hermitian Schrodinger representation of the extended Maxwell

system of equations,

$$
\begin{aligned}
& i\frac{\partial}{\partial t}\begin{bmatrix} \hat{W}_0^{1/2}\boldsymbol{u} \\ \hat{W}_0^{1/2}\hat{\Omega}_l\hat{\omega}_l\mathscr{P}_l \\ W_0^{1/2}\hat{\Omega}_l\mathscr{P}_{l,t} \end{bmatrix} = \begin{bmatrix} c\hat{M} & 0 & -i\hat{\Omega}_l \\ 0 & 0 & i\hat{\omega}_l \\ i\hat{\Omega}_l & -i\hat{\omega}_l & 0 \end{bmatrix} \begin{bmatrix} W_0^{1/2}\boldsymbol{u} \\ \hat{W}_0^{1/2}\hat{\Omega}_l\hat{\omega}_l\mathscr{P}_l \\ W_0^{1/2}\hat{\Omega}_l\mathscr{P}_{l,t} \end{bmatrix}, \\
& l = 1,2,...,N,
\end{aligned} \tag{4.74}
$$

where $c = (\varepsilon_0\mu_0)^{-1/2}$ is the speed of light in vacuum. The evolution equation (4.74) can be compactly written as,

$$
i\frac{\partial \boldsymbol{\psi}}{\partial t} = \hat{D}\boldsymbol{\psi}, \quad \hat{D} = \hat{D}^{\dagger}, \tag{4.75}
$$

with initial condition $\boldsymbol{\psi}_0 = (\hat{W}_0^{1/2}\boldsymbol{u}_0, 0, 0)^T$ with $\boldsymbol{u}_0 = (\boldsymbol{E}_0, \boldsymbol{H}_0)^T$ being the initial electromagnetic field quantities. Equation (4.75) is called the Schrodinger representation of Maxwell equations for dispersive media due to its quantal form similar in mathematical properties to Schrodinger equation. The state vector $\boldsymbol{\psi}$ includes all the physically relevant electromagnetic fields that are necessary to understand propagation and scattering of waves in a lossless Lorentz medium. A generalization of Eq.(4.74) to a tensor Lorentz medium can be found in [118].

The unitary evolution described by Eq.(4.75) leads to conservation of the extended electromagnetic energy E_{total} which corresponds to the norm of the state vector, $\|\boldsymbol{\psi}\|^2$

$$
\begin{aligned}
E_{total}(t) = \frac{1}{2}\|\boldsymbol{\psi}\|^2 = \frac{1}{2}\hat{W}_0\int_{\mathscr{V}}\|\boldsymbol{u}\|^2 d\,\boldsymbol{r} \\
+ \frac{1}{2}\hat{W}_0\sum_{l=1}^{N}\int_{\mathscr{V}}\hat{\Omega}_l^2\left(\hat{\omega}_l^2\|\mathscr{P}_l\|^2 + \left\|\mathscr{P}_{l,t}\right\|^2\right) d\,\boldsymbol{r}.
\end{aligned} \tag{4.76}
$$

The first term on the right hand side of Eq.(4.76) the electromagnetic energy of the vacuum,

$$
E_{el}(t) = \frac{1}{2}\int_{\Omega}\varepsilon_0\left(\|\boldsymbol{E}\|^2 + \mu_0\|\boldsymbol{H}\|^2\right) d\,\boldsymbol{r} \leq E_{total}(0) = E_{el}(0). \tag{4.77}
$$

The Energy expression in Eq.(4.76) holds beyond the plane-wave, harmonic and semi-harmonic approximations for the fields, as imposed by Landau and Brillouin [98].

4.3.2 Cold magnetized plasmas

On the other hand, gyrotropic media such as cold magnetized plasmas are tensor dielectric dispersive media. This translates into a frequency dependent permittivity matrix $\tilde{\varepsilon}(\omega)$.

Following the Stix notation [14],

$$\tilde{\varepsilon}(\omega) = \begin{bmatrix} S & -iD & 0 \\ iD & S & 0 \\ 0 & 0 & P \end{bmatrix}, \quad \mu = \mu_0. \tag{4.78}$$

with

$$\begin{aligned} S =& \varepsilon_0 \Big(1 - \sum_{j=i,e} \frac{\omega_{pj}^2}{\omega^2 - \omega_{cj}^2}\Big) \\ D =& \varepsilon_0 \sum_{j=i,e} \frac{\omega_{cj}\omega_{pj}^2}{\omega(\omega^2 - \omega_{cj}^2)} \\ P =& \varepsilon_0 \Big(1 - \sum_{j=i,e} \frac{\omega_{pj}^2}{\omega^2}\Big). \end{aligned} \tag{4.79}$$

of the Stix permittivity tensor are defined for a two-species plasma consisting of ions (i) and electrons (e). The plasma features an inhomogeneous plasma frequency $\omega_{pj}^2(\boldsymbol{r}) = \frac{n_j(\boldsymbol{r})q_j^2}{m_j\varepsilon_0}$ and cyclotron frequency $\omega_{cj} = \frac{q_j B_0}{m_j}$. The homogeneous magnetic field B_0 is aligned along the z axis with m_j and q_j the mass and charge of the j-species respectively. Finally, $n_j(\mathbf{r})$ represents the j^{th} species number density.

Calculating the integral transformation of Eq.(4.67) for the Stix permittivity tensor in Eq.(4.78) we obtain the electric susceptibility kernel $\hat{K}^e(\boldsymbol{r},t)$ (see Eq.(4.7)),

$$\hat{K}^e(\boldsymbol{r},t) = \varepsilon_0 \sum_{j=i,e} \begin{bmatrix} \frac{\omega_{pj}^2}{\omega_{cj}} \sin\omega_{cj}t & \frac{\omega_{pj}^2}{\omega_{cj}}(\cos\omega_{cj}t - 1) & 0 \\ \frac{\omega_{pj}^2}{\omega_{cj}}(1 - \cos\omega_{cj}t) & \frac{\omega_{pj}^2}{\omega_{cj}} \sin\omega_{cj}t & 0 \\ 0 & 0 & \omega_{pj}^2 t \end{bmatrix}. \tag{4.80}$$

Thus, the $\hat{G}_A$ kernel in Eq.(4.9) reads,

$$\hat{G}_A = \begin{bmatrix} \frac{1}{\varepsilon_0}\frac{\partial \hat{K}^e}{\partial t} & 0_{3\times3} \\ 0_{3\times3} & 0_{3\times3} \end{bmatrix}, \quad \frac{1}{\varepsilon_0}\frac{\partial \hat{K}^e}{\partial t} = \sum_{j=i,e} \omega_{pj}^2(\boldsymbol{r}) \begin{bmatrix} \cos\omega_{cj}t & -\sin\omega_{cj}t & 0 \\ \sin\omega_{cj}t & \cos\omega_{cj}t & 0 \\ 0 & 0 & 1 \end{bmatrix}. \tag{4.81}$$

Since $\tilde{\varepsilon}(\omega)$ in Eq.(4.78), is Hermitian, this ensures that the conductivity current does not produce dissipation inside the plasma, i.e. the cold magnetized plasma behaves as a lossless dispersive dielectric. As a result, based on the considerations on Sec.3.1.1 it is possible to construct a Schrodinger representation of Maxwell equations that admits unitary evolution, corresponding to the conservation of electromagnetic energy.

Similarly to Eq.(4.68), defining the total conductivity current density $\boldsymbol{J}_c$ as

$$\boldsymbol{J}_c = \int_0^t \frac{\partial \hat{K}}{\partial t}\boldsymbol{E}(\boldsymbol{r},\tau)d\,\tau = \boldsymbol{J}_{ce} + \boldsymbol{J}_{ci}, \tag{4.82}$$

and exploiting the rotational symmetry of $\frac{\partial \hat{K}^e}{\partial t}$ in Eq.(4.81) to reformulate Maxwell equations as

$$\begin{aligned} i\frac{\partial \boldsymbol{E}}{\partial t} &= \frac{i}{\varepsilon_0}\nabla\times\boldsymbol{H} - \frac{i}{\varepsilon_0}\boldsymbol{J}_c, \\ i\frac{\partial \boldsymbol{H}}{\partial t} &= -\frac{i}{\mu_0}\nabla\times\boldsymbol{E}, \\ i\frac{\partial \boldsymbol{J}_{cj}}{\partial t} &= i\varepsilon_0\omega_{pj}^2(\boldsymbol{r})\boldsymbol{E} + \omega_{cj}\hat{S}_z\boldsymbol{J}_{cj}, \quad j = i,e. \end{aligned} \tag{4.83}$$

The set of equations in Eq.(4.83) represents the augmented Maxwell system, which self-consistently describes the behavior of electromagnetic fields within a cold magnetized plasma. We point out that Eq.(4.83) forms the basis for finite-difference time-domain (FDTD) simulations [119, 120]. The Hermitian matrix $\hat{S}_z$ given by,

$$\hat{S}_z = \begin{bmatrix} 0 & -i & 0 \\ i & 0 & 0 \\ 0 & 0 & 0 \end{bmatrix} \tag{4.84}$$

represents the projection of spin-1 onto the z-axis.

Once again, to obtain an explicit Schrodinger representation of Eq.(4.83) we apply a Dyson transformation [93] to Eq.(4.83),

$$\hat{\eta} = diag(\varepsilon_0^{1/2}I_{3\times3}, \mu_0^{1/2}I_{3\times3}, \frac{1}{\varepsilon_0^{1/2}\omega_{pi}}I_{3\times3}, \frac{1}{\varepsilon_0^{1/2}\omega_{pe}}I_{3\times3}) \tag{4.85}$$

resulting into

$$i\frac{\partial}{\partial t}\begin{bmatrix} \varepsilon_0^{1/2}\boldsymbol{E} \\ \mu_0^{1/2}\boldsymbol{H} \\ \frac{1}{\varepsilon_0^{1/2}\omega_{pi}}\boldsymbol{J}_{ci} \\ \frac{1}{\varepsilon_0^{1/2}\omega_{pe}}\boldsymbol{J}_{ce} \end{bmatrix} = \begin{bmatrix} 0_{3\times3} & ic\boldsymbol{\nabla}\times & -i\omega_{pi} & -i\omega_{pe} \\ -ic\boldsymbol{\nabla}\times & 0_{3\times3} & 0_{3\times3} & 0_{3\times3} \\ i\omega_{pi} & 0_{3\times3} & \omega_{ci}\hat{S}_z & 0_{3\times3} \\ i\omega_{pe} & 0_{3\times3} & 0_{3\times3} & \omega_{ce}\hat{S}_z \end{bmatrix} \begin{bmatrix} \varepsilon_0^{1/2}\boldsymbol{E} \\ \mu_0^{1/2}\boldsymbol{H} \\ \frac{1}{e_0^{1/2}\omega_{pi}}\boldsymbol{J}_{ci} \\ \frac{1}{e_0^{1/2}\omega_{pe}}\boldsymbol{J}_{ce} \end{bmatrix} \Leftrightarrow i\frac{\partial \boldsymbol{\psi}}{\partial t} = \hat{D}\boldsymbol{\psi}, \tag{4.86}$$

or compactly,

$$i\frac{\partial \boldsymbol{\psi}}{\partial t} = \hat{D}\boldsymbol{\psi}, \quad \hat{D} = \hat{D}^\dagger. \tag{4.87}$$

Equation (4.86) can be easily extended to incorporate different ions species by adding the respective ion-species current components in the stave vector $\boldsymbol{\psi}$. In realistic fusion

experiments there will be hydrogen, deuterium and tritium ions, so their contribution must be included in Eq.(4.86) for a complete description of the total inhomogeneity profiles.

Similarly with Eq.(4.76), the evolution operator $\hat{\mathscr{U}} = e^{-it\hat{D}}$ of Eq.(4.87) is unitary and corresponds to the conservation of an extended electromagnetic energy $E(t)$ through the inner product,

$$\begin{aligned} E(t) = \langle \boldsymbol{\psi} | \boldsymbol{\psi} \rangle &= \int_{\mathscr{V}} \Big(\varepsilon_0 |\boldsymbol{E}|^2 + \frac{|\boldsymbol{B}|^2}{\mu_0} \Big) d\boldsymbol{r} + \int_{\mathscr{V}} \Big(\frac{|\boldsymbol{J}_{ci}|^2}{\varepsilon_0 \omega_{pi}^2(\mathbf{r})} + \frac{|\boldsymbol{J}_{ce}|^2}{\varepsilon_0 \omega_{pe}^2(\mathbf{r})} \Big) d\boldsymbol{r} \\ &= E(0) = \int_{\mathscr{V}} \Big(\varepsilon_0 |\boldsymbol{E}_0|^2 + \frac{|\boldsymbol{B}_0|^2}{\mu_0} \Big) d\boldsymbol{r}, \quad \mathscr{V} \subset \mathbb{R}^3. \end{aligned} \tag{4.88}$$

The extended electromagnetic energy Eq.(4.88) consists of two terms. The first term is the standard electromagnetic energy in a vacuum whereas the second term reflects the energy associated with the cold plasma response. We have denoted with $\boldsymbol{E}_0$ and $\boldsymbol{B}_0$ the initial values of the electromagnetic fields. Notice that due to the causality constraint in the plasma response, the initial values of the conductivity currents according to Eq.(4.82) are zero, $\boldsymbol{J}_{ce,i}(t \leq 0) = 0$.

4.3.2.1 Quantum algorithm

To construct a quantum walk algorithm for simulation of Eq.(4.86) we must first decompose the generator of dynamics $\hat{D}$ into simpler parts [94],

$$\hat{D} = \hat{D}_{vac} + \sum_{j=i,e} [\hat{D}_{\omega_{pj}} + \hat{D}_{\omega_{cj}}], \tag{4.89}$$

with

$$\begin{aligned} \hat{D}_{vac} &= -\frac{c}{2}(I_{2\times 2} + \hat{Z}) \otimes \hat{Y} \otimes \boldsymbol{\nabla}\times \\ \hat{D}_{\omega_{pi}} &= \frac{1}{2}\hat{Y} \otimes (I_{2\times 2} + \hat{Z}) \otimes \omega_{pi} \\ \hat{D}_{\omega_{pe}} &= \frac{1}{2}(\hat{X} \otimes \hat{Y} + \hat{Y} \otimes \hat{X}) \otimes \omega_{pe} \\ \hat{D}_{\omega_{ci}} &= \frac{1}{4}(I_{2\times 2} - \hat{Z}) \otimes (I_{2\times 2} + \hat{Z}) \otimes \omega_{ci}\hat{S}_z \\ D_{\omega_{ce}} &= \frac{1}{4}(I_{2\times 2} - \hat{Z}) \otimes (I_{2\times 2} - \hat{Z}) \otimes \omega_{ce}\hat{S}_z. \end{aligned} \tag{4.90}$$

Given the operators in Eq.(4.89), the assigned task is to recover them to order δ^2, through a quantum walk in a $x-y$ lattice with discretization step δ. The amplitude or coin register $\{|q\rangle\}$ is 12-dimensional, hence the number of particles-walkers corresponds to $n_q = 4$ qubits. Using the 12-dimensional canonical representation [121] for 4 qubits we

assign quantum to classical amplitudes and states in the following manner:

$$\begin{aligned}
&\psi_0 \leftrightarrow E_x \rightarrow |q=0\rangle \leftrightarrow |0000\rangle \\
&\psi_1 \leftrightarrow E_y \rightarrow |q=1\rangle \leftrightarrow |0100\rangle \\
&\psi_2 \leftrightarrow E_z \rightarrow |q=2\rangle \leftrightarrow |0101\rangle \\
&\psi_3 \leftrightarrow H_x \rightarrow |q=3\rangle \leftrightarrow |0110\rangle \\
&\psi_4 \leftrightarrow H_y \rightarrow |q=4\rangle \leftrightarrow |1000\rangle \\
&\psi_5 \leftrightarrow H_z \rightarrow |q=5\rangle \leftrightarrow |1001\rangle \\
&\psi_6 \leftrightarrow J_{cix} \rightarrow |q=6\rangle \leftrightarrow |1010\rangle \\
&\psi_7 \leftrightarrow J_{ciy} \rightarrow |q=7\rangle \leftrightarrow |1011\rangle \\
&\psi_8 \leftrightarrow J_{ciz} \rightarrow |q=8\rangle \leftrightarrow |1100\rangle \\
&\psi_9 \leftrightarrow J_{cey} \rightarrow |q=9\rangle \leftrightarrow |1101\rangle \\
&\psi_{10} \leftrightarrow J_{cey} \rightarrow |q=10\rangle \leftrightarrow |1110\rangle \\
&\psi_{11} \leftrightarrow J_{cez} \rightarrow |q=11\rangle \leftrightarrow |1111\rangle
\end{aligned} \tag{4.91}$$

Thus, the interior "spin" state of the walkers in this 12-dimensional subspace $\mathscr{H}_C$ is

$$|\psi_q\rangle = \sum_q \psi_q |q\rangle . \tag{4.92}$$

The walk between the $N = N_x N_y$ nodes for the $x-y$ lattice is realized by introducing the $n_p = \log_2 N$ qubit $\mathscr{H}_S$ space in which the swift/streaming operator acts controlled by the spin space. Therefore, the total plasma state reads,

$$|\psi(t)\rangle = \sum_{q,p} \psi_{q,p}(t) |q\rangle \otimes |p\rangle . \tag{4.93}$$

The QLA evolution of the state is,

$$|\psi(t+\Delta t)\rangle = \hat{V}_{pe}\hat{V}_{pi}\hat{V}_{ce}\hat{V}_{ci}\hat{U}_Y\hat{U}_X |\psi(t)\rangle + O(\delta^4), \tag{4.94}$$

where the participating operators in evolution Eq.(4.94) are all unitary to order $O(\delta^4)$. The $\hat{U}_X$ and $\hat{U}_Y$ operators recover differential $\hat{D}_{vac}$ operator in Eq.(4.90) following the same sequence as in Eq.(4.54) since its action regards only the $\{q_0 - q_5\}$ subspace. Therefore,

$$\begin{aligned}
\hat{U}_X &= \hat{S}^{+x}_{25}\hat{C}^{\dagger}_X\hat{S}^{-x}_{25}\hat{C}_X\hat{S}^{-x}_{14}\hat{C}^{\dagger}_X\hat{S}^{+x}_{14}\hat{C}_X\hat{S}^{-x}_{25}\hat{C}_X\hat{S}^{+x}_{25}\hat{C}^{\dagger}_X\hat{S}^{+x}_{14}\hat{C}_X\hat{S}^{-x}_{14}\hat{C}^{\dagger}_X, \\
\hat{U}_Y &= \hat{S}^{+y}_{25}\hat{C}^{\dagger}_Y\hat{S}^{-y}_{25}\hat{C}_Y\hat{S}^{-y}_{03}\hat{C}^{\dagger}_Y\hat{S}^{+y}_{03}\hat{C}_Y\hat{S}^{-y}_{25}\hat{C}_Y\hat{S}^{+y}_{25}\hat{C}^{\dagger}_Y\hat{S}^{+y}_{03}\hat{C}_Y\hat{S}^{-y}_{03}\hat{C}^{\dagger}_Y.
\end{aligned} \tag{4.95}$$

Consequently, the participating unitary 12-dimensional coin/collision operators $\hat{C}_X$ and

$\hat{C}_Y$ are the 12-dimensional variants of Eqs. (4.52) and (4.53) respectively,

$$\hat{C}_X = \begin{bmatrix} \hat{C}_x & 0_{6\times6} \\ 0_{6\times6} & I_{6\times6} \end{bmatrix}, \quad \hat{C}_x = \begin{bmatrix} 1 & 0 & 0 & 0 & 0 & 0 \\ 0 & \cos\theta & 0 & 0 & 0 & -\sin\theta \\ 0 & 0 & \cos\theta & 0 & -\sin\theta & 0 \\ 0 & 0 & 0 & 1 & 0 & 0 \\ 0 & 0 & \sin\theta & 0 & \cos\theta & 0 \\ 0 & \sin\theta & 0 & 0 & 0 & \cos\theta \end{bmatrix}, \tag{4.96}$$

and

$$\hat{C}_Y = \begin{bmatrix} \hat{C}_y & 0_{6\times6} \\ 0_{6\times6} & I_{6\times6} \end{bmatrix}, \quad \hat{C}_y = \begin{bmatrix} \cos\theta & 0 & 0 & 0 & 0 & \sin\theta \\ 0 & 1 & 0 & 0 & 0 & 0 \\ 0 & 0 & \cos\theta & \sin\theta & 0 & 0 \\ 0 & 0 & -\sin\theta & \cos\theta & 0 & 0 \\ 0 & 0 & 0 & 0 & 1 & 0 \\ -\sin\theta & 0 & 0 & 0 & 0 & \cos\theta \end{bmatrix}, \tag{4.97}$$

with rotation angle $\theta \sim c\delta/4$. The quantum circuit implementation of the non-trivial part $\hat{C}_x$ and $\hat{C}_y$ is analogous with the ones presented in Fig.4.1 but for a 4-qubit $\{|q\rangle\}$ register. For completeness, we provide their implementation in Fig.4.7. As a reminder,

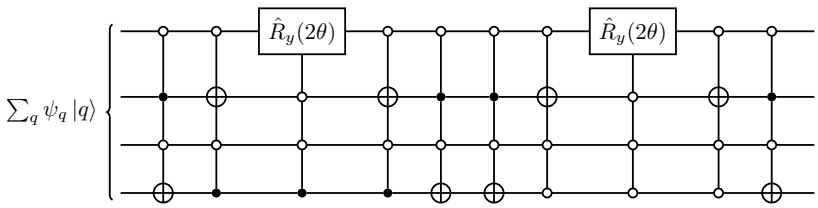

(a) Quantum circuit implementation of $\hat{C}_X$ operator in Eq.(4.96). The spatial dependence has been suppressed for simplicity.

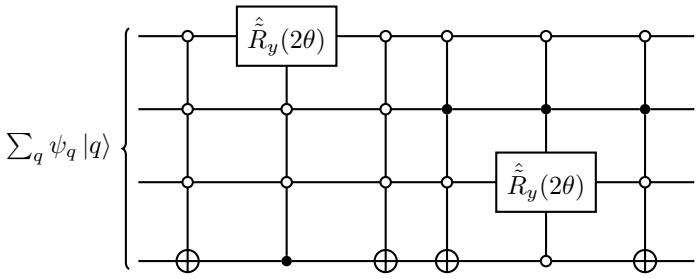

(b) Quantum circuit implementation of $\hat{C}_Y$ operator in Eq.(4.97). The spatial dependence has been suppressed for simplicity and the single qubit rotation $\hat{\hat{R}}_y$ is $\hat{\hat{R}}_y = \hat{Z}\hat{R}_y\hat{Z}$

Figure 4.7: The quantum circuit implementation of the collision operators $\hat{C}_X$ and $\hat{C}_Y$ in Eqs.(4.96) and (4.97) in the $\{|q\rangle\}$ register.

the implementation cost of streaming operator $\hat{S}$ in the $\{|p\rangle\}$ register is $O(n_p^2)$ and the respective quantum circuit implementation has been presented in Fig.3.2. The streaming operator is a controlled operator $\hat{S}^{q_i q_j}$,

$$\hat{S}^{q_i q_j} = |q_i\rangle\langle q_i| \otimes \hat{S} + |q_j\rangle\langle q_j| \otimes \hat{S}, \quad \hat{S}|p\rangle = |p+1\rangle, \quad \hat{S}^{\dagger}|p\rangle = |p-1\rangle. \tag{4.98}$$

To recover the non-differential terms associated with the diagonal magnetic cyclotron terms (see the underline structure of operators $\hat{D}_{\omega_{ci,e}}$ in Eq.(4.90)), we define the $\hat{V}_{ci,e}$ operators,

$$\hat{V}_{ci} = \begin{bmatrix} I_{6\times 6} & 0_{6\times 6} \\ 0_{6\times 6} & \hat{v}_{ci} \end{bmatrix}, \quad \hat{V}_{ce} = \begin{bmatrix} I_{6\times 6} & 0_{6\times 6} \\ 0_{6\times 6} & \hat{v}_{ce} \end{bmatrix}, \tag{4.99}$$

with

$$\hat{v}_{ci} = \begin{bmatrix} \cos\theta_{ci} & -\sin\theta_{ci} & 0 & 0 & 0 & 0 \\ \sin\theta_{ci} & \cos\theta_{ci} & 0 & 0 & 0 & 0 \\ 0 & 0 & 1 & 0 & 0 & 0 \\ 0 & 0 & 0 & 1 & 0 & 0 \\ 0 & 0 & 0 & 0 & 1 & 0 \\ 0 & 0 & 0 & 0 & 0 & 1 \end{bmatrix}, \quad \hat{v}_{ce} = \begin{bmatrix} 1 & 0 & 0 & 0 & 0 & 0 \\ 0 & 1 & 0 & 0 & 0 & 0 \\ 0 & 0 & 1 & 0 & 0 & 0 \\ 0 & 0 & 0 & \cos\theta_{ce} & -\sin\theta_{ce} & 0 \\ 0 & 0 & 0 & \sin\theta_{ce} & \cos\theta_{ce} & 0 \\ 0 & 0 & 0 & 0 & 0 & 1 \end{bmatrix}. \tag{4.100}$$

The rotation angles now read $\theta_{ci,e} \sim \delta^2\omega_{ci,e}$. For simplicity we assume homogeneous magnetic field so $\omega_{ci,e} = constant$. The implementation of these rotations in the amplitude register is very simple and the quantum circuit for the product $\hat{V}_{ce}\hat{V}_{ci}$ is depicted in Fig.4.8.

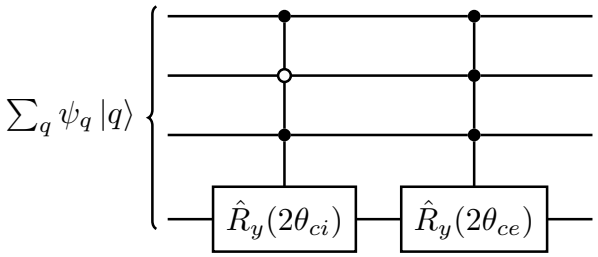

Figure 4.8: Quantum circuit implementation of the product $\hat{V}_{ce}\hat{V}_{ci}$ in the $\{|q\rangle\}$ coin register. The spatial dependence has been suppressed for simplicity.

Finally, moving on to the off-diagonal plasma frequency terms, we define

$$\hat{V}_{pi} = \begin{bmatrix} \cos\theta_{pe} & 0_{3\times 3} & -\sin\theta_{pi} & 0_{3\times 3} \\ 0_{3\times 3} & I_{3\times 3} & 0_{3\times 3} & 0_{3\times 3} \\ \sin\theta_{pi} & 0_{3\times 3} & \cos\theta_{pi} & 0_{3\times 3} \\ 0_{3\times 3} & 0_{3\times 3} & 0_{3\times 3} & I_{3\times 3} \end{bmatrix}, \quad \hat{V}_{pe} = \begin{bmatrix} \cos\theta_{pi} & 0_{3\times 3} & 0_{3\times 3} & -\sin\theta_{pe} \\ 0_{3\times 3} & I_{3\times 3} & 0_{3\times 3} & 0_{3\times 3} \\ 0_{3\times 3} & 0_{3\times 3} & I_{3\times 3} & 0_{3\times 3} \\ \sin\theta_{pe} & 0_{3\times 3} & 0 & \cos\theta_{pe} \end{bmatrix}, \tag{4.101}$$

with $\theta_{pi,e} \sim \delta^2 \omega_{pi,e}$ and the respective $\cos, \sin$ elements in Eq.(4.101) are diagonal 3×3 matrices. The quantum circuit implementation of the $\hat{V}_{pi,e}$ matrices of Eq.(4.101) is illustrated in Fig.4.9.

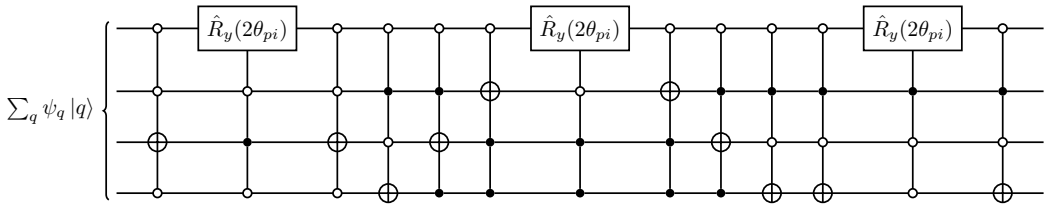

(a) Quantum circuit implementation of $\hat{V}_{pi}$ operator in Eq.(4.101). The spatial dependence has been suppressed for simplicity.

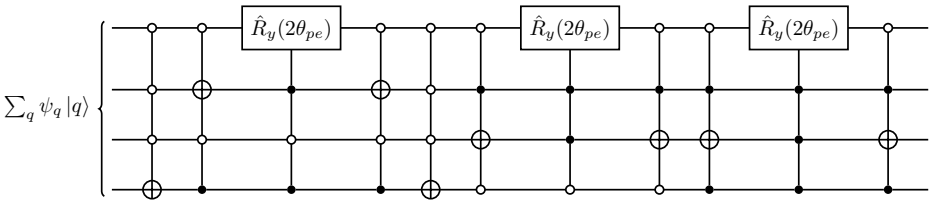

(b) Quantum circuit implementation of $\hat{V}_{pe}$ operator in Eq.(4.101). The spatial dependence has been suppressed for simplicity.

Figure 4.9: The quantum circuit implementation of $\hat{V}_{pi,e}$ operators in Eq.(4.101) and in the $\{|q\rangle\}$ register.

The locality of the collision operators in the $\mathscr{H}_C$ space guarantees that their implementation cost as shown in Figs.4.7-4.9 is constant $\sim O(4^2)$ for each of their two-level components. However, assuming an inhomogeneous plasma profile means that $\omega_{pi,e} = \omega_{pi,e}(\boldsymbol{r})$ and therefore the angles $\theta_{pi,e}$ take different values for each lattice cite $|p\rangle$. As a result, implementing the collision operators $\hat{V}_{pi,e}$ scales as $O(2^{n_p})$. Overall, the total implementation cost of the algorithm is $O(n_p^2 2^{n_p})$ in terms of the number of single qubit and CNOT gates. However, for applications in plasma physics, for example studying the electromagnetic scattering from localized inhomogeneous blobs and filaments [122, 123] it is safe to assume that

$$\left|\omega_{pi,e}\right\rangle = \sum_{p}^{poly(n_p)} \omega_{pi,e}(p) \left|p\right\rangle . \tag{4.102}$$

Equation (4.102) implies that the description of the inhomogeneity requires a sparse subset of the total 2^{n_p} states in $\mathscr{H}_S$. Then, the total implementation cost is reduced to $O[poly(n_p)]$. Since $n_p = \log_2(N)$ where $N = N_x N_y$ are the total lattice points the implementation scaling in terms of the spatial resources are $O[poly(log(N))]$.

Notably, the QLA implementation for magnetized plasmas achieves the same asymptotic scaling as the non-dispersive case, $O[poly(log(N))]$. This a direct consequence of the quantum walking process in the lattice which is handled efficiently through the streaming operator. As a result, the same considerations regarding the quantum advantage in-

dicator S_1 from Eq.(4.63) apply. However, now, the FDTD implementation scaling is actually worst than $O(N_x N_y)$ because for general anisotropic media (dispersive and non-dispersive), the staggered lattice segmentation of space means that the evolution of fields on each lattice side is not directly available at the required grid points. Consequently, an interpolation process is necessary [112, 120], introducing an additional complexity overhead that must be accounted for.

The total simulation time t_{total} is obtained after N_t applications of the evolution operator in Eq.(4.94) with $t_{total} = N_t \Delta t$ and the total simulation error ε reads,

$$\varepsilon = N_t \delta^4 = \frac{t_{total}^2}{N_t}. \tag{4.103}$$

Thus, the number N_t of time steps Δt is $N_t = t_{total}^2/\varepsilon$.

4.3.3 Clifford Geometric Algebra approach

The theoretical formulation of Maxwell equations for a cold inhomogeneous plasma, as described in Sec.4.3.2, can be geometrically extended in analogy to the full state-vector description in Eq. (4.74). This extension leverages the formalism of Clifford geometric algebras for electromagnetism [108, 109], thereby generalizing the standard RSW vector in Eq. (4.13).

To establish a Maxwell-Dirac isomorphism we employ the Clifford Geometric Algebra $\mathscr{C}l(\mathbb{R}^{1,3})$ which is called Dirac Algebra, $\mathscr{DA}$, or, alternatively, spacetime geometric algebra (STGA), which refers to the four dimensional Minkowskian spacetime, $\mathbb{R}^{1,3}$, with the metric $(1,-1,-1,-1)$. The mathematical structure and necessary involutions for the discussion that follows are detailed in Appendix A. can be found in the Appendix A. The underlying correspondence between this approach and Maxwell equations has been the subject of early work by Vaz and Rodrigues [124, 125].

In Clifford algebra $\mathscr{C}l(\mathbb{R}^{1,3})$, the electromagnetic bivector, along with its Clifford conjugate, (see Eq.(A.11)), are defined as follows:

$$\mathscr{F} = \mathscr{E} + c\mathscr{I}\mathscr{B}, \quad \mathscr{F}^\dagger = \mathscr{E} - c\mathscr{I}\mathscr{B}, \tag{4.104}$$

where $\mathscr{E}$ and $\mathscr{B}$ are space-time bivectors of the electric field intensity and the magnetic induction, respectively and $\mathscr{I}$ is the pseudo-scalar element of $\mathscr{DA}$,

$$\mathscr{I} = \gamma_{0123} = \gamma_0\gamma_1\gamma_2\gamma_3, \tag{4.105}$$

In components form (summation convention is adopted) one may write:

$$\mathscr{E} = E_m\gamma_m\gamma_0, \quad \mathscr{B} = B_m\gamma_m\gamma_0, \tag{4.106}$$

where the scalar amplitudes E_m, B_m, according to Eq.(A.2), read

$$E_m = \gamma_0 \cdot \mathscr{E} \cdot \gamma_m, \quad B_m = \gamma_0 \cdot \mathscr{B} \cdot \gamma_m. \tag{4.107}$$

Also, the electromagnetic bivector and its Clifford conjugate bear the property of a sign change upon reversion (defined in Sec.(A)), that is,

$$\tilde{\mathscr{F}} = -\mathscr{F}, \quad \tilde{\mathscr{F}}^\dagger = -\mathscr{F}^\dagger. \tag{4.108}$$

Considering the differential operator $\mathscr{D}$ operating geometrically on the electromagnetic bivector $\mathscr{F}$, that is, in accordance with Eq.(A.12),

$$\mathscr{D}\mathscr{F} = \mathscr{D} \cdot \mathscr{F} + \mathscr{D} \wedge \mathscr{F}, \tag{4.109}$$

as well as the polarization space-time bivector $\mathscr{P}$,

$$\mathscr{P} = P_m \gamma_m \gamma_0, \tag{4.110}$$

Maxwell equations for a general dielectric medium obtain the the compact Clifford form [109],

$$\begin{bmatrix} \mathscr{D} & 0 \\ 0 & \mathscr{D}^\dagger \end{bmatrix} \begin{bmatrix} \mathscr{F} \\ \mathscr{F}^\dagger \end{bmatrix} = -\frac{1}{\varepsilon_0} \begin{bmatrix} \mathscr{D}^\dagger & 0 \\ 0 & \mathscr{D} \end{bmatrix} \cdot \begin{bmatrix} \mathscr{P} \\ \mathscr{P} \end{bmatrix}. \tag{4.111}$$

For a cold magnetized plasma consisting of a-species,the explicit form of the polarization space-time bivector $\mathscr{P}$ in Eq.(4.110) depends on the space-time representation of the $\hat{K}^e$ operator in Eq.(4.80). This representation is also linked to the definition of the space-time conductivity current $\mathscr{J}$, as in Eq.(4.82),

$$\mathscr{J} \equiv \partial^0 \mathscr{P}, \tag{4.112}$$

which is also a bivector. Therefore, by gathering all the bivectorial entities $\mathscr{F}$, $\mathscr{F}^\dagger$, $\mathscr{P}^{(\alpha;L,R,\|)}$ and $\mathscr{J}^{(\alpha,;L,R,\|)}$ over all a-species and across the Left (L), Right (R) and parallel ($\|$) directions relative to the plasma magnetic axis, a Clifford spinor representing the quantum state $|\Psi\rangle$ is constructed,

$$|\Psi\rangle \equiv \left[\mathscr{F} \quad \mathscr{F}^\dagger \quad \left(\alpha; \tfrac{\mathscr{P}^L}{\varepsilon_0}\right) \quad \left(\alpha; \tfrac{\mathscr{P}^R}{\varepsilon_0}\right) \quad \left(\alpha; \tfrac{\mathscr{P}^\|}{\varepsilon_0}\right) \quad \left(\alpha; \tfrac{\mathscr{J}^L}{\varepsilon_0}\right) \quad \left(\alpha; \tfrac{\mathscr{J}^R}{\varepsilon_0}\right) \quad \left(\alpha; \tfrac{\mathscr{J}^\|}{\varepsilon_0}\right)\right]^T, \tag{4.113}$$

where $(\alpha; -)$ denotes contribution from each of the a-species. This leads to a Dirac-like representation,

$$\partial_0 |\Psi\rangle = \mathscr{W} \cdot |\Psi\rangle, \tag{4.114}$$

where the operator $\mathscr{W}$ is given by,

$$\mathscr{W} = \begin{bmatrix} \partial^l\gamma_{l0} & 0 & (\partial^l\gamma_{0l}\cdot,\alpha) & (\partial^l\gamma_{0l}\cdot,\alpha) & (\partial^l\gamma_{0l}\cdot,\alpha) & (-1,\alpha) & (-1,\alpha) & (-1,\alpha) \\ 0 & \partial^l\gamma_{0l} & (\partial^l\gamma_{0}\cdot,\alpha) & (\partial^l\gamma_{0}\cdot,\alpha) & (\partial^l\gamma_{0}\cdot,\alpha) & (-1,\alpha) & (-1,\alpha) & (-1,\alpha) \\ (0,\alpha) & (0,\alpha) & (0,\alpha) & (0,\alpha) & (0,\alpha) & (1,\alpha) & (0,\alpha) & (0,\alpha) \\ (0,\alpha) & (0,\alpha) & (0,\alpha) & (0,\alpha) & (0,\alpha) & (0,\alpha) & (1,\alpha) & (0,\alpha) \\ (0,\alpha) & (0,\alpha) & (0,\alpha) & (0,\alpha) & (0,\alpha) & (0,\alpha) & (0,\alpha) & (1,\alpha) \\ \left(\mathscr{S}^{(\alpha,L)}\cdot,\alpha\right) & \left(\mathscr{S}^{(\alpha,L)}\cdot,\alpha\right) & (0,\alpha) & (0,\alpha) & (0,\alpha) & \left(\frac{\varepsilon_\alpha\omega_{c\alpha}}{c},\alpha\right) & (0,\alpha) & (0,\alpha) \\ \left(\mathscr{S}^{(\alpha,R)}\cdot,\alpha\right) & \left(\mathscr{S}^{(\alpha,R)}\cdot,\alpha\right) & (0,\alpha) & (0,\alpha) & (0,\alpha) & (0,\alpha) & \left(-\frac{\varepsilon_\alpha\omega_{c\alpha}}{c},\alpha\right) & (0,\alpha) \\ \left(\mathscr{S}^{(\alpha,\|)}\cdot,\alpha\right) & \left(\mathscr{S}^{(\alpha,\|)}\cdot,\alpha\right) & (0,\alpha) & (0,\alpha) & (0,\alpha) & (0,\alpha) & (0,\alpha) & (0,\alpha) \end{bmatrix}, \tag{4.115}$$

with

$$\mathscr{S}^{(\alpha,L)} = -\varepsilon_0\frac{\omega_{p\alpha}^2}{4c^2}\left(\gamma_1\gamma_1+\gamma_2\gamma_2-2\gamma_0\gamma_3\right), \tag{4.116a}$$

$$\mathscr{S}^{(\alpha,R)} = -\varepsilon_0\frac{\omega_{p\alpha}^2}{4c^2}\left(\gamma_1\gamma_1+\gamma_2\gamma_2+2\gamma_0\gamma_3\right), \tag{4.116b}$$

$$\mathscr{S}^{(\alpha,\|)} = -\varepsilon_0\frac{\omega_{p\alpha}^2}{2c^2}\gamma_3\gamma_3. \tag{4.116c}$$

Equation (4.114) provides the Clifford representation of Eq.(4.75) for the plasma case, where the operator $\mathscr{W}$ is Hermitian under Clifford conjugation, satisfying $\mathscr{W} = \mathscr{W}^\dagger$.

4.4 Formulating dissipation

Returning to the Lorentz media Eqs.(4.65) and (4.66) with $\gamma_{e,l} \geq 0$ and $\gamma_{m,l} \geq 0$ (analogous considerations will apply to the plasma case for collisional dissipation). Consequently, the denominators in Eqs.(4.68) and (4.69) now include the appropriate factors of $-i\gamma_{e,l}$ and $-i\gamma_{m,l}$, respectively. As a result, the Hermitian structure of the Maxwell-Schrodinger evolution equation (4.75) is not preserved. While the first two Maxwell equations in (4.71) are not affected by dissipation, the third equation now reads,

$$i\frac{\partial\mathscr{P}_{l,t}}{\partial t} = i\boldsymbol{u} - i\hat{\omega}_l^2\mathscr{P}_l - i\hat{\gamma}_l\mathscr{P}_{l,t}, \qquad l = 1,2...N, \tag{4.117}$$

where,

$$\hat{\gamma}_l = \begin{bmatrix} \gamma_{e,l} & 0 \\ 0 & \gamma_{m,l} \end{bmatrix}. \tag{4.118}$$

The dissipative counterpart to Eq.(4.71) has the form,

$$i\frac{\partial\boldsymbol{\psi}}{\partial t} = [\hat{D} - i\hat{D}_{diss}]\boldsymbol{\psi}. \tag{4.119}$$

The diagonal matrix $\hat{D}_{diss} = diag(0,0,\hat{\gamma}_l)$ is Hermitian and positive definite ($\gamma_{e,l} \geq 0$ and $\gamma_{m,l} \geq 0$) so the anti-Hermitian term $-i\hat{D}_{diss}$ is purely dissipative. As a consequence, the non-Hermitian generator of dynamics $\hat{D} - i\hat{D}_{diss}$ in Eq.(4.119) possesses both real eigenvalues as well as complex eigenvalues but with negative imaginary part, indicating the absence of any global Parity-Time ($\mathscr{P}\mathscr{T}$) [44] or pseudo-Hermitian structure [49]. An example of $\mathscr{P}\mathscr{T}$-symmetry in electrodynamics is two coupled optical systems with balanced gain and loss [126] whereas a paradigm on unbroken pseudo-Hermitian structure of Maxwell equations in passive media for wave propagation can be found in [93]. Moreover, it has to be highlighted that even if $\mathscr{P}\mathscr{T}$ symmetry was present, by permitting gain (now some of $\gamma_{e,l}$ and $\gamma_{m,l}$ can be negative) in constitutive relations Eqs.(4.65) and (4.66), an unbroken $\mathscr{P}\mathscr{T}$ region where the non-Hermitian operator $\hat{D} - i\hat{D}_{diss}$ possesses only real eigenvalues will be present at discrete frequencies [126], due to Kramers-Kroning causality relations [99].

For an infinitesimal time step δt, starting at $t = 0$, a first order Suzuki-Trotter approximation [36] of the non-unitary operator $\hat{\mathscr{U}}(t) = \exp\{-it[\hat{D} - i\hat{D}_{diss}]\}$ yields,

$$\exp\{-i\delta t[\hat{D} - i\hat{D}_{diss}]\} = e^{-i\delta t\hat{D}} e^{-\delta t\hat{D}_{diss}} + O(\delta t^2). \tag{4.120}$$

This allows us to separate out the non-unitary term $\exp\{-\delta t\hat{D}_{diss}\}$. The diagonal dissipative operator $\hat{D}_{diss}$ contains at most $6N$ positive elements $(\gamma_{e,l}, \gamma_{m,l})$, $l = 1,\ldots N$. Then,

$$\exp\{-\delta t\hat{D}_{diss}\} = \hat{K}_0 = diag(I_{6\times 6}, I_{6N\times 6N}, \hat{\Gamma}), \tag{4.121}$$

where,

$$\hat{\Gamma} = \begin{bmatrix} e^{-\delta t\gamma_{e,l}} I_{3\times 3} & 0 \\ 0 & e^{-\delta t\gamma_{m,l}} I_{3\times 3} \end{bmatrix}. \tag{4.122}$$

The dimensions of the diagonal sub-matrix $\hat{\Gamma}$ are $6N \times 6N$.

4.4.1 Treating dissipation in the context of quantum channels

In the density matrix framework, the Suzuki-Trotter evolution (4.120) is,

$$\bar{\rho}(\delta t) = e^{-i\delta t\hat{D}} \hat{K}_0 \rho(0) \hat{K}_0^{\dagger} e^{i\delta t\hat{D}}, \tag{4.123}$$

where the initial density matrix $\rho(0)$ is,

$$\rho(0) = |\psi_0\rangle\langle\psi_0|, \quad |\psi_0\rangle = \frac{1}{\sqrt{E_0}} \sum_{j=0}^{d-1} \psi_{0j} |j\rangle, \quad d = (6+12N)N_xN_yN_z, \tag{4.124}$$

where $N_xN_yN_z$ are the number of nodes in the $3D$ lattice discetization. It should be noted that $\bar{\rho}(\delta t)$ is not a proper quantum mechanical density matrix, as the operation $\hat{K}_0\rho(0)\hat{K}_0^{\dagger}$

is not trace preserving (TP). Non-TP quantum channels emerge when a measurement is performed in the environment and selecting over a specific outcome [25]. Consequently, we can think of classical dissipation as a post-selective outcome from the interaction between a quantum represented lossless system and an unspecified environment. Accordingly, to retrieve the TP property we augment Eq.(4.123) with the term,

$$\hat{K}_1 \rho(0) \hat{K}_1, \tag{4.125}$$

where the second Kraus operator $\hat{K}_1$ satisfies $\hat{K}_1^\dagger \hat{K}_1 = I_{d\times d} - \hat{K}_0^\dagger \hat{K}_0$, and has an upper-triangular form,

$$\hat{K}_1 = \begin{bmatrix} 0 & \sqrt{I_{r\times r} - \hat{\Gamma}^2} \\ 0 & 0 \end{bmatrix}, \tag{4.126}$$

with $r = 6NN_xN_yN_z$ being the dimension of the dynamic space occupied by dissipation. The operator $\hat{K}_1$ corresponds to a transition – a quantum jump from the dissipative state of interest to a different state. The operators $\hat{K}_0$ and $\hat{K}_1$ are the multi-dimensional analogs of the amplitude damping channel operators in Eq.(2.58) The augmented quantum dissipative evolution for the open quantum system is similar to Eq.(4.57),

$$\rho_{aug}(\delta t) = e^{-i\delta t \hat{D}} \rho_{diss}(\delta t) e^{i\delta t \hat{D}}, \tag{4.127}$$

where,

$$\rho_{diss}(\delta t) = \hat{K}_0 \rho(0) \hat{K}_0^\dagger + \hat{K}_1 \rho(0) \hat{K}_1^\dagger. \tag{4.128}$$

The constructed linear CPTP quantum channel in Eqs.(4.127),(4.128) describes the evolution of the linear dynamics of an open quantum system, generated by the effective Hamiltonian $\hat{H}_{eff}$,

$$\hat{H}_{eff} = \hat{D} - i\hat{L}^\dagger \hat{L}, \quad \hat{L} = \begin{bmatrix} 0 & \sqrt{\hat{\gamma}_r} \\ 0 & 0 \end{bmatrix}. \tag{4.129}$$

The diagonal matrix $\hat{\gamma}_r$ represents dissipation in the r-dimensional subspace. The operator $\hat{L}$ is a Lindblad jump operator [41] and the generated Gorini–Kossakowski–Sudarshan–Lindblad (GKSL) master equation [41, 42] (also see Sec.2.4.2) is then,

$$\frac{\partial \rho}{\partial t} = -i\hat{H}_{eff}\rho + i\rho\hat{H}_{eff}^\dagger + 2\hat{L}\rho\hat{L}^\dagger. \tag{4.130}$$

For an infinitesimal time evolution $0 \to \delta t$, the density matrix evolution, to first order in δt, can be generated through the master equation (4.130) for the classical, non-Hermitian operator,

$$\rho(\delta t) = \hat{E}_0 \rho(0) \hat{E}_0^\dagger + \hat{E}_1 \rho(0) \hat{E}_1^\dagger, \tag{4.131}$$

with

$$\hat{E}_0 = I_{d\times d} - i\delta t\hat{D} - \delta t\hat{D}_{diss}, \quad \hat{E}_1 = \sqrt{2\delta t}\hat{L}. \tag{4.132}$$

By expanding in a Taylor series the Kraus operators in the augmented evolution Eq.(4.127) we obtain,

$$\rho_{aug}(\delta t) = \rho(\delta t) + O(\delta t^2). \tag{4.133}$$

Equation (4.133) confirms that treating the classical non-Hermitian operator $\hat{D} - i\hat{D}_{diss}$ as a quantum effective Hamiltonian generates, to first order, the same dynamics with the quantum channel establishing that this minimal augmented form is sufficient to capture the classical dissipative dynamics.

Since the set of Kraus operators $\hat{K}_0$ and $\hat{K}_1$ in Eq.(4.128) define a linear CPTP quantum channel, they are contractions [83]. Thus, a guaranteed minimal unitary dilation $\hat{\mathscr{U}}_{diss}$ can be formulated for according to Sec.3.3.2,

$$\hat{\mathscr{U}}_{diss} = \begin{bmatrix} \hat{K}_0 & -\hat{K}_1^\dagger \\ \hat{K}_1 & \hat{\mathscr{X}}\hat{K}_0\hat{\mathscr{X}} \end{bmatrix}. \tag{4.134}$$

The operator $\hat{\mathscr{X}}$ is an appropriate extension of the Pauli $\hat{X}$ operator to d-dimensions. The unitary $\hat{\mathscr{U}}_{diss}$ is a $2d \times 2d$ matrix operator acting on $n+1$ qubits with $n = \log_2 d$. The ancillary qubit represents the environment; the lossless system together with the environment form a closed conservative system that evolves under the unitary operator $\hat{\mathscr{U}}_{diss}$. This minimal dilation is related to the Sz. Nagy dilation (Sec.3.3.2) of $\hat{K}_0$ operator by a rotational transformation.

The action of $\hat{\mathscr{U}}_{diss}$ on the composite initial state $|0\rangle|\boldsymbol{\psi}_0\rangle$ yields,

$$|0\rangle\hat{K}_0|\boldsymbol{\psi}_0\rangle + |1\rangle\hat{K}_1|\boldsymbol{\psi}_0\rangle. \tag{4.135}$$

Next, we apply a controlled $e^{-i\delta t\hat{D}}$ operation to state (4.135) with respect to the 0-bit environment qubit, leading to the composite state,

$$|0\rangle e^{-i\delta t\hat{D}}\hat{K}_0|\boldsymbol{\psi}_0\rangle + |1\rangle\hat{K}_1|\boldsymbol{\psi}_0\rangle. \tag{4.136}$$

Subsequently, a projective measurement in the first qubit with operator $\hat{P}_0 = |0\rangle\langle 0| \otimes I_{d\times d}$ followed by tracing out the environment, leads to the non-unitary Suzuki-Trotter evolution equation (4.120) for the lossy, dispersive medium, up to a normalization factor with success probability $p_0(\delta t) = \langle\boldsymbol{\psi}_0|\hat{K}_0^2|\boldsymbol{\psi}_0\rangle$. The steps in Eqs.(4.135)-(4.136) along with the post-selection of the output state are illustrated in the quantum circuit in Fig.4.10.

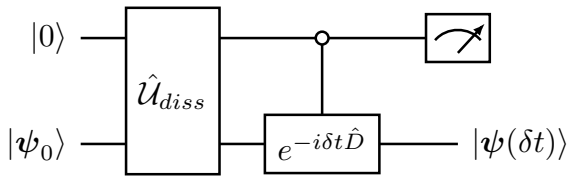

Figure 4.10: Quantum circuit for simulation of the non-unitary classical evolution Eq.(4.120) in a dissipative and dispersive electromagnetic medium.

The explicit form of $\hat{\mathscr{U}}_{diss}$ in Eq.(4.134) is,

$$\hat{\mathscr{U}}_{diss} = \begin{bmatrix} I_{(d-r)\times(d-r)} & 0 & 0 & 0 \\ 0 & \hat{\Gamma} & -\sqrt{I_{r\times r}-\hat{\Gamma}^2} & 0 \\ 0 & \sqrt{I_{r\times r}-\hat{\Gamma}^2} & \hat{\Gamma} & 0 \\ 0 & 0 & 0 & I_{(d-r)\times(d-r)} \end{bmatrix}. \tag{4.137}$$

Setting $\cos\theta_l/2 = \hat{\Gamma}_{ll}$, we can decompose $\hat{\mathscr{U}}_{diss}$ into r two-level unitary y-rotations, $\hat{\mathscr{R}}_y(\theta_l)$, acting on $n+1$ qubits,

$$\hat{\mathscr{U}}_{diss} = \prod_{l=1}^{r} \hat{\mathscr{R}}_y(\theta_l). \tag{4.138}$$

Hence, to leading order, we can implement $\hat{\mathscr{U}}_{diss}$ in $O(rn^2)$ CNOTs and a single qubit rotations $\hat{R}_y(\theta_l)$. Since $d = (6+12N)N_xN_yN_z = 6N_xN_yN_z + 2r = 2^n$ then $r = 2^{n-1}(1 - \frac{1}{1+2N})$, and the implementation of $\hat{\mathscr{U}}_{diss}$ is achieved using $O(2^{n-1}n^2)$ simple gates.

4.4.2 An optimized approach employing the LCU method

In the previous section, we showed a pathway to convert the non-unitary, diagonal, dissipative $\exp\{-\delta t\hat{D}_{diss}\}$ into $O(2^{n-1}n^2)$ elementary unitary gates, based on a constructed interconnection between dissipative and post-selective open quantum systems and classical dissipation. A different approach is to refrain from associating classical dissipation with a quantum process but treat $\hat{K}_0$ with the LCU method of Sec.3.2.1. Specifically, $\hat{K}_0$ in Eq.(4.121) can be written as a sum of two unitary matrices,

$$\hat{K}_0 = \frac{1}{2}(\hat{K}_{0z} + \hat{K}_{0z}^{\dagger}), \tag{4.139}$$

where,

$$\hat{K}_{0z} = \begin{bmatrix} I_{(d-r)\times(d-r)} & 0 \\ 0 & e^{-i\theta_l/2} \end{bmatrix}, \quad l = 1,2,...,r. \tag{4.140}$$

As previous, we have set $\cos\theta_l/2 = \hat{\Gamma}_{ll}$ and the unitary components in Eq.(4.139) remain diagonal. In order to apply the LCU method as described in Sec.3.2.1, we need one auxiliary qubit as in the dilation process of Sec.4.4.1. Then, according to Eqs.(3.35) and

(3.36) we introduce the unitary operators,

$$\hat{U}_{prep} : |0\rangle \rightarrow \frac{1}{\sqrt{2}}(|0\rangle + |1\rangle), \tag{4.141}$$

$$\hat{U}_{select} = |0\rangle\langle 0| \otimes \hat{K}_{0z} + |1\rangle\langle 1| \otimes \hat{K}_{0z}^{\dagger}, \tag{4.142}$$

where $\hat{U}_{prep} = \hat{H}$ is the Hadamard gate. We can probabilistically implement $\hat{K}_0$ using the unitary dilated operator,

$$\hat{\mathscr{U}}_{diss} = (\hat{H} \otimes I_{d\times d})\hat{U}_{select}(\hat{H} \otimes I_{d\times d}). \tag{4.143}$$

The action of $\hat{\mathscr{U}}_{diss}$ on the initial state $|0\rangle|\boldsymbol{\psi}_0\rangle$ is,

$$\hat{\mathscr{U}}_{diss}|0\rangle|\boldsymbol{\psi}_0\rangle = |0\rangle\hat{K}_0|\boldsymbol{\psi}_0\rangle + \frac{1}{2}|1\rangle(\hat{K}_{0z} - \hat{K}_{0z}^{\dagger})|\boldsymbol{\psi}_0\rangle. \tag{4.144}$$

Again, a measurement on the first qubit provides the desired result. Then, the quantum circuit representation for simulation of the Suzuki-Trotter dynamics (4.120), is depicted in Fig.4.11.4.11 The probability of measuring the 0-bit value qubit in the output state

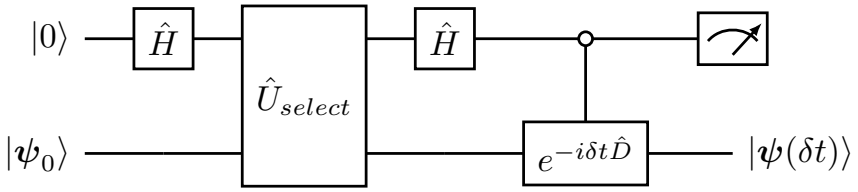

Figure 4.11: Quantum circuit for simulation of the non-unitary classical evolution (4.120) in a dissipative and dispersive medium using the LCU method.

(4.144) is agiain $p_0 = \langle\boldsymbol{\psi}_0|\hat{K}_0^2|\boldsymbol{\psi}_0\rangle$.

The remaining question is whether the implementation cost of $\hat{U}_{select}$ scales favorably compared to that of $\hat{\mathscr{U}}_{diss}$ from the previous section. Given the definition in (4.142), $\hat{U}_{select}$ is a $2d \times 2d$ diagonal operator,

$$\hat{U}_{select} = \begin{bmatrix} \hat{K}_{0z} & 0 \\ 0 & \hat{K}_{0z}^{\dagger} \end{bmatrix}, \tag{4.145}$$

which contains r two-level z-rotations $\hat{\mathscr{R}}_z(\theta_l)$ compared to the r two-level y-rotations $\hat{\mathscr{R}}_y(\theta_l)$ of Eq.(4.137). As a result, the diagonal nature of $\hat{U}_{select}$ allows for an implementation in $2^n(1 - \frac{1}{1+2N}) - 3$ alternating CNOTs and single-qubit $\hat{R}_z(\theta_l)$ rotations [127]. Thus, to leading order, a quadratic improvement is achieved as compared to the scaling of the physical dilation of the previous section. The LCU method produces the same dilation method, specialized for diagonal operators, as in [79].

4.4.3 Post-selection, time and total complexity of the algorithm

To first order in δt, the probability $p_0(\delta t) = \langle \boldsymbol{\psi}_0 | \hat{K}_0^2 | \boldsymbol{\psi}_0 \rangle$ for a successful post-selection is,

$$p_0(\delta t) = 1 - 2\delta t \sum_{q=d-r}^{d-1} \gamma_q \frac{|\psi_{0q}|^2}{E_0}. \tag{4.146}$$

where $p_0(\delta t)$ is bounded $p_{0min}(\delta t) \leq p_0(\delta t) \leq p_{0max}(\delta t)$,

$$p_{0min}(\delta t) = 1 - 2\gamma_{max}\delta t \sum_{q=d-r}^{d-1} \frac{|\psi_{0q}|^2}{E_0}, \tag{4.147}$$

$$p_{0max}(\delta t) = 1 - 2\gamma_{min}\delta t \sum_{q=d-r}^{d-1} \frac{|\psi_{0q}|^2}{E_0}, \tag{4.148}$$

with $r = 6NN_xN_yN_z$, $\gamma_{max} = \max\{\gamma_{e,l}, \gamma_{m,l}\}$, and $\gamma_{min} = \min\{\gamma_{e,l}, \gamma_{m,l}\}$, $l = 1, \ldots, r$. From Eq.(4.146), the optimal time-step δt for a high success post-selection out of the output state requires,

$$\delta t << \frac{1}{2\sum_{q=d-r}^{d-1} \gamma_q \frac{|\psi_{0q}|^2}{E_0}}. \tag{4.149}$$

Based on (4.147), the upper bound on δt is,

$$\Delta t_{diss} = \frac{1}{2\gamma_{max}\sum_{q=d-r}^{d-1} \frac{|\psi_{0q}|^2}{E_0}}, \tag{4.150}$$

with $\delta t << \Delta t_{diss}$, where the time step Δt_{diss} corresponds to the fast time scale $1/\gamma_{max}$ associated with dissipation – since $\sum_{q=d-r}^{d-1} \frac{|\psi_{0q}|^2}{E_0} \sim r/d \sim 1/2$, $\Delta t_{diss} \sim 1/\gamma_{max}$. Thus, for an accurate modeling of dissipation we have to select a simulation time step that is smaller than the fastest dissipative time scale. We have realized this physical conclusion solely from the quantum operational requirement of a highly successive post-selection process.

The non-normality of operator $\hat{D} - i\hat{D}_{diss}$ dictates that besides the dissipation time scale Δt_{diss} which is dominant for large simulation time, there is also a time scale $\Delta t_{uni} = 1/\lambda_{max}$ associated with the Hermitian part $\hat{D}$ with $\lambda_{max} = \lambda_{max}(n, \Omega_{e,m}, \omega_{e,m})$ the largest eigenvalue of operator $\hat{D}$ [128], depending on the number of qubits n and on the parameters present in operator $\hat{D}$. This time scale is dominant for small simulation time.

The quantum circuit in Figs.4.10 and 4.11 can be interpreted as a building blocks for a quantum simulation of total time $t_{total} = N_t \delta t$ in two different ways [129]. The first one utilizes the extra qubit globally and applies the quantum circuits of Figs.4.10,4.11, N_t consecutive times. Then, a single post-selection on the total output state is enough to

obtain the desired normalized non-unitary evolution,

$$|\psi(t_{total})\rangle = \frac{e^{-it_{total}(\hat{D}-i\hat{D}_{diss})}|\psi_0\rangle}{\left\|e^{-it_{total}(\hat{D}-i\hat{D}_{diss})}|\psi_0\rangle\right\|}. \tag{4.151}$$

However, taking into consideration the probability p_{total} for a successful post-selection at the final stage, this decays exponentially [128] as

$$p_{total} = \left\|e^{-it_{total}(\hat{D}-i\hat{D}_{diss})}|\psi_0\rangle\right\|^2. \tag{4.152}$$

Thus, Eq.(4.152) implies that we need an exponentially large number, N_t/p_{total}, of repetitions for obtaining the state (4.151) to within a desired error. This picture refers to monitoring only the continuous evolution of a quantum trajectory from a collection of them by disposing the trajectories with quantum jumps with a global post-selection process [128, 130]. The second implementation path for the total evolution is a repetition of the quantum circuits to be followed by a a post-selection with success probability p_0 each time. This local re-usage of the extra qubit in each step exploits the magnitude optimization Eq.(4.150) of probability p_0 relying on the dissipation characteristics. The post-selection complexity for the total evolution now reads $N_t/p_0^{N_t}$.

While the global method incorporates only one post-selection the exponentially small success rate of it, Eq.(4.152), renders it extremely costly in terms of resources for large time-scale simulation. Conversely, the local method demands of N_t post-selections which introduces a readout error, but the overall success rate is realizable after suitable selection of the δt time step.

For the local simulation method with the intermediate post-selections to be efficiently applied, a suitable selection of δt has to made in relation with the physical time scales Δt_{diss} and Δt_{uni} to capture the transient physical phenomena. However, a fine-meshing in the temporal domain directly affects the number of Trotter steps N_t required for a complete simulation time $t_{total} = N_t\delta t$ within an error ε. After N_t Trotter repetitions the error of the resulting (without considering the post-selection complexity overhead) non-unitary evolution $(e^{-i\delta t\hat{D}}e^{-i\delta t\hat{D}_{diss}})^{N_t}$ is [54],

$$\varepsilon \sim \frac{\gamma_{max}\lambda_{max}t_{total}^2}{N_t}\exp\left\{\frac{2(\lambda_{max}+\gamma_{max})}{N_t}t_{total}\right\} \tag{4.153}$$

reflecting the trade-off between the smallness of the time step δt and the number of repetitions N_t for the desired error scaling. Considering a more sophisticated and higher order product formulas [54] can lead to an optimized selection between the quantities $\varepsilon, N_t, \delta t$ and p_0.

Let us now combine the previous considerations of the case of a weakly dissipative

homogeneous dielectric medium. For such a simple $N = 1$ medium the diagonal matrix $\hat{U}_{select}$ contains repetitive values. It is then possible to further reduce the implementation cost of $\hat{U}_{select}$ to polynomial scaling $O[poly(n)]$, [131]. Similarly, according to the discussion in Sec.4.3.2, a QLA implementation of the unitary part $e^{-i\delta t\hat{D}}$ for the homogeneous case scales as $O(n^2)$. Consequently, the overall implementation scaling of the LCU quantum circuit of Fig.4.11 is $O[poly(n)+n^2]$. For a quantum simulation of total time $t_{total} = N_t\delta t$ the overall number of gates, taking into consideration the the local post-selection complexity reads $O\big[\frac{N_t}{p_0^{N_t}}(poly(n)+n^2)\big]$.

For a weakly dissipative medium in a specific frequency window [98] applies that,

$$\lambda_{max} >> \gamma, \quad \Delta t_{uni} << \Delta t_{diss}. \tag{4.154}$$

Hence, the dissipative time scale Δt_{diss} corresponds to the large scale temporal dynamics. Therefore, selecting a Trotter time scale $\delta t \sim \Delta t_{uni}$ a high success local post-selection process, Eq.(4.149), is guaranteed. The number N_t of the required Trotter steps to obtain the desired approximation within an error ε is provided in Eq.(4.153),

$$N_t = \frac{2\lambda_{max}t_{total}}{W(2\varepsilon/\gamma t_{total})}, \tag{4.155}$$

where $W(x)$ is the Lambert W function. The scaling law Eq.(4.155) for the number of Trotter steps N_t is interwoven with the different physical time-scales. For instance, aiming to simulate the dynamics for long total time $t_{total} \sim \kappa\Delta t_{diss}$ with $\kappa >> 1$ with constant error $\varepsilon \sim O(1)$ we obtain from Eq.(4.155),

$$N_t^l \sim \kappa^2\frac{\lambda_{max}}{\gamma}. \tag{4.156}$$

For simulation time $t_{total} = \kappa\Delta t_{uni} < \Delta t_{diss}$ with $\kappa > 1$, reflecting the transient dynamics, the number of required Trotter steps for constant error is,

$$N_t^t \sim \frac{2\kappa}{W(2\lambda_{max}/\kappa\gamma)}. \tag{4.157}$$

Finally, for short-scale simulation time $t_{total} = \kappa\Delta t_{uni}$ with $\kappa \sim O(1)$,

$$N_t^s \sim \frac{2\kappa}{\ln(2\lambda_{max}/\kappa\gamma)}. \tag{4.158}$$

In derivation of Eqs.(4.156)-(4.158) the following approximations $W(x << 1) \approx x$, $W(x >> 1) \approx \ln x$ have been used.

Consequently, the total number of gates N_{gates}, including the post-selection complex-

ity, required for simulation of the various temporal regimes with constant error ε is,

$$N_{gates} = \begin{cases} O\left[\kappa^2 \frac{\lambda_{max}}{\gamma p_0^{N_t^s}} (poly(n) + n^2)\right], & \text{for} \quad \kappa >> 1, \\ O\left[\frac{2\kappa}{p_0^{N_t^l} W(2\lambda_{max}/\kappa\gamma)} (poly(n) + n^2)\right], & \text{for} \quad \kappa > 1, \\ O\left[\frac{2\kappa}{p_0^{N_t^s} \ln(2\lambda_{max}/\kappa\gamma)} (poly(n) + n^2)\right], & \text{for} \quad \kappa \sim O(1), \end{cases} \tag{4.159}$$

where $p_0^{N_t^m} = \langle \psi_0 | \hat{K}_0^{2N_t^m} | \psi_0 \rangle$, for $m = s,t,l$. and $\lambda_{max} = \lambda_{max}(n, \Omega_e, \omega_e)$. Evidently, Eq.(4.159) proves a polynomial overall scaling of our algorithm as well as it is in accordance with the physical constrains and the transient nature of evolution, features that cannot be captured through quantum imaginary time evolution approaches [132, 133] which would be more suitable for calculation of low frequency modes rather than physical evolution implementation. In the same manner, allowing for different and inhomogeneous dissipation rates will result into complex temporal dynamics with different local basins of attraction, rendering the task of finding the correct solution very difficult even for modern variational quantum algorithms [134].

Chapter 5

Conclusions and Future Research

In concluding this thesis, the reader may find themselves with more questions than definitive answers to the question: "*Can quantum computers eventually surpass classical machines for scientific computing purposes?*" In the context of this work—where the Maxwell equations in plasmas and complex media are considered—the response leans towards "There are theoretical indications that quantum algorithms can be resource-efficient compared to classical counterparts for certain studies of electromagnetic wave propagation and scattering in plasmas and similar media."

However, a significant gap exists between the theoretical performance of quantum algorithms and their actual implementation, especially in the current Noisy Intermediate-Scale Quantum (NISQ) era. Noise and constraints on circuit depth and width heavily influence performance, highlighting the need for advances in quantum hardware to realize the practical potential of these algorithms. The ultimate answer will hinge on these advancements, which will determine the feasibility and efficiency of quantum algorithms for a variety of tasks.

To mitigate potential confusion and provide clarity, we asses our findings, suggest pathways for extending this research, and highlight open problems that may inspire the curious minds to address them in the future.

5.1 Key takeaways

- **Theoretical contributions**

    1. Established that every linear dynamics with a positive definite conserved quantity possess unitary dynamics which are explicitly retrieved by transforming the governing dynamical equations into a Hermitian structured Schrodinger representation. As a result, every conservative plasma physics problem admits an explicit unitary representation for wave dynamics.

2. Explored the quantum implementation of non-unitary operators within the framework of open quantum systems and unitary dilations.
3. Reformulating Maxwell equations in both dispersive and non-dispersive regimes. In the non-dissipative regime, the equations are treated as a closed quantum system, whereas in the dissipative regime, classical dissipation is mapped to a multi-dimensional analog of a quantum amplitude damping channel. While this post-selective open quantum system interpretation of classical dissipation scales quadratically worse than the LCU method, it can potentially benefit from leveraging the native quantum noise of the quantum hardware [135] as part of simulation better rather than serving as a pathway to unitary dilation.

- **Contributions on quantum computation**

1. Proposed a quantum walk based algorithm (QLA) for the quantum simulation of Maxwell equations in conservative media such as cold magnetized plasmas. The main advantages of the algorithm is its explicit nature in terms of scaling and error. For homogeneous media, whether dispersive or not, the primary computational cost is the walking process on the spatial lattice, which scales as $O(n_p^2)$, where n_p represents the number of qubits required to describe the grid points in the discretized space. For scattering from localized inhomogeneities, the quantum algorithm maintains an appealing scaling of $O(\text{poly}(n_p))$.
2. The explicit implementation complexity of the algorithm in terms quantum gates, demonstrates that simple test cases such as the propagation of a pulse in a uniform medium can be used to benchmark quantum computer performance under realistic error conditions for a physical problem. This will highlight a paradigm shift in using quantum computers for scientific computing, as shown in similar applications to hydrodynamics [136].
3. As supported by Eq.(4.63), that the proposed quantum algorithm exhibits an exponential quantum advantage in implementation resources compared to the widely used classical FTDTD method.
4. Finally, a post-selective quantum algorithm has been developed to handle simple collisional dissipation using the LCU method, achieving polynomial scaling for multiple dissipation rates as well as capturing distinct transient regimes effectively.

5.2 Open problems and future research directions

Two significant challenges that quantum computing faces in quantum simulation is addressing general non-unitary evolution and non-linear dynamics.

The quantum simulation of linear but non-unitary dynamics is typically addressed using dilation methods, as outlined in Sec. 3.3.2, with notable examples including the LCU method [74] and Schrodingerization [137]. However, these methods become less efficient when the dynamics involve not only dissipation but also amplification components, which may represent instabilities in classical dynamics or PTP open quantum systems. To address this challenge, we have proposed a biorthogonal dilation method [138] as an alternative approach tailored to such scenarios.

As quantum mechanics is inherently a linear physical theory, handling non-linear dynamics remains an area of active research and debate. In the design of quantum algorithms for non-linear dynamics, particularly in the context of partial differential equations, the community has explored linear embedding methods such as the Koopman–von Neumann formulation of classical mechanics and Carleman linearization [8, 139, 140]. However, these methods encounter limitations when attempting to delve into the chaotic or turbulent regimes [141], which are often where the most interesting physics occurs. A primary issue with these linear embedding techniques is that, while they enable the quantum simulation of non-linear classical systems, the necessary projection into a finite-dimensional space can introduce numerical artifacts. These artifacts are difficult to control or even to eliminate tehm, hence comprising the accuracy of the simulation [142].

An alternative approach, motivated by the works of Childs and Geller [143, 144] explores performing ”impossible tasks” through consistent non-linear extensions of quantum mechanics as well as probabilistic non-linear transformations [145]. Towards the former direction, one can establish connections with classical dynamical systems theory [146] or develop non-linear quantum representations for simulation [147]. In the latter, the non-linear transformations can be incorporated as components of the quantum algorithms [148].

References

[1] J. P. Dowling and G. J. Milburn. "Quantum technology: the second quantum revolution". In: *Phil. Trans. R. Soc. A.* 361 (2003), pp. 1655–1674. DOI: 10.1098/rsta.2003.1227.

[2] J. Preskill. "Quantum Computing in the NISQ era and beyond". In: *Quantum* 2 (2018), p. 79. DOI: 10.22331/q-2018-08-06-79.

[3] J. Yin et al. "Satellite-based entanglement distribution over 1200 kilometers". In: *Science* 356.6343 (2017), pp. 1140–1144. DOI: 10.1126/science.aan3211.

[4] F. Arute et al. "Quantum supremacy using a programmable superconducting processor." In: *Nature* 574 (2019), pp. 505–510. DOI: 10.1038/s41586-019-1666-5.

[5] Y. Wu et al. "Strong Quantum Computational Advantage Using a Superconducting Quantum Processor". In: *Phys. Rev. Lett.* 127 (18 2021), p. 180501. DOI: 10.1103/PhysRevLett.127.180501.

[6] A. Robert, P. K. Barkoutsos, S. Woerner, and I. Tavernelli. "Resource-efficient quantum algorithm for protein folding". In: *npj Quantum Inf.* 07 (38 2021). DOI: 10.1038/s41534-021-00368-4.

[7] J. Biamonte, P. Wittek, N. Pancotti, P. Rebentrost, N. Wiebe, and S. Lloyd. "Quantum machine learning". In: *Nature* 549 (2017), pp. 195–202. DOI: 10.1038/nature23474.

[8] I. Joseph. "Koopman–von Neumann approach to quantum simulation of nonlinear classical dynamics". In: *Phys. Rev. Res.* 2 (4 2020), p. 043102. DOI: 10.1103/PhysRevResearch.2.043102.

[9] S. Succi, W. Itani, K. Sreenivasan, and R. Steijl. "Quantum computing for fluids: Where do we stand?" In: *EPL* 144.1 (2023), p. 10001. DOI: 10.1209/0295-5075/acfdc7.

[10] T. Schenkel, B. Dorland, A. Baczewski, M. Boshier, G. Collins, J. Dubois, A. Houck, T. Humble, N. Loureiro, C. Monroe, et al. *Fusion Energy Sciences Roundtable on Quantum Information Science*. Tech. rep. May 2018. DOI: 10.2172/1615242.

[11] I. Y. Dodin and E. A. Startsev. "On applications of quantum computing to plasma simulations". In: *Phys. Plasmas* 28.9 (2021), p. 092101. DOI: 10.1063/5.0056974.

[12] I. Joseph, Y. Shi, M. D. Porter, A. R. Castelli, V. I. Geyko, F. R. Graziani, S. B. Libby, and J. L. DuBois. "Quantum computing for fusion energy science applications". In: *Phys. Plasmas* 30.1 (2023), p. 010501. DOI: 10.1063/5.0123765.

[13] Ó. Amaro and D. Cruz. *A Living Review of Quantum Computing for Plasma Physics*. 2023. arXiv: 2302.00001 [physics.plasm-ph].

[14] H. T. Stix. *Waves in Plasmas*. American Institute of Physics, 1992.

[15] D. G. Swanson. *Plasma Waves*. CRC Press, 2003. DOI: 10.1201/9780367802721.

[16] C. Lau, E. Jaeger, N. Bertelli, L. Berry, D. Green, M. Murakami, J. Park, R. Pinsker, and R. Prater. "AORSA full wave calculations of helicon waves in DIII-D and ITER". In: *Nucl. Fusion* 58.6 (2018), p. 066004. DOI: 10.1088/1741-4326/aab96d.

[17] P. A. M. Dirac. *The Principles of Quantum Mechanics*. Oxford, Clarendon Press, 1930.

[18] L. D. Landau and E. M. Lifshits. *Quantum Mechanics: Non-Relativistic Theory*. Vol. v.3. Course of Theoretical Physics. Oxford: Butterworth-Heinemann, 1991. ISBN: 978-0-7506-3539-4.

[19] J. Audretsch. *Entangled Systems: New Directions in Quantum Physics*. John Wiley & Sons, Ltd, 2007. ISBN: 9783527619153. DOI: 10.1002/9783527619153.

[20] D. J. Griffiths and D. F. Schroeter. *Introduction to Quantum Mechanics*. 3rd ed. Cambridge University Press, 2018. DOI: 10.1017/9781316995433.

[21] J. J. Sakurai and J. Napolitano. *Modern Quantum Mechanics*. 3rd ed. Cambridge University Press, 2020. DOI: 10.1017/9781108587280.

[22] R. A. Horn and C. R. Johnson. *Matrix Analysis*. Cambridge University Press, 1985. DOI: d10.1017/CBO9780511810817.

[23] M. H. Stone. "On One-Parameter Unitary Groups in Hilbert Space". In: *Ann. Math.* 33.3 (1932), pp. 643–648. DOI: 10.2307/1968538.

[24] C. Helstrom. "Quantum detection and estimation theory". In: *J. Stat. Phys.* 1 (2 1969), pp. 231–252. DOI: 10.1007/BF01007479.

[25] M. A. Nielsen and I. L. Chuang. *Quantum Computation and Quantum Information: 10th Anniversary Edition*. Cambridge University Press, 2010. DOI: 10.1017/CBO9780511976667.

[26] A. Barenco, C. H. Bennett, R. Cleve, D. P. DiVincenzo, N. Margolus, P. Shor, T. Sleator, J. A. Smolin, and H. Weinfurter. "Elementary gates for quantum computation". In: *Phys. Rev. A* 52 (5 1995), pp. 3457–3467. DOI: 10.1103/PhysRevA.52.3457.

[27] M. Möttönen, J. J. Vartiainen, V. Bergholm, and M. M. Salomaa. "Quantum Circuits for General Multiqubit Gates". In: *Phys. Rev. Lett.* 93 (13 2004), p. 130502. DOI: 10.1103/PhysRevLett.93.130502.

[28] A. J. da Silva and D. K. Park. "Linear-depth quantum circuits for multiqubit controlled gates". In: *Phys. Rev. A* 106 (4 2022), p. 042602. DOI: 10.1103/PhysRevA.106.042602.

[29] B. Claudon, J. Zylberman, C. Feniou, F. Debbasch, A. Peruzzo, and J.-P. Piquemal. *Polylogarithmic-depth controlled-NOT gates without ancilla qubits*. 2024. arXiv: 2312.13206 [quant-ph].

[30] R. Vale, T. M. D. Azevedo, I. C. S. Araújo, I. F. Araujo, and A. J. da Silva. "Circuit Decomposition of Multicontrolled Special Unitary Single-Qubit Gates". In: *IEEE Transactions on Computer-Aided Design of Integrated Circuits and Systems* 43.3 (2024), pp. 802–811. DOI: 10.1109/TCAD.2023.3327102.

[31] P. W. Shor. "Polynomial-Time Algorithms for Prime Factorization and Discrete Logarithms on a Quantum Computer". In: *SIAM J. Comput.* 26.5 (1997), pp. 1484–1509. DOI: 10.1137/S0097539795293172.

[32] G. H. Low and I. L. Chuang. "Optimal Hamiltonian Simulation by Quantum Signal Processing". In: *Phys. Rev. Lett.* 118 (1 2017), p. 010501. DOI: 10.1103/PhysRevLett.118.010501.

[33] A. W. Harrow, A. Hassidim, and S. Lloyd. "Quantum Algorithm for Linear Systems of Equations". In: *Phys. Rev. Lett.* 103 (15 2009), p. 150502. DOI: 10.1103/PhysRevLett.103.150502.

[34] R. P. Feynman. "Simulating physics with computers". In: *Int. J. Theor. Phys.* 21 (05 1982), pp. 467–488. DOI: 10.1007/BF02650179.

[35] S. Lloyd. "Universal Quantum Simulators". In: *Science* 273.5278 (1996), pp. 1073–1078. DOI: 10.1126/science.273.5278.1073.

[36] M. Suzuki. "General theory of fractal path integrals with applications to many–body theories and statistical physics". In: *J. Math. Phys.* 32.2 (1991), pp. 400–407. DOI: 10.1063/1.529425.

[37] D. W. Berry, G. Ahokas, and B. C. Cleve Richard andSanders. "Efficient Quantum Algorithms for Simulating Sparse Hamiltonians". In: *Commun. Math. Phys.* 270 (2 2007), pp. 359–371. DOI: 10.1007/s00220-006-0150-x.

[38] L. K. Grover. "A fast quantum mechanical algorithm for database search". In: *Proceedings of the Twenty-Eighth Annual ACM Symposium on Theory of Computing*. STOC '96. Philadelphia, Pennsylvania, USA: Association for Computing Machinery, 1996, pp. 212–219. ISBN: 0897917855. DOI: 10.1145/237814.237866.

[39] G. Brassard, P. Høyer, M. Mosca, and A. Tapp. "Quantum amplitude amplification and estimation". In: *Quantum computation and information*. Vol. 305. Contemporary Mathematics, 2002, pp. 53–74. DOI: doi.org/10.1090/conm/305.

[40] H.-P. Breuer and F. Petruccione. *The Theory of Open Quantum Systems*. Oxford University Press, Jan. 2007. ISBN: 9780199213900. DOI: 10.1093/acprof:oso/9780199213900.001.0001.

[41] G. Lindblad. "On the generators of quantum dynamical semigroups". In: *Commun. Math. Phys.* 48 (02 1976), pp. 119–130. DOI: 10.1007/BF01608499.

[42] V. Gorini, A. Kossakowski, and E. C. G. Sudarshan. "Completely positive dynamical semigroups of *N*–level systems". In: *Journal of Mathematical Physics* 17.5 (1976), pp. 821–825. DOI: 10.1063/1.522979.

[43] F. J. Dyson. “General Theory of Spin-Wave Interactions”. In: *Phys. Rev.* 102 (5), pp. 1217–1230. DOI: 10.1103/PhysRev.102.1217.

[44] C. M. Bender and S. Boettcher. “Real Spectra in Non-Hermitian Hamiltonians Having PT Symmetry”. In: *Phys. Rev. Lett.* 80 (24 1998), pp. 5243–5246. DOI: 10.1103/PhysRevLett.80.5243.

[45] A. Mostafazadeh. “Pseudo-Hermiticity versus PT symmetry: The necessary condition for the reality of the spectrum of a non-Hermitian Hamiltonian”. In: *J. Math. Phys.* 43.1 (Jan. 2002), pp. 205–214. DOI: 10.1063/1.1418246.

[46] A. Mostafazadeh. “Pseudo-Hermiticity versus PT-symmetry. II. A complete characterization of non-Hermitian Hamiltonians with a real spectrum”. In: *J. Math. Phys.* 43.5 (May 2002), pp. 2814–2816. DOI: 10.1063/1.1461427.

[47] A. Mostafazadeh. “Pseudo-Hermiticity versus PT-symmetry III: Equivalence of pseudo-Hermiticity and the presence of antilinear symmetries”. In: *J. Math. Phys.* 43.8 (Aug. 2002), pp. 3944–3951. DOI: 10.1063/1.1489072.

[48] M. Znojil. “Time-dependent version of crypto-Hermitian quantum theory”. In: *Phys. Rev. D* 78 (8 2008), p. 085003. DOI: 10.1103/PhysRevD.78.085003.

[49] A. Mostafazadeh. “Pseudo-Hermitian representation of quantum mechanics”. In: *Int. J. Geom. Methods Mod.* 07.07 (2010), pp. 1191–1306. DOI: 10.1142/S0219887810004816.

[50] A. Fring and M. H. Y. Moussa. “Unitary quantum evolution for time-dependent quasi-Hermitian systems with nonobservable Hamiltonians”. In: *Phys. Rev. A* 93 (4 2016), p. 042114. DOI: 10.1103/PhysRevA.93.042114.

[51] M. Znojil. “Hybrid form of quantum theory with non-Hermitian Hamiltonians”. In: *Phys. Lett. A* 457 (2023), p. 128556. DOI: https://doi.org/10.1016/j.physleta.2022.128556.

[52] J. P. H. Goedbloed and S. Poedts. *Principles of Magnetohydrodynamics: With Applications to Laboratory and Astrophysical Plasmas*. Cambridge University Press, 2004. DOI: 10.1017/CBO9780511616945.

[53] D. W. Berry. “High-order quantum algorithm for solving linear differential equations”. In: *J. Phys. A* 47.10 (2014), p. 105301. DOI: 10.1088/1751-8113/47/10/105301.

[54] A. M. Childs, Y. Su, M. C. Tran, N. Wiebe, and S. Zhu. “Theory of Trotter Error with Commutator Scaling”. In: *Phys. Rev. X* 11 (1 2021), p. 011020. DOI: 10.1103/PhysRevX.11.011020.

[55] G. H. Low and I. L. Chuang. “Hamiltonian Simulation by Qubitization”. In: *Quantum* 3 (2019), p. 163. DOI: 10.22331/q-2019-07-12-163.

[56] H. Krovi. “Improved quantum algorithms for linear and nonlinear differential equations”. In: *Quantum* 7 (2023), p. 913. DOI: 10.22331/q-2023-02-02-913.

[57] D. W. Berry, A. M. Childs, R. Cleve, R. Kothari, and R. D. Somma. “Simulating Hamiltonian Dynamics with a Truncated Taylor Series”. In: *Phys. Rev. Lett.* 114 (9 2015), p. 090502. DOI: 10.1103/PhysRevLett.114.090502.

[58] A. M. Childs and N. Wiebe. “Hamiltonian simulation using linear combinations of unitary operations”. In: *Quantum Info. Comput.* 12.11–12 (2012), pp. 901–924. DOI: 10.26421/QIC12.11-12-1.

[59] D. W. Berry, A. M. Childs, and R. Kothari. “Hamiltonian Simulation with Nearly Optimal Dependence on all Parameters”. In: *Proceedings of the 2015 IEEE 56th Annual Symposium on Foundations of Computer Science (FOCS)*. FOCS ’15. 2015, pp. 792–809. DOI: 10.1109/FOCS.2015.54.

[60] A. M. Childs, R. Cleve, E. Deotto, E. Farhi, S. Gutmann, and D. A. Spielman. “Exponential algorithmic speedup by a quantum walk”. In: *Proceedings of the Thirty-Fifth Annual ACM Symposium on Theory of Computing*. STOC ’03. San Diego, CA, USA: Association for Computing Machinery, 2003, pp. 59–68. ISBN: 1581136749. DOI: 10.1145/780542.780552.

[61] A. M. Childs, D. Maslov, Y. Nam, N. J. Ross, and Y. Su. “Toward the first quantum simulation with quantum speedup”. In: *PNAS* 115.38 (2018), pp. 9456–9461. DOI: 10.1073/pnas.1801723115.

[62] Y. Aharonov, L. Davidovich, and N. Zagury. “Quantum random walks”. In: *Phys. Rev. A* 48 (2 1993), pp. 1687–1690. DOI: 10.1103/PhysRevA.48.1687.

[63] A. Ambainis, E. Bach, A. Nayak, A. Vishwanath, and J. Watrous. “One-dimensional quantum walks”. In: *Proceedings of the Thirty-Third Annual ACM Symposium on Theory of Computing*. STOC ’01. Hersonissos, Greece: Association for Computing Machinery, 2001, pp. 37–49. ISBN: 1581133499. DOI: 10.1145/380752.380757.

[64] I. Bialynicki-Birula. “Weyl, Dirac, and Maxwell equations on a lattice as unitary cellular automata”. In: *Phys. Rev. D* 49 (12 1994), pp. 6920–6927. DOI: 10.1103/PhysRevD.49.6920.

[65] F. ç. Fillion-Gourdeau, S. MacLean, and R. Laflamme. “Algorithm for the solution of the Dirac equation on digital quantum computers”. In: *Phys. Rev. A* 95 (4 2017), p. 042343. DOI: 10.1103/PhysRevA.95.042343.

[66] L. Mlodinow and T. A. Brun. “Discrete spacetime, quantum walks, and relativistic wave equations”. In: *Phys. Rev. A* 97 (4 2018), p. 042131. DOI: 10.1103/PhysRevA.97.042131.

[67] U. Nzongani, N. Eon, I. Márquez-Martín, A. Pérez, G. Di Molfetta, and P. Arrighi. “Dirac quantum walk on tetrahedra”. In: *Phys. Rev. A* 110 (4 2024), p. 042418. DOI: 10.1103/PhysRevA.110.042418.

[68] B. M. Boghosian and W. Taylor. “Quantum lattice-gas model for the many-particle Schrödinger equation in d dimensions”. In: *Phys. Rev. E* 57 (1 1998), pp. 54–66. DOI: 10.1103/PhysRevE.57.54.

[69] J. Yepez and B. Boghosian. “An efficient and accurate quantum lattice-gas model for the many-body Schrödinger wave equation”. In: *Computer Physics Communications* 146.3 (2002), pp. 280–294. DOI: https://doi.org/10.1016/S0010-4655(02)00419-8.

[70] S. Succi, F. Fillion-Gourdeau, and S. Palpacelli. “Dirac quantum walk on tetrahedra”. In: *EPJ Quantum Technol.* 02 (01 2015), p. 042418. DOI: 10.1140/epjqt/s40507-015-0025-1.

[71] J. Yepez and B. Boghosian. “An efficient and accurate quantum lattice-gas model for the many-body Schrodinger wave equation”. In: *Comput. Phys. Commun.* 146.3 (2002), pp. 280–294. DOI: 10.1016/S0010-4655(02)00419-8.

[72] J. Yepez. *An efficient and accurate quantum algorithm for the Dirac equation*. 2002. DOI: 10.48550/arXiv.quant-ph/0210093. arXiv: quant-ph/0210093 [quant-ph].

[73] L. Gui-Lu. “General Quantum Interference Principle and Duality Computer”. In: *Commun. Theor. Phys.* 45.5 (2006), p. 825. DOI: 10.1088/0253-6102/45/5/013.

[74] D. An, J.-P. Liu, and L. Lin. “Linear Combination of Hamiltonian Simulation for Nonunitary Dynamics with Optimal State Preparation Cost”. In: *Phys. Rev. Lett.* 131 (15 2023), p. 150603. DOI: 10.1103/PhysRevLett.131.150603.

[75] P. Wu. “Additive combinations of special operators”. In: *Banach Center Publ.* 30.1 (1994), pp. 337–361. URL: http://eudml.org/doc/262750.

[76] O. M. Shalit. “Dilation Theory: A Guided Tour”. In: *Operator Theory, Functional Analysis and Applications*. Ed. by M. A. Bastos, L. Castro, and A. Y. Karlovich. Springer International Publishing, 2021, pp. 551–623. DOI: 10.1007/978-3-030-51945-2_28.

[77] “A quantum algorithm for evolving open quantum dynamics on quantum computing devices”. In: *Sci. Rep.* 10 (01 2020), p. 3301. DOI: 10.1038/s41598-020-60321.

[78] A. W. Schlimgen, K. Head-Marsden, L. M. Sager, P. Narang, and D. A. Mazziotti. “Quantum Simulation of Open Quantum Systems Using a Unitary Decomposition of Operators”. In: *Phys. Rev. Lett.* 127 (27 2021), p. 270503. DOI: 10.1103/PhysRevLett.127.270503.

[79] A. W. Schlimgen, K. Head-Marsden, L. M. Sager-Smith, P. Narang, and D. A. Mazziotti. “Quantum state preparation and nonunitary evolution with diagonal operators”. In: *Phys. Rev. A* 106 (2 2022), p. 022414. DOI: 10.1103/PhysRevA.106.022414.

[80] A. W. Schlimgen, K. Head-Marsden, L. M. Sager-Smith, P. Narang, and D. A. Mazziotti. *Quantum Simulation of Open Quantum Systems Using Density-Matrix Purification*. 2022. DOI: 10.48550/arXiv.2207.07112. arXiv: 2207.07112 [quant-ph].

[81] N. Suri, J. Barreto, S. Hadfield, N. Wiebe, F. Wudarski, and J. Marshall. “Two-Unitary Decomposition Algorithm and Open Quantum System Simulation”. In: *Quantum* 7 (2023), p. 1002. DOI: 10.22331/q-2023-05-15-1002.

[82] J. Hubisz, B. Sambasivam, and J. Unmuth-Yockey. "Quantum algorithms for open lattice field theory". In: *Phys. Rev. A* 104 (5 2021), p. 052420. DOI: 10.1103/PhysRevA.104.052420.

[83] R. Hu Z.and Xia and S. Kais. "A quantum algorithm for evolving open quantum dynamics on quantum computing devices". In: *Sci. Rep.* 10 (2020), p. 3301. DOI: 10.1038/s41598-020-60321-x.

[84] S. Sinha and P. Russer. "Quantum computing algorithm for electromagnetic field simulation". In: *Quantum Inf. Process.* 09.3 (2010), pp. 385–404. DOI: 10.1007/s11128-009-0133-x.

[85] P. C. S. Costa, S. Jordan, and A. Ostrander. "Quantum algorithm for simulating the wave equation". In: *Phys. Rev. A* 99 (1 2019), p. 012323. DOI: 10.1103/PhysRevA.99.012323.

[86] J. Zhang, F. Feng, and Q. J. Zhang. "Quantum Method for Finite Element Simulation of Electromagnetic Problems". In: *2021 IEEE MTT-S International Microwave Symposium (IMS)*. 2021, pp. 120–123. DOI: 10.1109/IMS19712.2021.9574852.

[87] R. Novak. "Quantum Algorithms in Electromagnetic Propagation Modelling for Telecommunications". In: *IEEE Access* 11 (2023), pp. 111545–111565. DOI: 10.1109/ACCESS.2023.3322446.

[88] I. Novikau, I. Dodin, and E. Startsev. "Simulation of Linear Non-Hermitian Boundary-Value Problems with Quantum Singular-Value Transformation". In: *Phys. Rev. Appl.* 19 (5 2023), p. 054012. DOI: 10.1103/PhysRevApplied.19.054012.

[89] Jin, Shi, Liu, Nana, and Ma, Chuwen. "Quantum simulation of Maxwell's equations via Schrödingerisation". In: *ESAIM: M2AN* 58.5 (2024), pp. 1853–1879. DOI: 10.1051/m2an/2024046.

[90] N. Nguyen and R. Thompson. *Solving Maxwells Equations using Variational Quantum Imaginary Time Evolution*. 2024. arXiv: 2402.14156 [quant-ph]. URL: https://arxiv.org/abs/2402.14156.

[91] G. Vahala, L. Vahala, M. Soe, and A. K. Ram. "Unitary quantum lattice simulations for Maxwell equations in vacuum and in dielectric media". In: *J. Plasma Phys.* 86.5 (2020), p. 905860518. DOI: 10.1017/S0022377820001166.

[92] A. K. Ram, G. Vahala, L. Vahala, and M. Soe. "Reflection and transmission of electromagnetic pulses at a planar dielectric interface: Theory and quantum lattice simulations". In: *AIP Advances* 11.10 (2021), p. 105116. DOI: 10.1063/5.0067204.

[93] E. Koukoutsis, K. Hizanidis, A. K. Ram, and G. Vahala. "Dyson maps and unitary evolution for Maxwell equations in tensor dielectric media". In: *Phys. Rev. A* 107 (4 2023), p. 042215. DOI: 10.1103/PhysRevA.107.042215.

[94] E. Koukoutsis, K. Hizanidis, G. Vahala, M. Soe, L. Vahala, and A. K. Ram. "Quantum computing perspective for electromagnetic wave propagation in cold magnetized plasmas". In: *Phys. Plasmas* 30.12 (2023), p. 122108. DOI: 10.1063/5.0177589.

[95] G. Vahala, M. Soe, L. Vahala, A. K. Ram, E. Koukoutsis, and K. Hizanidis. "Qubit lattice algorithm simulations of Maxwell's equations for scattering from anisotropic dielectric objects". In: *Comput. Fluids* 266 (2023), p. 106039. DOI: https://doi.org/10.1016/j.compfluid.2023.106039.

[96] G. Vahala, M. Soe, E. Koukoutsis, K. Hizanidis, L. Vahala, and A. K. Ram. "Qubit Lattice Algorithms Based on the Schrödinger-Dirac Representation of Maxwell Equations and Their Extensions". In: *Schrödinger Equation*. Ed. by M. B. Tahir, M. Sagir, M. I. Khan, and M. Rafique. Rijeka: IntechOpen, 2023. Chap. 7. DOI: 10.5772/intechopen.112692.

[97] E. Koukoutsis, K. Hizanidis, A. K. Ram, and G. Vahala. "Quantum simulation of dissipation for Maxwell equations in dispersive media". In: *Future Gener. Comput. Syst.* 159 (2024), pp. 221–229. DOI: 10.1016/j.future.2024.05.028.

[98] L. D. Landau, L. P. Pitaevskii, and E. M. Lifshitz. *Electrodynamics of Continuous Media*. Butterworth-Heinemann, 1984.

[99] J. D. Jackson. *Classical Electrodynamics*. New York: Wiley, 1998.

[100] A. S. I.V. Lindell and K. Suchy. "Six-vector formalism in electromagnetics of bi-anisotropic media". In: *J. Electromagn. Waves Appl.* 9.7-8 (1995), pp. 887–903. DOI: 10.1163/156939395X00631.

[101] G. F. Roach, I. G. Stratis, and A. N. Yannacopoulos. *Mathematical Analysis of Deterministic and Stochastic Problems in Complex Media Electromagnetics*. Princeton University Press, 2012. ISBN: 9780691142173. URL: http://www.jstor.org/stable/j.ctt7t1xz.

[102] A. Bossavit, G. Griso, and B. Miara. "Modelling of periodic electromagnetic structures bianisotropic materials with memory effects". In: *J. Math. Pures Appl.* 84.7 (2005), pp. 819–850. DOI: 10.1016/j.matpur.2004.09.015.

[103] I. Bialynicki-Birula. "On the Wave Function of the Photon". In: *Acta Phys. Pol. A* 86.1 (1994), pp. 245–294. DOI: 10.1016/S0079-6638(08)70316-0.

[104] S. A. Khan. "An Exact Matrix Representation of Maxwell's Equations". In: *Phys. Scr.* 71 (2005), p. 440. DOI: 10.1238/Physica.Regular.071a00440.

[105] O. Laporte and G. E. Uhlenbeck. "Application of Spinor Analysis to the Maxwell and Dirac Equations". In: *Phys. Rev.* 37 (1931), pp. 1380–1397. DOI: 10.1103/PhysRev.37.1380.

[106] J. R. Oppenheimer. "Note on Light Quanta and the Electromagnetic Field". In: *Phys. Rev.* 38 (1931), pp. 725–746. DOI: 10.1103/PhysRev.38.725.

[107] R. H. Good. "Particle Aspect of the Electromagnetic Field Equations". In: *Phys. Rev.* 105 (1957), pp. 1914–191. DOI: 10.1103/PhysRev.105.1914.

[108] J. Dressel, K. Y. Bliokh, and F. Nori. "Spacetime algebra as a powerful tool for electromagnetism". In: *Phys. Reports* 589 (2015), pp. 1–71. DOI: https://doi.org/10.1016/j.physrep.2015.06.001.

[109] K. Hizanidis, E. Koukoutsis, P. Papagiannis, A. K. Ram, and G. Vahala. *Space Time Algebra Formulation of Cold Magnetized Plasmas*. 2024. DOI: 10.48550/arXiv.2412.05009. arXiv: 2412.05009 [physics.plasm-ph].

[110] G. K. Jonas Fridén and A. Sihvola. "Effect of Dissipation on the Constitutive Relations of Bi-Anisotropic Media—the Optical Response". In: *Electromagnetics* 17.3 (1997), pp. 251–267. DOI: 10.1080/02726349708908535.

[111] K. Yee. "Numerical solution of initial boundary value problems involving maxwell's equations in isotropic media". In: *IEEE Trans. Antennas Propag.* 14.3 (1966), pp. 302–307. DOI: 10.1109/TAP.1966.1138693.

[112] J. Schneider and S. Hudson. "A finite-difference time-domain method applied to anisotropic material". In: *IEEE Trans. Antennas Propag.* 41.7 (1993), pp. 994–999. DOI: 10.1109/8.237636.

[113] A. Papageorgiou and J. F. Traub. "Measures of quantum computing speedup". In: *Phys. Rev. A* 88 (2 2013), p. 022316. DOI: 10.1103/PhysRevA.88.022316.

[114] J. Taylor, S. Smith, and J. Yepez. *Spin-2 BEC spinor superfluid soliton-soliton scattering in one and two space dimensions*. 2019. DOI: 10.48550/arXiv.1907.12834.

[115] A. Tip. "Linear absorptive dielectrics". In: *Phys. Rev. A* 57 (1998), pp. 4818–4841. DOI: 10.1103/PhysRevA.57.4818.

[116] A. Figotin and J. Schenker. "Spectral Theory of Time Dispersive and Dissipative Systems". In: *J. Stat. Phys* 118 (2005), pp. 199–263. DOI: 10.1007/s10955-004-8783-7.

[117] M. Cassier, P. Joly, and M. Kachanovska. "Mathematical models for dispersive electromagnetic waves: An overview". In: *Comput. Math. with Appl.* 74 (2017), pp. 2792–2830. DOI: https://doi.org/10.1016/j.camwa.2017.07.025.

[118] M. G. Silveirinha. "Chern invariants for continuous media". In: *Phys. Rev. B* 92 (2015), p. 125153. DOI: 10.1103/PhysRevB.92.125153.

[119] J. H. Lee and D. Kalluri. "Three-dimensional FDTD simulation of electromagnetic wave transformation in a dynamic inhomogeneous magnetized plasma". In: *IEEE Trans. Antennas Propag.* 47.7 (1999), pp. 1146–1151. DOI: 10.1109/8.785745.

[120] C. Tsironis and A. Papadopoulos. "Parallelization of a 3D FDTD code and physics studies of electromagnetic wave propagation in fusion plasmas". In: *J. Electromagn. Waves Appl.* 37.16 (2023), pp. 1366–1393. DOI: 10.1080/09205071.2023.2241862.

[121] M. G. Ghahi and S. J. Akhtarshenas. "Entangled graphs: a classification of four-qubit entanglement". In: *Eur. Phys. J. D* 70 (54 2016), p. 042418. DOI: 10.1140/epjd/e2016-60729-1.

[122] A. K. Ram, K. Hizanidis, and Y. Kominis. “Scattering of radio frequency waves by blobs in tokamak plasmasa)”. In: *Phys. Plasmas* 20.5 (2013), p. 056110. DOI: 10.1063/1.4803898.

[123] A. K. Ram and K. Hizanidis. “Scattering of radio frequency waves by cylindrical density filaments in tokamak plasmas”. In: *Phys. Plasmas* 23.2 (2016), p. 022504. DOI: 10.1063/1.4941588.

[124] J. J. Vaz and J. W.A. Rodrigues. “Equivalence of the Dirac and Maxwell equations and quantum mechanics”. In: *Int. J. Theor. Phys* 32 (1993), pp. 945–586.

[125] J. J. Vaz and J. W.A. Rodrigues. “Maxwell and Dirac theories as an already unified theory”. In: *arXiv:hep-th/9511181* 1 (1995).

[126] A. A. Zyablovsky, A. P. Vinogradov, A. A. Pukhov, A. V. Dorofeenko, and A. A. Lisyansky. “PT-symmetry in optics”. In: *Phys.-Usp.* 57 (2014), p. 1063. DOI: 10.3367/UFNe.0184.201411b.1177.

[127] S. S. Bullock and I. L. Markov. “Asymptotically optimal circuits for arbitrary n-qubit diagonal comutations”. In: *Quantum Inf. Comput.* 4 (2004), pp. 27–47. DOI: 10.5555/2011572.2011575.

[128] N. Okuma and Y. O. Nakagawa. “Nonnormal Hamiltonian dynamics in quantum systems and its realization on quantum computers”. In: *Phys. Rev. B* 105 (5 2022), p. 054304. DOI: 10.1103/PhysRevB.105.054304.

[129] R. Shen, T. Chen, B. Yang, and C. H. Lee. *Observation of the non-Hermitian skin effect and Fermi skin on a digital quantum computer*. 2024. DOI: doi.org/10.48550/arXiv.2311.10143. arXiv: 2311.10143 [quant-ph].

[130] A. J. Daley. “Quantum trajectories and open many-body quantum systems”. In: *Advances in Physics* 63.2 (2014), pp. 77–149. DOI: 10.1080/00018732.2014.933502.

[131] T. Hogg, C. Mochon, W. Polak, and E. Rieffel. “Tools For Quantum Algorithms”. In: *Int. J. Mod. Phys. C* 10 (1999), pp. 1347–1361. DOI: 10.1142/S0129183199001108.

[132] M. Motta, C. Sun, A. T. K. Tan, M. J. Oberourke, E. Ye, A. J. Minnich, F. G. S. L. Brand£o, and G. K.-L. Chan. “Determining eigenstates and thermal states on a quantum computer using quantum imaginary time evolution”. In: *Nat. Phys.* 16 (2 2020), pp. 205–210. DOI: 10.1038/s41567-019-0704-4.

[133] H. Kamakari, S.-N. Sun, M. Motta, and A. J. Minnich. “Digital Quantum Simulation of Open Quantum Systems Using Quantum Imaginary–Time Evolution”. In: *PRX Quantum* 3 (1 2022), p. 010320. DOI: 10.1103/PRXQuantum.3.010320.

[134] T. M. Watad and N. H. Lindner. “Variational quantum algorithms for simulation of Lindblad dynamics”. In: *Quantum Sci. Technol.* 9.2 (2024), p. 025015. DOI: 10.1088/2058-9565/ad17d8. URL: https://dx.doi.org/10.1088/2058-9565/ad17d8.

[135] P. Stadler, M. Lodi, A. Khedri, R. Reiner, K. Bark, N. Vogt, M. Marthaler, and J. Leppäkangas. *Demonstration of system-bath physics on gate-based quantum computer*. 2024. DOI: 10.48550/arXiv.2404.18828. arXiv: 2404.18828 [quant-ph].

[136] J. Zhong, S. Xu, K. Wang, J. Chen, F. Jin, X. Zhu, Y. Gao, Y. Wu, C. Zhang, N. Wang, et al. "Simulating unsteady flows on a superconducting quantum processor". In: *Commun. Phys.* 7 (1 2024), p. 349. DOI: 10.1038/s42005-024-01845-w.

[137] S. Jin, N. Liu, and Y. Yu. "Quantum simulation of partial differential equations: Applications and detailed analysis". In: *Phys. Rev. A* 108 (3 2023), p. 032603. DOI: 10.1103/PhysRevA.108.032603.

[138] E. Koukoutsis, P. Papagiannis, K. Hizanidis, A. K. Ram, G. Vahala, O. Amaro, L. I. I. Gamiz, and D. Vallis. *Quantum implementation of non-unitary operations with biorthogonal representations*. 2024. arXiv: 2410.22505 [quant-ph]. URL: https://arxiv.org/abs/2410.22505.

[139] A. Engel, G. Smith, and S. E. Parker. "Linear embedding of nonlinear dynamical systems and prospects for efficient quantum algorithms". In: *Phys. Plasmas* 28.6 (June 2021), p. 062305. DOI: 10.1063/5.0040313.

[140] J.-P. Liu, H. Ø. Kolden, H. K. Krovi, N. F. Loureiro, K. Trivisa, and A. M. Childs. "Efficient quantum algorithm for dissipative nonlinear differential equations". In: *Proc. Natl. Acad. Sci. U.S.A.* 118.35 (2021), e2026805118. DOI: 10.1073/pnas.2026805118.

[141] D. Lewis, S. Eidenbenz, B. Nadiga, and Y. Subaşı. "Limitations for Quantum Algorithms to Solve Turbulent and Chaotic Systems". In: *Quantum* 8 (2024), p. 1509. DOI: 10.22331/q-2024-10-24-1509.

[142] Y. T. Lin, R. B. Lowrie, D. Aslangil, Y. Subaşı, and A. T. Sornborger. *Challenges for quantum computation of nonlinear dynamical systems using linear representations*. 2024. arXiv: 2202.02188 [quant-ph]. URL: https://arxiv.org/abs/2202.02188.

[143] A. M. Childs and J. Young. "Optimal state discrimination and unstructured search in nonlinear quantum mechanics". In: *Phys. Rev. A* 93 (2 2016), p. 022314. DOI: 10.1103/PhysRevA.93.022314.

[144] M. R. Geller. "Fast Quantum State Discrimination with Nonlinear Positive Trace-Preserving Channels". In: *Advanced Quantum Technologies* 6.6 (2023), p. 2200156. DOI: 10.1002/qute.202200156.

[145] Z. Holmes, N. J. Coble, A. T. Sornborger, and Y. ğ. Suba ş ı. "Nonlinear transformations in quantum computation". In: *Phys. Rev. Res.* 5 (1 2023), p. 013105. DOI: 10.1103/PhysRevResearch.5.013105.

[146] S. Das and J. R. Green. "Density matrix formulation of dynamical systems". In: *Phys. Rev. E* 106 (5 2022), p. 054135. DOI: 10.1103/PhysRevE.106.054135.

[147] M. Soe, G. Vahala, L. Vahala, A. K. Ram, E. Koukoutsis, and K. Hizanidis. *Quantum Lattice Representation of Nonlinear Classical Physics*. 2024. arXiv: 2409.17520 [physics.plasm-ph]. URL: https://arxiv.org/abs/2409.17520.

[148] E. Esmaeilifar, D. Ahn, and R. S. Myong. “Quantum algorithm for nonlinear Burgers’ equation for high-speed compressible flows”. In: *Phys. Fluids* 36.10 (2024), p. 106110. DOI: 10.1063/5.0231994.

Appendix A

Basics of $\mathscr{C}l(\mathbb{R}^{1,3})$

The Dirac Algebra, $\mathscr{DA}$ is a remarkably powerful tool that describes scalars along with 4-dimensional objects such as vectors, planes, volumes and pseudo-scalars. It contains all of the familiar vector operations, but most importantly a new type of algebraic product, the so-called Geometric or Clifford product. For vectors, denoted by bold face letters, $\boldsymbol{a},\boldsymbol{b} \in \mathbb{R}^3$

$$\boldsymbol{ab} = \boldsymbol{a}\cdot\boldsymbol{b} + \boldsymbol{a}\wedge\boldsymbol{b} \tag{A.1}$$

The result is the sum of a scalar (the so-called inner product) and the so-called wedge ($\wedge$) or exterior product which is called *bivector*. Thus, it produces the sum of two distinct objects that forms a *multivector* just like the sum in the complex numbers. Orthonormal vectors render, by definition, zero inner product. In the Dirac Algebra we choose an orthonormal basis of vectors denoted with $\{\gamma_\nu, \nu = 0,1,2,3\}$, or, equivalently, with $\{\gamma_0, \gamma_m, m = 1,2,3\}$ that satisfy the following generalized orthonormality conditions:

$$\gamma_0\gamma_0 = 1, \quad \gamma_m\cdot\gamma_n = -\delta_{mn}, \quad \gamma_0\cdot\gamma_m = 0, \quad m,n = 1,2,3, \tag{A.2a}$$

as well as:

$$\gamma_\mu\wedge\gamma_\mu = 0, \quad \mu = 0,1,2,3, \tag{A.2b}$$

The $\mathbb{R}^{1,3}$ space now has been equipped with the product of Eq.(A.1), hence the basis set of the $\mathscr{DA}$ is generated from the orthonormal basis $\{\gamma_\mu\}$ vectors, rendering five different bases for the respective five geometrical grades, namely the scalars and 4-dimensional (spacial and temporal) vectors, the 4-dimensional bivectors (space-space and space-time planes or blades), the trivectors (spatial oriented volumes and spacetime oriented volumes) and the pseudo-scalars (the highest grade geometrical element). Furthermore, because of (A.2) one can actually suppress the exterior product in the process of defining the bases for the various grades:

$$\{1\} \tag{A.3a}$$

$$\{\gamma_0, \gamma_1, \gamma_2, \gamma_3\} \tag{A.3b}$$

$$\{\gamma_1\gamma_0, \gamma_2\gamma_0, \gamma_3\gamma_0, \gamma_1\gamma_2, \gamma_2\gamma_3, \gamma_3\gamma_1\} \tag{A.3c}$$

$$\{\gamma_1\gamma_2\gamma_3, \gamma_1\gamma_2\gamma_0, \gamma_2\gamma_3\gamma_0, \gamma_3\gamma_1\gamma_0\} \tag{A.3d}$$

$$\{\gamma_0\gamma_1\gamma_2\gamma_3\} \tag{A.3e}$$

The latter basis element is usually denoted as $\mathscr{I} = \gamma_0\gamma_1\gamma_2\gamma_3$. All the elements of $\mathscr{D}\mathscr{A}$ can be decomposed in elements (multivectors) that belong to different grades. On the other hand, the pseudoscalar has a paramount intrinsic geometrical significance: It commutes with elements of even grade and anti-commutes with elements of odd grade. If $\mathscr{A}_r$ is a multivector of grade r (a pure multivector), then:

$$\mathscr{A}_r\mathscr{I} = (-1)^{3r}\mathscr{I}\mathscr{A}_r \tag{A.4}$$

As a consequence of the choice of the Minkowskian metric $(1,-1,-1,-1)$, the geometric product of the pseudo-scalar with itself (its square) is scalar and:

$$\mathscr{I}\mathscr{I} = \mathscr{I}^2 = -1 \tag{A.5}$$

The LHS of (A.4) is the (minus) so called dual (prefix $\star$) of the pure blade $\mathscr{A}_r$, or, equivalently, its orthogonal complement (superscript $\perp$). Generally speaking, going from a multivector to a multivector via multiplication by the pseudoscalar is the so-called *duality transformation*:

$$\star\mathscr{A}_r \equiv \mathscr{A}_r{}^{\perp} \equiv -\mathscr{A}_r\mathscr{I} \tag{A.6}$$

The orthogonal complement of a pure blade of grade r does not contain vectors that "lie on" the blade, since the grade of the orthogonal complement is $4-r$. For bivectors, this amounts to going (for example) from space-time bivectors to purely spatial ones.

The duality transform is of tantamount importance in reformulating Maxwell equation to a Schrodinger-Dirac form. In the framework of $\mathscr{D}\mathscr{A}$, the proper "tools" are (1) the so-called *grade involution*, specifically called *space conjugation*: It is the geometric multiplication of an object $\mathscr{A}$ from both sides by the time-like direction γ_0 (superscript $\star$):

$$\mathscr{A}^{\star} \equiv \gamma_0\mathscr{A}\gamma_0, \tag{A.7}$$

and (2) *reversion* (over $\sim$). In terms of a geometric product of grade one objects (vectors) this can readily defined as follows:

$$\widetilde{(abc...z)} \equiv (z...cba) \tag{A.8}$$

This amounts to the following change of signs (from plus) in the separation of grades

(signified by $\langle\rangle_r, r = 0...4$) in an object $\mathscr{A}$ of $\mathscr{DA}$:

$$\mathscr{A} = \langle\mathscr{A}\rangle_0 + \langle\mathscr{A}\rangle_1 + \langle\mathscr{A}\rangle_2 + \langle\mathscr{A}\rangle_3 + \langle\mathscr{A}\rangle_4, \quad \widetilde{\mathscr{A}} = \langle\mathscr{A}\rangle_0 + \langle\mathscr{A}\rangle_1 - \langle\mathscr{A}\rangle_2 - \langle\mathscr{A}\rangle_3 + \langle\mathscr{A}\rangle_4 \tag{A.9}$$

Both involutions (grade and reversion) commute by definition. The application of both is called Clifford conjugation (†) in $\mathscr{DA}$. It is an extension of Hermitian conjugation from the Pauli Algebra $\mathscr{PA}$ to the Dirac Algebra $\mathscr{DA}$ (that is why the same symbol is used, although there are different symbolisms in the literature). It is also called relative (relative to the time-like direction γ_0) reversion-involution:

$$\mathscr{A}^\dagger \equiv \gamma_0 \widetilde{\mathscr{A}} \gamma_0 = \widetilde{\mathscr{A}^\star} \tag{A.10}$$

As far as the EM bivector is concerned, it is straightforward to obtain its reversion as well as its Clifford conjugate :

$$\tilde{\mathscr{F}} = -\mathscr{F}, \quad \mathscr{F}^\dagger = \mathscr{E} - \mathscr{I}\mathscr{B} \tag{A.11}$$

It is also important in our application to generalize the geometric product (A.1) to the one between a vector or vector operator $\boldsymbol{a}$ (grade 1 objects) and a bivector $\mathscr{B}$:

$$\boldsymbol{a}\mathscr{B} = \boldsymbol{a} \cdot \mathscr{B} + \boldsymbol{a} \wedge \mathscr{B} \tag{A.12}$$

Above, both the vector and the bivector are expressed in the basis (A.3) and the inner and exterior products are executed in accordance with (A.2).

We now introduce the Dirac differential operator. It is a grade 1 (vectorial) differential operator and it involves the 4-tangent vectors in the Minkowskian space and the partial differentiation of the differentiated object of $\mathscr{DA}$. Its form is (summation convention is adapted):

$$\mathscr{D} \equiv \gamma_\mu \partial^\mu, \quad \mu = 0,1,2,3 \tag{A.13}$$

Seeing this gradient operator as a four-vector operator, operating in $\mathscr{DA}$, one can "split" it by its right geometric product with the time-like direction γ_0 as follows (summation convention is adapted):

$$\mathscr{D}\gamma_0 = \mathscr{D} \cdot \gamma_0 + \mathscr{D} \wedge \gamma_0 = \partial^0 + \gamma_m \wedge \gamma_0 \partial^m = \partial^0 + \gamma_m \gamma_0 \partial^m, \quad m = 1,2,3 \tag{A.14}$$

The second part is clearly a differential bivector acting on each space-time blade $\gamma_m\gamma_0$. We introduce the double arrow to signify this space-time differential operator:

$$\overleftrightarrow{\nabla} \equiv \gamma_0 \wedge \gamma_m \partial^m = \gamma_0 \gamma_m \partial^m \tag{A.15}$$

Thus, similarly:

$$\mathscr{D} = (\partial^0 - \overleftrightarrow{\nabla})\gamma_0 = \gamma_0(\partial^0 + \overleftrightarrow{\nabla}) = \tilde{\mathscr{D}}, \tag{A.16}$$

That is, the time-like direction splits the 4-dimensional gradient into two mutually orthogonal parts: the time-like scalar differential operator and the space-like bivectorial one. The Clifford conjugate of the operator $\mathscr{D}$ can be easily deduced in analogy to the Clifford conjugation of the 4-vectors. Because of (A.16):

$$\mathscr{D}^\dagger = (\partial^0 + \overleftrightarrow{\nabla})\gamma_0 = \gamma_0(\partial^0 - \overleftrightarrow{\nabla}) = \tilde{\mathscr{D}}^\dagger = \mathscr{D}^\star \tag{A.17}$$

That is, the Clifford (Hermitian) conjugate (or relative reversed) of the 4-dimensional differential operator $\mathscr{D}$ with its space-conjugate. This is something to be expected from the very definition of the relative inversion acting on grade 1 objects and operators. Notice that both the differential bivector and its Clifford conjugate coincide with their reverse ones.

In Sec.4.3.3 one needs to evaluate the Clifford conjugate of the operation of $\mathscr{D}$ on the electromagnetic bivector $\mathscr{F}$:

$$(\mathscr{D}\mathscr{F})^\dagger = \gamma_0\tilde{\mathscr{F}}\tilde{\mathscr{D}}\gamma_0 = \mathscr{F}^\dagger\mathscr{D}^\dagger = \widetilde{\tilde{\mathscr{D}}^\dagger\tilde{\mathscr{F}}^\dagger} = -\widetilde{\mathscr{D}^\dagger\mathscr{F}^\dagger} \tag{A.18}$$

or, equivalently:

$$\mathscr{D}^\dagger\mathscr{F}^\dagger = -\widetilde{(\mathscr{D}\mathscr{F})^\dagger} \tag{A.19}$$

From (A.19) one has to reverse the RHS of this equation and then take its Clifford conjugate. Before we proceed, one must easily notice that the inner product part of the differential operator (a one-vector operator) as well as its Clifford conjugate with a bivector coincides with its reverse:

$$\widetilde{\mathscr{D}^\dagger \cdot \mathscr{P}} = \mathscr{D}^\dagger \cdot \mathscr{P} \tag{A.20}$$

and,via the relations (A.16) and (A.17) one obtains:

$$\left(\widetilde{\mathscr{D}^\dagger \cdot \mathscr{P}}\right)^\dagger = (\mathscr{D}^\dagger \cdot \mathscr{P})^\dagger = -\mathscr{D} \cdot \mathscr{P}. \tag{A.21}$$